

## ABSTRACT

Volatile Organic Compounds (VOCs), which may cause short and long term adverse health effects, constitute a significant class of indoor gaseous pollutants. To reduce the VOC concentration of indoor environment, an in-depth understanding of the performance of the air cleaning technologies that address VOCs is important. Although many studies have been conducted to evaluate the performance of air cleaning devices, most of them were performed at elevated concentration level ( $\sim$ ppmv). The performance of the sorbent media at realistic VOC concentration (ppbv) is still not clear due to lack of experiment data and theoretical study. The test conducted under the low concentration is not cost-effective and difficult to perform. Currently, no mathematical model can be effectively used for sorbent media performance simulation at ppb level.

The main objective of the presented research is to investigate the adsorption mechanism, address the existing problems through a model-based testing and evaluation method, develop and validate reliable methodologies to predict the long-term performance of filter sorbent media, when exposed to the realistic indoor concentration of VOCs.

A series of long-term tests were conducted at six concentration levels from 100 ppm to 66 ppb, and different test conditions (particle size, flow rate and sorbent bed length) to reveal the different behavior of the filter media at different concentration levels. A new mechanistic model named convective & diffusion mass transfer model with variable partition coefficient (C&DMT-VP) was proposed to simulate the performance of adsorption-based air cleaning devices under the typical indoor VOC concentrations. The applications of this model were demonstrated, including the determination of the surface diffusion coefficient, prediction of sorbent media filter performance via C&DMT-VP at typical indoor concentration level based on the model parameters determined from different test methods, including the ASHRAE

standard test 145.1, ground pellet test and thin layer with ground pellet test. Finally, the proposed methods were compared and validated with the experimental data.

It was found that 1) the partition coefficient varied with the concentration in the form of  $K_{ma} = aC^b$  (or  $\log(K_{ma}) = A + B\log(C)$ ); 2) The C&DMT-VP model incorporating the K(C) relationship significantly improved the representation of the performance at the low concentration as well as being able to represent the high concentration performance as in previous model; 3) The three accelerated methods were able to provide the data needed to determine the  $K_{ma}(C)$  function for a given adsorption media's performance at low concentrations typically found indoors.

MODEL-BASED TESTING AND EVALUATION OF SORPTION MEDIA FOR  
REMOVING VOLATILE ORGANIC COMPOUNDS IN INDOOR AIR

by

Chuan He

B.S., China University of Mining and Technology (Beijing), 2010  
M.S., Syracuse University, 2013

Dissertation Submitted in partial fulfillment of the requirements for the degree of  
Doctor of Philosophy in *Civil Engineering*.

Syracuse University  
May 2018

ProQuest Number: 10750536

All rights reserved

INFORMATION TO ALL USERS

The quality of this reproduction is dependent upon the quality of the copy submitted.

In the unlikely event that the author did not send a complete manuscript and there are missing pages, these will be noted. Also, if material had to be removed, a note will indicate the deletion.



ProQuest 10750536

Published by ProQuest LLC (2018). Copyright of the Dissertation is held by the Author.

All rights reserved.

This work is protected against unauthorized copying under Title 17, United States Code  
Microform Edition © ProQuest LLC.

ProQuest LLC.  
789 East Eisenhower Parkway  
P.O. Box 1346  
Ann Arbor, MI 48106 – 1346

Copyright © Chuan He 2018

All Rights Reserved

## ACKNOWLEDGEMENTS

I would love to extend thanks to the many people, in both US and China, who supported me from many aspects from 2011 to 2016. My sincere gratitude goes to my advisor, Dr. Jensen Zhang, wholeheartedly. My five-year Ph.D. program cannot be such an amazing experience without Jensen, not only for his tremendous academic support, but also for giving me so many wonderful opportunities and helping me in life.

Similar, profound gratitude goes to my parents, who supported me both financially and emotionally. I am particularly indebted to them for their constant faith in me.

The time that I had in the Building Energy Environmental Systems Laboratory (BEESL), Department of Mechanical and Aerospace Engineering at Syracuse University was meaningful and unforgettable. The memory of the day and night in the lab is still fresh like yesterday. When I walked into the lab space for the very first time, I did not realize that I would spend 6 years in this small and lovely town. I consider Syracuse as my second hometown, the BEESL folks are my family members. The knowledge, skills, and attitude I learned from this lab will benefit me in both work and life, forever. I would like to particularly thank Dr. Jingjing Pei and Beverly

Guo who helped me tremendously in conducting the modeling and experimental work in my research.

I am also hugely appreciative to the friends who I made in Syracuse University. The Ph.D. life can be very tough without the joy that came from the friendship. I would like to apply my knowledge gained from my research in the real world and make it a better place.

# CONTENTS

|   |              |
|---|--------------|
| <b>ACKNOWLEDGEMENTS</b>                                 | <b>V</b>     |
| <b>LIST OF ABBREVIATIONS AND ACRONYMS</b>               | <b>X</b>     |
| <b>LIST OF TABLES</b>                                   | <b>XIII</b>  |
| <b>LIST OF FIGURES</b>                                  | <b>XIV</b>   |
| <b>LIST OF APPENDICES</b>                               | <b>XVIII</b> |
| <b>1 INTRODUCTION</b>                                   | <b>1</b>     |
| 1.1 BACKGROUND AND PROBLEM DEFINITION                   | 1            |
| 1.2 OBJECTIVE AND SCOPE                                 | 5            |
| 1.3 THESIS OUTLINE                                      | 6            |
| <b>2 LITERATURE REVIEW</b>                              | <b>9</b>     |
| 2.1 INTRODUCTION  | 9            |
| 2.2 VOC PHYSICAL ADSORPTION IN ACTIVATED CARBON         | 9            |
| 2.2.1 <i>Activated carbon</i>                           | 11           |
| 2.2.2 <i>Mass transport in a sorbent bed</i>            | 16           |
| 2.3 EXPERIMENTAL EVALUATION OF FILTER MEDIA PERFORMANCE | 27           |
| 2.4 MODELLING AND SIMULATION OF SORBENT BED             | 28           |
| 2.4.1 <i>Empirical/semi-empirical model</i>             | 28           |
| 2.4.2 <i>Adsorption isotherm</i>                        | 32           |
| 2.4.3 <i>Mechanistic model</i>                          | 38           |
| 2.5 MAJOR FINDINGS                                      | 41           |
| <b>3 EXPERIMENTAL INVESTIGATION</b>                     | <b>43</b>    |
| 3.1 INTRODUCTION  | 43           |
| 3.2 TEST SYSTEM AND METHOD                              | 44           |



|  |           |
|--|-----------|
| 3.3 TEST MATERIAL  | 48        |
| 3.4 TEST CONDITION   | 50        |
| 3.5 RESULTS AND DISCUSSIONS  | 52        |
| 3.6 MAJOR FINDINGS   | 62        |
| <b>4 MODELING AND SIMULATIONS</b>  | <b>64</b> |
| 4.1 INTRODUCTION   | 64        |
| 4.2 MODEL DESCRIPTION  | 65        |
| 4.2.1 <i>Convective &amp; Diffusion Mass Transfer with Constant Partition Coefficient (C&amp;DMT-CP)</i> | 65        |
| 4.2.2 <i>Convective &amp; Diffusion Mass Transfer with Variable Partition Coefficient (C&amp;DMT-VP)</i> | 69        |
| 4.3 MODEL IMPLEMENTATION   | 71        |
| 4.3.1 <i>C&amp;DMT-CP model implementation</i>   | 71        |
| 4.3.2 <i>C&amp;DMT-VP model implementation</i>   | 73        |
| 4.4 MODEL EVALUATION   | 75        |
| 4.4.1 <i>C&amp;DMT-CP model evaluation</i>   | 79        |
| 4.4.2 <i>C&amp;DMT-VP model evaluation</i>   | 82        |
| 4.5 DISCUSSION   | 89        |
| 4.6 MAJOR FINDINGS   | 94        |
| <b>5 MODEL-BASED TESTING METHOD FOR PREDICTING MEDIA PERFORMANCE AT LOW CONCENTRATIONS</b>               | <b>95</b> |
| 5.1 INTRODUCTION   | 95        |
| 5.2 MODEL-BASED TESTING AND EVALUATION METHOD  | 96        |
| 5.3 DETERMINATION OF P-C CORRELATION THROUGH ACCELERATED TESTS   | 97        |
| 5.4 RESULTS AND DISCUSSION   | 99        |

|   |            |
|---|------------|
| 5.5 MAJOR FINDINGS  | 107        |
| <b>6 SUMMARY AND CONCLUSIONS</b>  | <b>109</b> |
| 6.1 INTRODUCTION  | 109        |
| 6.2 PHYSICAL ADSORPTION TEST AT DIFFERENT CONCENTRATION LEVELS  | 109        |
| 6.3 MODEL-BASED TESTING AND EVALUATION METHOD   | 110        |
| 6.4 RECOMMENDATIONS FOR FUTURE WORKS  | 111        |
| <b>7 APPENDICES</b>   | <b>112</b> |
| APPENDIX A SPECIFICATION OF MONITORING DEVICE   | 112        |
| APPENDIX B. DERIVATION OF SORBENT BED EQUATION AND PELLET EQUATION                                    | 113        |
| APPENDIX C. COMPUTER PROGRAM (C++) FOR SIMULATION MODEL   | 116        |
| APPENDIX D. METHOD AND PROCEDURE IMPLEMENTED IN MODELS FOR REGRESSION ANALYSIS<br>WITH C&DMT-VP MODEL | 132        |
| <b>8 REFERENCES</b>   | <b>137</b> |

## LIST OF ABBREVIATIONS AND ACRONYMS

### Arbitrations

|         |   |
|---------|---|
| ASHRAE  | American Society of Heating, Refrigerating and Air-Conditioning Engineers |
| CDMT-CP | convective & diffusion mass transfer with constant partition coefficient  |
| CDMT-VP | convective & diffusion mass transfer with variable partition coefficient  |
| GAC     | granular activated carbon   |
| HVAC    | heating, ventilating, and air conditioning                                |
| MTZ     | mass transfer zone  |
| VOC     | volatile organic compounds  |

### Symbols

|          |  |
|----------|--|
| $A_s$    | Surface area of the pellet exposed to the bulk air, $m^2$        |
| $C$      | Gas phase concentration in the bulk air of sorbent bed, $mg/m^3$ |
| $C^*$    | Concentration at the gas-solid interface, $mg/m^3$               |
| $C_b$    | Gas phase concentration in the sorbent bed, ppm or $mg/m^3$      |
| $C_{in}$ | Inlet VOC concentration in the bulk air, $mg/m^3$                |
| $C_p$    | Gas phase concentration in the pores of sorbent pellet, $mg/m^3$ |
| $C_s$    | Sorbed phase concentration, ppm or $mg/m^3$                      |

|             |   |
|-------------|---|
| $C_r$       | Removal capacity, mg (VOC absorbed)/mg(adsorbent)   |
| $d_p$       | Diameter of the spherical sorbent pellet, m   |
| $D_{app}$   | Apparent diffusivity, which combines effective pore diffusion coefficient, surface coefficient and partition coefficient, $m^2/s$ |
| $D_{ax}$    | Axial diffusion coefficient through the sorbent bed, $m^2/s$  |
| $D_k$       | Knudsen diffusion coefficient, $m^2/s$  |
| $D_m$       | Molecular diffusion coefficient, $m^2/s$  |
| $D_p$       | Effective pore diffusion coefficient within pellet, $m^2/s$   |
| $D_{s,cri}$ | Surface diffusion coefficient when the Bi number is 1, $m^2/s$  |
| $D_s$       | Surface diffusion coefficient within pellet, $m^2/s$  |
| $E_r$       | Removal efficiency, %   |
| $h_m$       | Convective mass transfer coefficient, m/s   |
| $K_L$       | Langmuir constant   |
| $K_{ma}$    | VOC partition coefficient   |
| $L$         | Sorbent bed depth, m  |
| $M$         | Molecular weight of target compound, g/mol  |
| $Q$         | Air flow rate through the sorbent bed, $m^3/h$  |
| $q$         | Adsorbed mass of VOC per unit mass of the sorbent media, mg/mg  |
| $r_p$       | Radius of sorbent pellet, m   |
| $t$         | Elapsed time, h   |

|                 |  |
|-----------------|--|
| $u_p$           | Interstitial velocity (average velocity through the bed's void), m/s |
| $u_s$           | Superficial velocity (flow rate/sorbent bed cross area), m/s         |
| $W$             | Mass of the sorbent media, g   |
| $\varepsilon_b$ | Sorbent bed porosity, $m^3/m^3$                                      |
| $\varepsilon_p$ | Sorbent pellet porosity, $m^3/m^3$                                   |
| $\rho$          | Density of sorbent pellet, $g/m^3$                                   |

## LIST OF TABLES

|  |     |
|--|-----|
| TABLE 1-1 CHALLENGE CONCENTRATION IN ASHRAE STANDARD   | 3   |
| TABLE 2-1 TYPICAL CHARACTERISTICS OF ACTIVATED CARBON  | 13  |
| TABLE 2-2 ACTIVATED CARBON TYPE FOR AIR CLEANING (HENNING, 2001)   | 14  |
| TABLE 2-3 CORRELATIONS FOR CONVECTIVE MASS TRANSFER COEFFICIENT  | 22  |
| TABLE 2-4 LOW CONCENTRATION BREAKTHROUGH TEST IN PREVIOUS STUDIES  | 28  |
| TABLE 2-5 SUMMARY OF EMPIRICAL BREAKTHROUGH MODEL  | 28  |
| TABLE 2-6 SUMMARY OF ADSORPTION ISOTHERM   | 33  |
| TABLE 3-1 TEST MEDIA   | 49  |
| TABLE 3-2 TEST CONDITIONS  | 51  |
| TABLE 3-3 SUMMARY OF THE REMOVAL CAPACITY AND PARTITION COEFFICIENT AT DIFFERENT<br>CONCENTRATION LEVELS | 59  |
| TABLE 4-1 SIMULATION PARAMETERS FOR ADSORPTION TESTS   | 76  |
| TABLE 4-2 SUMMARY OF THE DETERMINED DS AND BI NUMBER   | 87  |
| TABLE 5-1 TEST CONDITIONS OF ACCELERATED TESTS   | 99  |
| TABLE 5-2 SIMULATION PARAMETERS FOR TEST III   | 101 |
| TABLE 8-1 SPECIFICATIONS FOR PPBRAE 30000  | 112 |

## LIST OF FIGURES

|  |    |
|--|----|
| FIGURE 1-1 COMPARISON OF CENTRAL TENDENCY AND MAXIMUM CONCENTRATIONS OF SELECTED VOCs BETWEEN EXISTING RESIDENCES AND OFFICE BUILDINGS (LEVIN & HODGSON, 2006) | 4  |
| FIGURE 1-2 ROADMAP OF THIS STUDY   | 7  |
| FIGURE 2-1 MASS TRANSFER OF VOCs IN THE SORTBENT BED   | 10 |
| FIGURE 2-2 PORE SIZE CLASSIFICATION IN ACTIVATED CARBON  | 12 |
| FIGURE 2-3 MASS TRANSFER ZONE (MTZ) AND BREAKTHROUGH CURVE   | 17 |
| FIGURE 2-4 SCHEMATIC DIAGRAM OF MASS BALANCE OF A CONTROL VOLUME   | 20 |
| FIGURE 2-5 THREE DIFFUSION MECHANISMS  | 27 |
| FIGURE 2-6 TYPICAL ADSORPTION ISOTHERM   | 35 |
| FIGURE 2-7 LINEARITY OF ADSORPTION ISOTHERM AT LOW CONCENTRATION(PEI & ZHANG, 2012)  | 36 |
| FIGURE 2-8 ILLUSTRATION OF DIFFERENT ADSORPTION MODEL IN PACKED BED  | 41 |
| FIGURE 3-1 AIR-CLEANING TECHNOLOGY TEST SYSTEM   | 44 |
| FIGURE 3-2 SCHEMATIC OF ACTTS SYSTEM   | 45 |
| FIGURE 3-3 SCHEMATIC OF TEST COLUMN  | 47 |
| FIGURE 3-4 ACTIVATED CARBON M#1 (LEFT) AND M#2 (RIGHT)   | 49 |
| FIGURE 3-5 GRINDING TOOL SET (A), SIEVING TOOL SET (B) AND GROUND PELLET (C)   | 52 |
| FIGURE 3-6 BREAKTHROUGH CURVE OF TOLUENE, $C_{IN}=107\pm 3.4$ PPM, TEST A  | 54 |
| FIGURE 3-7 BREAKTHROUGH CURVE OF TOLUENE, $C_{IN}=66.8\pm 8$ PPB, TEST A   | 54 |

|   |    |
|---|----|
| FIGURE 3-8 BREAKTHROUGH CURVE OF TOLUENE, $C_{IN}=50$ PPM ( $42\pm 0.8$ PPM), TEST B    | 56 |
| FIGURE 3-9 BREAKTHROUGH CURVE OF TOLUENE, $C_{IN}=5$ PPM ( $5\pm 0.37$ PPM), TEST B     | 56 |
| FIGURE 3-10 BREAKTHROUGH OF TOLUENE, $C_{IN}=500$ PPB ( $563\pm 32.6$ PPB), TEST B      | 57 |
| FIGURE 3-11 BREAKTHROUGH CURVE OF TOLUENE, $C_{IN}=100$ PPB ( $103\pm 6.0$ PPB), TEST B | 57 |
| FIGURE 3-12 CORRELATION OF PARTITION COEFFICIENT AND INLET CONCENTRATION                | 61 |
| FIGURE 3-13 CORRELATION OF PARTITION COEFFICIENT AND INLET CONCENTRATION, LOG AXIS      | 61 |
| FIGURE 4-1 ILLUSTRATION OF MASS TRANSFER ZONE IN A SORBENT BED                          | 70 |
| FIGURE 4-2 DISCRETE REPRESENTATION OF THE SORBENT BED                                   | 71 |
| FIGURE 4-3 FLOW CHART OF SIMULATION WITH THE C&DMT-CP                                   | 73 |
| FIGURE 4-4 IMPLEMENT OF P-C CORRELATION IN THE MODEL                                    | 74 |
| FIGURE 4-5 FLOW CHART OF SIMULATION WITH THE C&DMT-VP                                   | 75 |
| FIGURE 4-6 C&DMT-CP MODEL SIMULATION, 100 PPM   | 80 |
| FIGURE 4-7 C&DMT-CP MODEL SIMULATION, 50 PPB  | 80 |
| FIGURE 4-8 C&DMT-CP MODEL SIMULATION, 50 PPM  | 81 |
| FIGURE 4-9 C&DMT-CP MODEL SIMULATION, 5 PPM   | 81 |
| FIGURE 4-10 C&DMT-CP MODEL SIMULATION, 500 PPB  | 82 |
| FIGURE 4-11 C&DMT-CP MODEL SIMULATION, 100 PPB  | 82 |
| FIGURE 4-12 C&DMT-VP MODEL SIMULATION, 100 PPM, TEST A                                  | 83 |
| FIGURE 4-13 C&DMT-VP SIMULATION, 50 PPB, TEST A   | 83 |
| FIGURE 4-14 C&DMT-VP MODEL SIMULATION, 42 PPM, TEST B                                   | 84 |



|  |     |
|--|-----|
| FIGURE 4-15 C&DMT-VP MODEL SIMULATION, 5 PPM, TEST B   | 84  |
| FIGURE 4-16 C&DMT-VP MODEL SIMULATION, 577 PPB, TEST B   | 85  |
| FIGURE 4-17 C&DMT-VP MODEL SIMULATION, 103 PPB, TEST B   | 85  |
| FIGURE 4-18 EFFECT OF SURFACE DIFFUSION COEFFICIENT IN C&DMT-CP, M#1, TEST B   | 91  |
| FIGURE 4-19 CONCENTRATION PROFILE IN THE SORBENT BED (X/L, NORMALIZED BED LOCATION),<br>M#1, 100 PPM, TEST A.                      | 93  |
| FIGURE 4-20 CONCENTRATION PROFILE IN THE SORBENT BED (X/L, NORMALIZED BED LOCATION),<br>M#1, 50 PPB, TEST A                        | 93  |
| FIGURE 5-1 EFFECTING FACTORS OF MEDIA SORPTION PERFORMANCE, MES  | 96  |
| FIGURE 5-2 MODEL-BASED EVALUATION METHOD   | 97  |
| FIGURE 5-3 SCHEMATIC OF ACCELERATED TEST (TEST III)  | 98  |
| FIGURE 5-4 BREAKTHROUGH OF LOW CONCENTRATION-ACCELERATED TEST, (M#1: 107±9 PPB;<br>M#2: 99±4 PPB)                                  | 101 |
| FIGURE 5-5 REGRESSION THROUGH LOW CONCENTRATION-ACCELERATED TEST, 100 PPB  | 103 |
| FIGURE 5-6 DETERMINATION OF THE P-C CURVE, M#1   | 104 |
| FIGURE 5-7 DETERMINATION OF THE P-C CURVE, M#1(LOG SCALE)  | 104 |
| FIGURE 5-8 DETERMINATION OF THE P-C CURVE, M#2   | 105 |
| FIGURE 5-9 DETERMINATION OF THE P-C CURVE, M#2(LOG SCALE)  | 105 |
| FIGURE 5-10 PREDICTION OF 50 PPB PERFORMANCE BASED ON THE P-C CURVE FROM THE<br>ACCELERATED TEST I: ASHRAE STANDARD TEST (100 PPM) | 106 |

FIGURE 5-11 PREDICTION OF 66 PPB PERFORMANCE BASED ON THE ACCELERATED TEST II:

GROUND PELLET TEST (50 PPM) 106

FIGURE 5-12 PREDICTION OF 66 PPB PERFORMANCE BASED ON THE ACCELERATED TEST III: LOW

CONCENTRATION-ACCELERATED TEST (100 PPB) 107

## LIST OF APPENDICES

Appendix A Specification of monitoring device

Appendix B Derivation of sorbent bed equation and pellet equation

Appendix C Computer program (C++) for Simulation Model

Appendix D Method and procedure implemented in models for regression analysis with the P-C model

# 1 INTRODUCTION

## 1.1 Background and Problem Definition

In both commercial and residential buildings in the U.S., the indoor air pollutants are primarily particulate matters and volatile/semi-volatile organic compounds (VOCs/SVOCs). VOCs could cause short and long term adverse effects on health and productivity (Fiedler et al., 2005). Over three hundred VOCs have been identified in indoor environments (Patel & Brown, 1994; Wolkoff, 1995). Consequently, ventilation is required in buildings to maintain acceptable indoor concentrations of pollutants. ASHRAE standard 62.1-2016: Standards For Ventilation And Indoor Air Quality. Meanwhile, energy agencies and many building owners seek to reduce the consumption of energy for ventilation and thermal conditioning, which accounted for 53% of the total energy consumption in residential buildings and 48% in office buildings (Pérez-Lombard, Ortiz, & Pout, 2008).

Indoor pollutant source control and air purification are another two approaches with the potential of reducing the required ventilation to maintain acceptable indoor air quality. However, practicing VOC source control is the most effective approach in theory, but it has limitations because of unavoidable VOCs emitted from materials, furniture and occupant behaviors. Air cleaning technologies for indoor air quality remains a high priority in engineering practice, especially for reducing the levels of known target compounds. Granular activated carbon (GAC) is an efficient type of sorbent media that can be placed in filters because it has a high capacity in adsorbing pollutants due to the high activated porous structure

and large specific surface area. The installation of GAC media filter in heating, ventilation and air conditioning (HVAC) systems has been proven to reduce VOC concentration in an energy efficient manner (Fisk, 2008). The application of GAC filter raises the importance to well understand the performance of activated carbon at different operation conditions, especially the conditions occurring frequently in the indoor environment.

In the past decades, studies have been conducted in physical adsorption of gaseous pollutants. For example, ASHRAE standard 145.1-2015 has been published to provide a standard laboratory test method for assessing the performance of loose granular media. Table 1 listed the challenge VOC concentration levels suggested in the latest ASHRAE standard, and Figure 1-1 illustrated the typical concentrations in the indoor environment(Levin & Hodgson, 2006). Three orders of magnitude difference exist between the testing concentration and indoor concentration. Indeed, conducting the test at high concentration levels could benefit the testing time and simplicity of VOC generation/measurement, but studying the challenging

concentration that is similar to those often found in the indoor air is necessary to obtain a better understanding of the GAC filters performance.

**Table 1-1 Challenge Concentration in ASHRAE standard**

| Compounds                       | Challenge concentration (10%) |          |
|---------------------------------|-------------------------------|----------|
|                                 | Mg/m <sup>3</sup>             | ppm      |
| Toluene                         | 377±38                        | 100±10   |
| Acetaldehyde                    | 180±18                        | 100±10   |
| Hexane                          | 352±35                        | 100±10   |
| 2-Butanone                      | 295±30                        | 100±10   |
| Isobutanol                      | 303±30                        | 100±10   |
| Dichloromethane                 | 347±35                        | 100±10   |
| Tetrachloroethylene             | 678±68                        | 100±10   |
| Air at 23 °C (75 °F) and 50% RH | Balanced                      | Balanced |

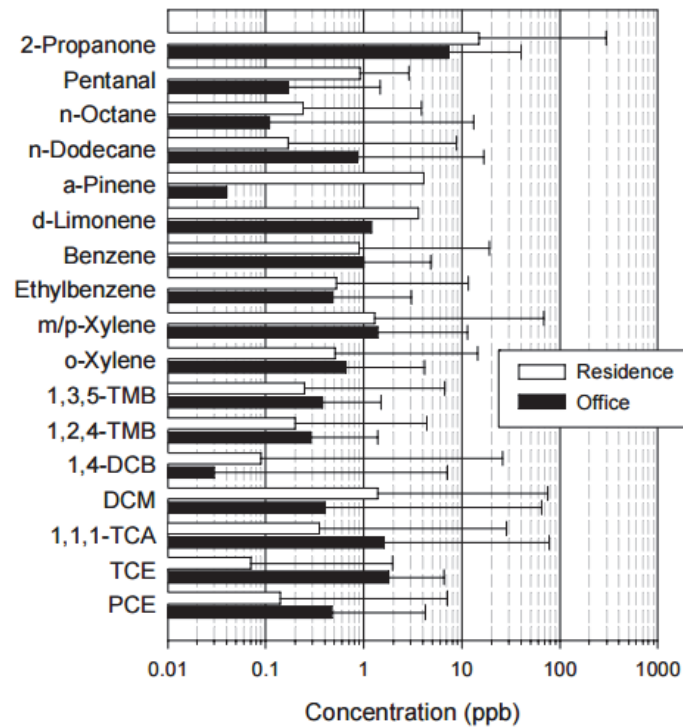


**Figure 1-1 Comparison of central tendency and maximum concentrations of selected VOCs between existing residences and office buildings (Levin & Hodgson, 2006)**

Commonly, high concentration tests have shorter time, easier gas generation, more abrupt breakthrough, and the experimental conditions are easier to maintain within a short time period. But conducting high concentration test needs excessive protection and precaution for the investigator because of the chance of chemical compound exposure and the possible leakage from the test system. Also, the exhaust system needs specific treatment before venting out into the urban air. Most importantly, the high concentration test results cannot represent the performance of the sorbent media in the indoor environment concentrations. On the other hand, low concentration test could reflect the performance of GAC filter in real application, but the test needs to take an extremely long time to reach meaningful breakthrough. In addition, maintaining a stable low concentration gas generation remains a challenge. As a result, very little systematic research has been carried out regarding the long-term performance of GAC

filter at the typical indoor concentration. Although adsorption of indoor VOCs onto GAC has been emphasized in some literatures (Pei & Zhang, 2012; Scahill et al., 2004; VanOsdell, Owen, Jaffe, & Sparks, 1996), the performance data on activated carbon under relative low concentration is still insufficient.

Recently, some researchers attempted to predict the sorbent performance at low concentrations by using mechanistic model with extrapolated model parameters from the high concentration tests, but the extrapolations remained questionable due to some unknown mass transfer mechanism at low concentration condition (He et al., 2014; Khazraei Vizhemehr et al., 2014). Few simulation methodologies are validated at very low concentration levels. In order to guide the design/maintenance of gas-phase air cleaning system, there is an urgent need to develop an effective method for evaluating the performance of sorbent media at the concentration level that can be actually found in the indoor environment.

## 1.2 Objective and Scope

The first objective of this research was to investigate the performance of sorbent media at different concentration levels, especially at typical indoor concentration (<100 ppb). The limitations of the current experimental methods and mathematical models at low concentration will be addressed. The second objective was to develop a new mechanistic model to describe the adsorption process with the consideration of concentration effects. The third objective was to develop a model-based testing and evaluation method to predict the sorbent media



performance at real operation conditions within a reasonable period (in hours). The scope of this study included both experimental and modeling tasks:

Experimental:

1. Conducted the performance test for the commercial activated carbon packed bed at different concentrations from elevated level to practical level.
2. Identified the limitations of current experimental methods
3. Developed accelerated test methods to evaluate the performance of sorbent media for air cleaning devices at VOC concentration levels typical found indoors.

Modelling:

4. Addressed the limitations of current models on physical adsorption at low concentration level.
5. Developed a new mechanistic model with the consideration of the correlation between concentration level and adsorption behavior.
6. Validated the developed physical adsorption model using the experimental data

### 1.3 Thesis Outline

Different parts of this study, their relationships and outcomes can be summarized in a roadmap shown in Figure 1-2. The development of each part will be explained in the following 5 chapters.

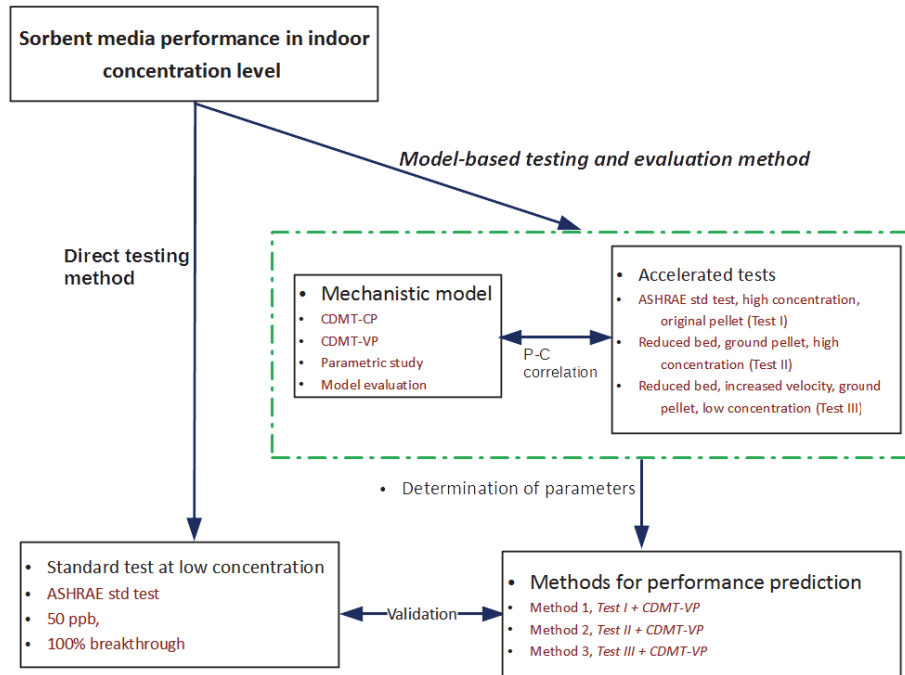


**Figure 1-2 Roadmap of this study**

Chapter 2 illustrates the adsorption principle and fundamentals of mass transfer in filter media.

A critical review of the previous studies on filter media performance test and modelling is

conducted. In addition, the characteristic parameters for activated carbon performance simulation are introduced.

Chapter 3 demonstrates the development of experimental system, test conditions and methodology of the sorbent media performance evaluation, including direct tests and accelerated tests. The test results are presented and discussed.

Chapter 4 is concerned with the development of the new mechanistic model for describing the adsorption dynamics. The evaluation of two different models is conducted. The performance each model in adsorption process simulation is analyzed.

Chapter 5 demonstrates an innovative model-based testing and evaluation method by using three different tests to predict the sorbent media performance at very low concentration level.

Chapter 6 present the conclusions of this study and recommendations for future work on the subject.

# 2 LITERATURE REVIEW

## 2.1 Introduction

In this chapter, the fundamentals of dynamic adsorption in porous media and the governing equations of the mass transport phenomena in activated carbon filter bed are explained. Empirical and mechanistic models are introduced, including different assumptions, governing equations, model parameters, simplifications and solutions. Performance index for adsorption filters such as breakthrough, removal efficiency and removal capacity are defined and interrelated.

## 2.2 VOC physical adsorption in activated carbon

The process by which gases and vapors are removed from air stream in air cleaning devices is called filtration/purification (filtration is more used for particle removal). Generally, the target gas is separated from the air flow which passes through a filter at a constant flow velocity. There are four major components in the purification system, including: the filter media (sorbent), the target gases (sorbates), filter structure (packed bed, or called sorbent bed) and the carrier flow. Each component affects the performance of the purification system differently. In Figure 2-1, the mass transfer process of the sorbates (VOCs in this study) is illustrated in the simplified schematic. There are several key steps: advection by bulk flow through the bed; axial diffusion through the bed voidage; convective mass transfer over the surface (film) of pellet, diffusion inside the sorbent pellet (intra-pellet diffusion, including pore diffusion and surface diffusion), and adsorption at the micropore surface. For active sorbent bed used in typical HVAC system, the axial diffusion is usually negligible comparing with advection

transport by air flow (K.-T. Liu & Weber Jr, 1981; Pei & Zhang, 2012; Xu, Cai, & Pan, 2013).

The details of each key step will be introduced in the rest of this chapter.

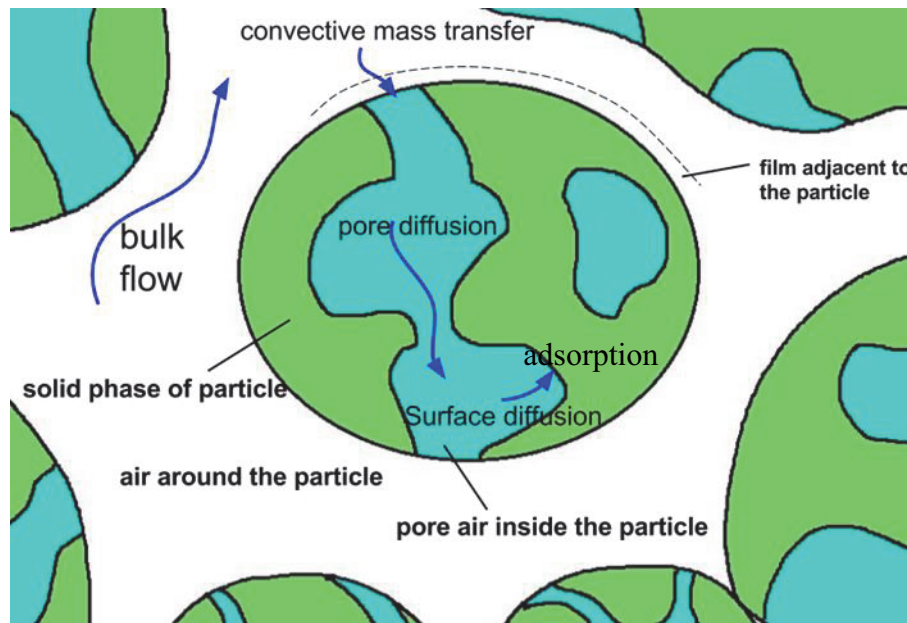


**Figure 2-1 Mass transfer of VOCs in the sorbent bed**

Adsorption refers to the accumulation of gas or liquid molecules on the inner and outer surfaces of a solid sorbent. The sorbent media is a porous medium in nature. Physical adsorption results from the physical attraction of gas or vapor molecules to a surface by relatively weak intermolecular forces termed van der Waals (dispersion-repulsion) (Ruthven, 1984). When considering physical adsorption between a solid and gas or vapor, dispersion forces are always present and will represent the major contribution to the total energy of adsorption, unless the adsorbate molecule possesses a strong dipole moment. The dispersion forces will be

considerably stronger in micropores than above plane surface and will be weakest on prominences (Sing, 1989).

### 2.2.1 Activated carbon

Among various filter media in HVAC applications, activated carbon is one of the most widely used materials due to its extremely high surface area and micropore volume. Moreover, its pore size distribution (can also be bimodal, sometimes trimodal) provides good access of adsorbate molecules to the interior (Laine & Yunes, 1992). The arrangement of carbon atoms in the graphitic structure is similar to that of pure graphite, so the true density of virgin activated carbon is almost the same with graphite. The linkage between graphite unit in the activated carbon is possible with strong cross linking(Li, Quinlivan, & Knappe, 2002). The interspace between those graphite units will form pore network and its size is usually in the range of

mesopore and macropore (Figure 2-2). The classification of pore size as recommended by IUPAC (Sing, 1985):

- Micropores,  $d < 2$  nm
- Mesopores,  $2 < d < 50$  nm
- Macropores,  $d > 50$  nm

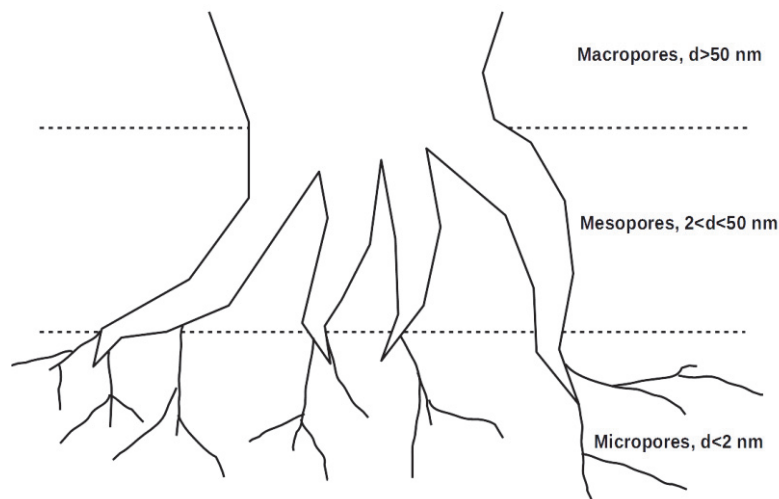


**Figure 2-2 Pore size classification in activated carbon**

Macropores are of little significance in terms of adsorption capacity but they act as transport pores to allow adsorbate molecules to diffuse from the bulk air phase into the particle interior. Micropores are generally slit-shaped. Because of their high dispersive force acting on adsorbate molecule. They provide space for storing most of VOC molecule, the mechanism of adsorption is via the process of volume filling in micropores (Ruthven, 1984). Mesopore can be treated as

a transient region between macropores and micropores. The typical characteristics of activated carbon are listed in Table 2-1(Do, 1998a).

**Table 2-1 Typical characteristics of activated carbon**

| <b>Characteristic</b>     | <b>Value</b>   |
|---------------------------|----------------|
| True density              | 2.2 g/cc       |
| Particle density          | 0.45~0.73 g/cc |
| Total porosity            | 0.4~0.71       |
| Mean macropore radius     | 800 nm         |
| Mean micropore half width | 1-2 nm         |
| Macropore porosity        | 0.31           |
| Micropore porosity        | 0.40           |

In engineering practice, cylindrically-shaped activated carbon pellets with a diameter of 3 or 4 mm are used for air cleaning applications, because they usually assure a relatively low pressure drop across the adsorbent bed. For different applications, different type of activated carbon



media with different physical properties (pore size distribution, porosity and particle shape) are used. (Table 2-2).

**Table 2-2 Activated carbon type for air cleaning (Henning, 2001)**

| <b>Adsorbent</b>              | <b>Applications</b>   | <b>Apparent density, g/cc</b> | <b>Pore volume, d&lt;20nm, ml/g</b> | <b>Pore volume, d&gt;20nm, ml/g</b> | <b>Specific surface area, m<sup>2</sup>/g</b> |
|-------------------------------|---|-------------------------------|-------------------------------------|-------------------------------------|---|
| Activated carbon, fine-pore   | Intake air and exhaust air cleanup, odor control, Adsorption of hydrocarbons<br>With low-boiling points | 0.4 – 0.5                     | 0.5 - 0.7                           | 0.3 - 0.5                           | 1000-1200                                     |
| Activated carbon, medium-pore | Solvent recovery, Adsorption of hydrocarbons with medium-high boiling points                            | 0.35 – 0.45                   | 0.4 - 0.6                           | 0.5 - 0.7                           | 1200-1400                                     |

|                             |  |           |           |           |           |
|-----------------------------|--|-----------|-----------|-----------|-----------|
| Activated carbon, wide-pore | Adsorption and recovery of hydrocarbons with high-boiling points | 0.3 – 0.4 | 0.3 - 0.5 | 0.5 - 1.1 | 1000-1500 |
|-----------------------------|--|-----------|-----------|-----------|-----------|

### 2.2.2 Mass transport in a sorbent bed

The adsorbent, e.g., activated carbon, is usually packed in a sorbent bed and the contaminated air is pushed through the sorbent media. When the contaminated air first enters the packed bed, most of the adsorbate is initially adsorbed near the inlet of the bed and the air passes on this region with little further adsorption occurring. When the zone near the inlet of the bed reaches saturation, adsorption takes place deeper downstream. According to the dynamics of the filtration process, three zones can be defined in the packed bed of gas filter (Figure 2-3): 1) the region near the inlet, where the sorbent has reached equilibrium; 2) the region in which the sorbent is partially equilibrium, which is also called mass transfer zone (MTZ) or wave front, and 3) the region near the outlet where the adsorbent remains clean. When the MTZ reaches the outlet, breakthrough occurs. Mathematically, breakthrough ratio in the adsorption process is defined as the ratio between the outlet concentration and inlet concentration. The outlet concentration continues to rise until it becomes the same as the inlet concentration, reaching

100% breakthrough. In applications, it is extremely important that the filter bed should be at least as long as the MTZ length of the component to be removed.

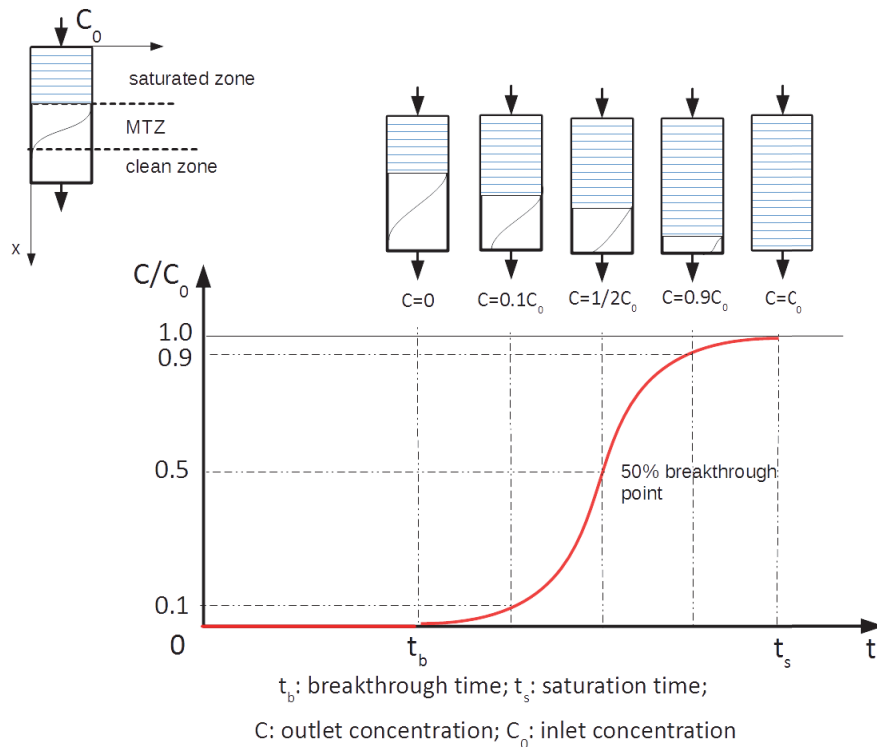


**Figure 2-3 Mass transfer zone (MTZ) and breakthrough curve**

The performance of packed bed is usually described through the concept of a breakthrough curve. As shown in Figure 2-3, a typical breakthrough curve is a plot of the concentration at the outlet with respect to time. Alternatively, it can be plotted in the dimensionless form by

normalizing the concentration with the inlet concentration,  $C/C_0$  (also called breakthrough ratio), so that the removal efficiency of sorbent bed,  $Er$ , can be defined as Eq. (2-1):

$$Er = \left( 1 - \frac{C}{C_0} \right) \times 100\% \quad (2-1)$$

The removal capacity,  $Cr$ , is defined as the ratio between the mass of adsorbed VOC and the mass of sorbent media, Eq. (2-2).

$$Cr = \frac{Q \cdot 0.001 \cdot \int_0^t (C_0(t) - C(t)) dt}{W} \times 100\% \quad (2-2)$$

Where  $Q$  is airflow rate through the media,  $m^3/h$ ;  $W$  is the mass of the media sample,  $mg$ ; and  $t$  is time,  $h$ .

Removal efficiency and removal capacity are often used together to describe the gas filter performance. A well-designed gas filter should have a high initial removal efficiency and maintain it as long as possible. Large removal capacity could indicate a long service life for a particular pollutant.

The breakthrough time and the shape of the curve are very important characteristics for determining the dynamic behavior of a sorbent column. The general characteristics of the breakthrough curve depends on the removal capacity of the column with respect to the inlet concentration and flow condition. Theoretically, the break-through curve would be a step function for favorable separations, i.e., there would be an instantaneous jump in the outlet concentration from zero to the feed concentration at the moment the column capacity is reached

(Goud, Mohanty, Rao, & Jayakumar, 2005). The slope of breakthrough depends on the overall mass transfer resistance in the packed bed, which requires a model to further understand.

To describe a gas-solid adsorption in packed-bed, it is necessary to divide it into four basic steps (Crittenden & Weber, 1978; K.-T. Liu & Weber Jr, 1981):

- a) Gas phase mass transfer including advection and molecular diffusion;
- b) Interface diffusion between gas phase and the exterior surface of the adsorbent (i.e., film diffusion)
- c) Intraparticle mass transfer involving pore diffusion and surface diffusion
- d) Adsorption-desorption reaction

➤ Gas phase mass transfer

The detailed structure of a porous medium is greatly irregular and just some statistical properties are known. An exact solution to characterize the flowing fluid through one of these structures is basically impossible. However, by the method of volume averaging, it is possible to obtain the mass balance equation in a porous sorbent bed (Delgado, 2006).

Molecules of VOCs in the packed bed can move in both axial and radial direction. For simplification, it is common to postulate that all cross-sections are homogeneous and the radial movement could be neglected (Mohan, Kannan, Upendra, Subha, & Kumar, 2009; Popescu, Blondeau, Jouandon, Costes, & Fanlo, 2013; Reguer, Sochard, Hort, & Platel, 2011; Xu et al., 2013). A macroscopic mass balance equation, Eq. (2-3), regarding a control volume as shown

in Figure 2-4 is essential to describe the mass transport process in the packed bed (Ruthven, 1984; Xu et al., 2013). Assumptions in this model are:

- the process is isothermal
- no chemical reaction occurs in the bed
- the particles are spherical and identical in size
- the bed is homogenous and the concentration gradient in radial direction of the bed is negligible

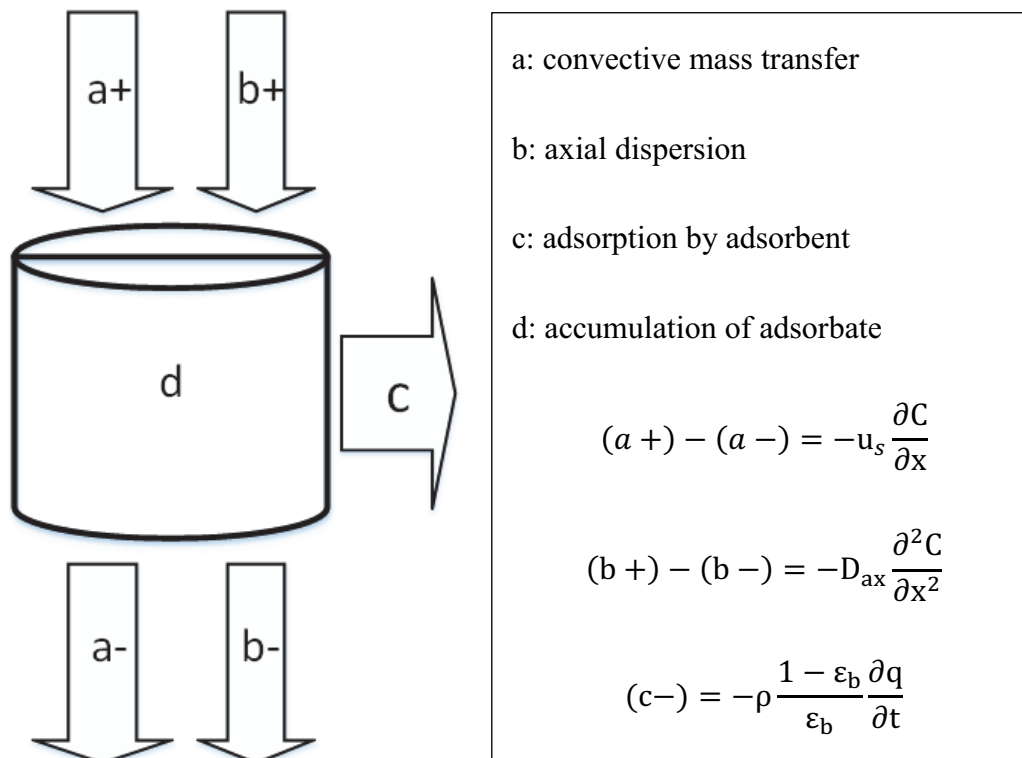


**Figure 2-4 Schematic diagram of mass balance of a control volume**

$$\frac{\partial C}{\partial t} = D_{ax} \frac{\partial^2 C}{\partial x^2} - u_s \frac{\partial C}{\partial x} - \rho \frac{1 - \epsilon_b}{\epsilon_b} \frac{\partial q}{\partial t} \quad (2-3)$$

Where the following initial and boundary conditions are used:

$$\begin{aligned}
C(x, t = 0) &= 0 \\
q(x, t = 0) &= 0 \\
C(x = 0, t > 0) &= C_{in} \\
\frac{\partial C}{\partial t}(x = L, t) &= 0
\end{aligned}
\tag{2-4}$$

Once the VOC molecules transfer from the bulk air into the voids between activated carbon particles, and then immigrate through the laminar film adjacent to the particle surface via convection, the mass flux penetrating the film is represented by the mass transfer coefficient,  $h_m$ ,

$$N = h_m(C - C^*) \tag{2-5}$$

Where  $N$  is the mass flux enter the activated carbon particle,  $C^*$  is the gas phase VOC concentration at the interphase.

Many studies have been done on the convective mass transfer coefficient in packed bed systems (Ranz & Marshall, 1952; Thoenes & Kramers, 1958; Wakao & Funazkri, 1978a). Experiments were designed to determine the heat and mass transfer coefficient in the spherical particle/packed bed systems. Table 2-3 shows a summary of the correlations which can be used for the determination of the mass transfer coefficient. Among these correlations, the Wakao and Funazkri correlation was derived by collecting the data from packed bed and limited to works that assume the particles in the bed (more than two layers) to be all active. The experiments involved in their research included the data of evaporation of water, evaporation of organic solvent, sublimation of naphthalene, diffusion-controlled reaction on particle surface



and dissolution of solid. The suggested application condition for the correlation is the cases with Reynolds number 3~10000(Wakao & Funazkri, 1978a).

**Table 2-3 Correlations for convective mass transfer coefficient**

| Correlation   | Condition   | Reference                 |
|---|---|---------------------------|
| $Sh = 2.0 + 0.6Re^{0.5}SC^{0.33}$   | NR  | (Ranz & Marshall, 1952)   |
| $Sh = 2.0 + 1.1Re^{0.6}SC^{1/3}$  | $3 < Re < 10000$  | (Wakao & Funazkri, 1978)  |
| $Sh = 2.4Re^{0.3}SC^{0.42}$   | $0.08 < Re < 125$<br>$150 < Sc < 1300$                  | (Williamson et al., 1963) |
| $Sh = 1.85 \left[ \frac{1 - \epsilon}{\epsilon} \right]^{1/3} Re^{1/3} SC^{1/3}$  | $Re \left[ \frac{\epsilon}{1 - \epsilon} \right] < 100$ | (kataoka et al., 1972)    |
| $Sh = \left( 2.0 + 0.644Re^{0.5}SC^{\frac{1}{3}} \right) [1 + 1.5(1 - \epsilon)]$ | NR  | (Chern & Huang, 1999)     |
| $Sh = \frac{0.325}{\epsilon Re^{0.36} SC^{1/3}}$                                  | NR  | (Ko et al., 2003)         |

\* Where  $Re = \frac{u_s d_p}{\nu}$ ,  $Sh = \frac{h_m d_p}{D_m}$ ,  $Sc = \frac{\nu}{D_m}$

\* NR: not reported

However, even from the same type of packing materials for which the mass transport correlations have been derived, this procedure usually introduces a potential error of approximately 20% (K.-T. Liu & Weber Jr, 1981). If the particle shape is irregular, the external mass transfer coefficient determined via experiments could be exerted a modified factor of two (Roberts, Cornel, & Summers, 1985). The present correlations usually have been summarized from the media that are significantly different in topographic properties from activated carbon particles and ion-exchange resins. It was demonstrated that the topography and roughness of an adsorbent is also an important factor relative to the operative mass transfer coefficient in fixed-bed (van Vliet & Weber Jr, 1981). Therefore, researchers developed alternative procedures that can determine the mass transfer coefficient via fitting the mechanistic model

from experimental data (Liu & Weber Jr, 1981; Pei & Zhang, 2010). The drawback of this method is that the system could have difficulty finding a true and unique set of mass transfer coefficient and intra-diffusion coefficient values if both external mass transfer and solid diffusion exert comparable rate-controlling resistance in the pack bed. Liu and Weber, 1981, concluded that it was found that for long column packed bed where the mass transfer wave front can be fully developed, the attempting to determine the mass transfer coefficient is difficult since both the film transfer and surface diffusion occur simultaneously along the entire range of the “S” shape breakthrough curve.

Following the mass transport through the adjacent film, the VOC molecules travel into the porous structure and eventually are adsorbed on the internal surface of the activated carbon. Since there is no flow motion inside the pore of particle, the mass transport is entirely contributed by diffusion. It is necessary to recognize these processes and use correct equations to quantify the internal diffusion resistance correspondingly. Generally, pore diffusion and surface diffusion are used to describe the entire intraparticle diffusion process.

➤ Pore diffusion

Diffusion in pores of activated carbon occurs through two process, molecular diffusion and Knudsen diffusion, depending on the pore size. Molecular diffusion, which results from collisions between molecules dominates in macropores. In other word, molecular diffusion prevails the mass transfer when the mean free path of the gas, which is defined as the average distance traveled by molecules between two consecutive molecular collisions, is small relative

to the pore diameter. The diffusion of any gas in carrier air is molecular diffusion, which can be represented by the diffusion coefficient (Nelson, 1992):

$$D_m = \frac{0.0043T^{\frac{3}{2}} \left( \frac{1}{M_1} + \frac{1}{M_2} \right)^{\frac{1}{2}}}{P\sigma_{12}^2} \quad (2-6)$$

Where T stands for the system temperature (K), M stands for molecular weight (g/mol), P is the pressure (atm) and  $\sigma$  is the collision diameter (m).

Knudsen diffusion happens between molecules and the pore wall when the mean free path is comparable with the pore diameter. As a rule of thumb, molecular diffusion prevails when the pore diameter is greater than 10 times of the mean free path. The value of the mean free path for air is  $2 \times 10^{-5}$  cm at 101.325 kPa and 300 K, and thus the Knudsen diffusion is usually the

dominant pore diffusion when the pore diameter is within the order of 50 nm (Do, 1998b).

Knudsen diffusion coefficient can be determined by equation (Ruthven, 1984):

$$D_k = 9700\lambda \left( \frac{T}{M} \right)^{1/2} \quad (2-7)$$

The mean pore radius  $\lambda$  (m) can be estimated with:

$$\lambda = \frac{2\varepsilon_p}{S_{bet}\rho_m} \quad (2-8)$$

Both molecular and Knudsen diffusion are involved in the intraparticle mass transport, so a compound diffusion coefficient, pore diffusion coefficient,  $D_p$  ( $m^2/s$ ), is defined as:

$$D_p = \frac{1}{\tau} \frac{1}{\frac{1}{D_m} + \frac{1}{D_k}} \quad (2-9)$$

Where  $\tau$  is the tortuosity (normally between 2~6) of the porous media that can be calculated by the equation (Mugge, Bosch, & Reith, 2001):

$$\tau = 1 + 0.5(1 - \varepsilon_p) \quad (2-10)$$

A general correlation for tortuosity shows that it increases with the decreasing pellet porosity (Ruthven, 1984).

#### ➤ Surface diffusion

When the VOC molecules are adsorbed on the surface of pores, they do not simply attach on the active sites. Another possibility of transport can drive the molecules to move along the surface, and hop between active sites. As a result, the surface diffusion coefficient,  $D_s$ , has a strong dependence on the surface concentration (or fractional surface coverage). Experimental measurement of the surface diffusion coefficient is not feasible because the gas phase diffusion

is always present in parallel. The limited literature and data for the surface diffusion coefficient may cause the neglecting of the surface diffusion in many models (Pei & Zhang, 2010; Xu et al., 2013). For gaseous systems, some researcher estimated the surface diffusion coefficient  $D_s$  is within a large range,  $10^{-17} \text{ m}^2/\text{s} \sim 10^{-7} \text{ m}^2/\text{s}$  (Tien, 1994). For physically adsorbed gas,  $D_s$  is typically in the order of  $10^{-7} \text{ m}^2/\text{s} \sim 10^{-9} \text{ m}^2/\text{s}$  (Treybal, 1980). In fact, it becomes dominant when both the surface area and the surface concentration are high. In commercial physical sorbent, both conditions are satisfied. For example, the surface diffusion contributes approximately 40%~80% of the total mass flux in the diffusion of methane, ethane and ethylene in activated carbon at 20 °C and pressure below 0.2 atm (Yang, 1988). An increase in the initial adsorbate concentration yields an increase in the surface diffusion coefficient. This may be attributed to a decrease in the adsorption forces for higher surface coverage (Vidic, Suidan, & Brenner, 1994). A strong dependence of surface diffusion on the concentration is more significant for the systems having higher affinity, except in the Henry's law region (Ruthven, 1984). At a high initial concentration, the surface diffusion coefficient exhibits its maximum value (when the slope of the Langmuir isotherm is close to zero).

In some cases, the effective diffusion coefficient, which is used to represent the overall intraparticle diffusion, combines all three diffusion mechanisms (Figure 2-5,  $D_p$  accounts for both molecular diffusion and Knudsen diffusion):

$$D_{app} = \frac{D_p}{K_{ma}} + D_s \quad (2-11)$$

Again,  $K_{ma}$  is the dimensionless partition coefficient. At low concentration region, the first term on the right-hand side is small compared with the  $D_s$  due to a large partition coefficient,

so that the effective diffusion coefficient is primarily contributed by the surface diffusion coefficient.

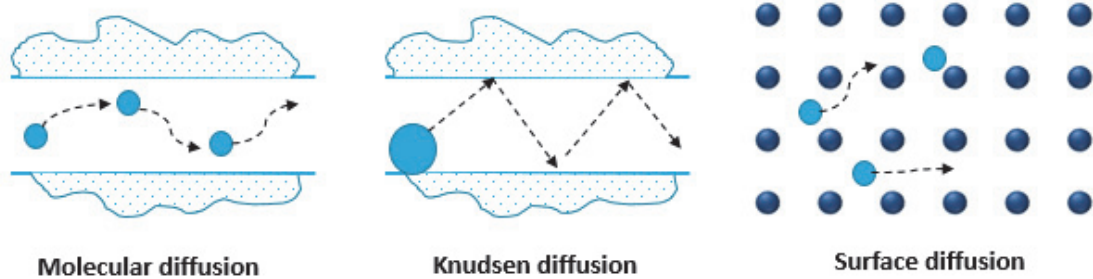


**Figure 2-5 Three diffusion mechanisms**

### 2.3 Experimental evaluation of filter media performance

Given the knowledge that the GAC filter could behave differently at high and low concentration levels, researchers have been investigating this topic in the very recent years. Some comparable research are listed in Table 2-4. Experiments with 100% breakthrough are very rare among these studies when the inlet concentration is below 100 ppb, which is the approximate level of typical indoor environment. It must be admitted that Table 2-4 is not an exhaustive list of relevant studies or test conditions. The properties of the test media and test conditions in these studies, are usually different from each other, hence developing an empirical correlation through literature review is very difficult. However, a common conclusion is reported that activated carbon indeed behave very differently at different concentration levels. The performance of the sorbent media obtained from high concentration standard test cannot

directly indicate in low concentration engineering applications in terms of removal efficiency and capacity.

**Table 2-4 Low concentration breakthrough test in previous studies**

| Reference  | Material-compound | Concentration, ppm |
|--|-------------------|--------------------|
| Seo, Kato, Ataka, & Chino, 2009  | AC, toluene       | 0.5, 0.8, 1, 1.6   |
| R.-T. Liu, 1990  | AC, heptane       | 118, 15, 2.7, 0.5  |
| Foster, Fuerman, Economy, Larson, & Rood, 1992                           | AC, toluene       | 95.8               |
| VanOsdell et al., 1996   | AC, toluene       | 0.5~100            |
| (Reguer et al., 2011)  | AC, toluene       | 0.47               |
| (Carratala-Abril, Lillo-Rodenas, Linares-Solano, & Cazorla-Amoros, 2009) | AC, toluene       | 200                |
| (Khazraei Vizhemehr et al., 2014)  | AC, MEK, Hexane   | 1~100 ppm          |

## 2.4 Modelling and simulation of sorbent bed

### 2.4.1 Empirical/semi-empirical model

In the application of packed-bed reactor, there are many empirical or semi-empirical equations proposed for modeling the breakthrough curves that characterize the performance of the sorbent bed (Table 2-5).

**Table 2-5 Summary of empirical breakthrough model**

| Model name   | Equation  | Parameters  | Assumptions   |
|--------------|---|---|---|
| Bohart-Adams | $\ln \frac{C_b}{C_{in}}$ $= k_{BA} C_{in} t - k_{BA} q \frac{L}{u}$ | <p><math>k_{BA}</math> is the kinetic constant (L/mg·min);</p> <p><math>q</math> is the saturation concentration(mg/L);</p> <p><math>L</math> is the bed depth (cm); and <math>u</math> is the flow velocity (cm/min)</p> | <p>Equilibrium is not instantaneous;</p> <p>Adsorption rate is proportional to the adsorption capacity which still remains on the sorbent.</p> <p>Adsorption rate is limited by the external mass transfer (Bohart &amp; Adams, 1920)</p> |



|               |   |   |  |
|---------------|---|---|--|
| <p>Thomas</p> | $\ln\left(\frac{C_{in}}{C_b} - 1\right)$ $= \frac{k_{Th}q_0M}{v}$ $- k_{Th}C_{in}t$ | <p><math>k_{Th}</math> is the Thomas rate constant (mL/mg·min);<br/> <math>q_0</math> is the equilibrium uptake per g of the adsorbent (mg/g)</p> | <p>The axial and radial dispersion are negligible.</p> <p>Adsorption is pseudo second order reaction which could reduce to a Langmuir isotherm at equilibrium.</p> <p>Intraparticle resistance is negligible (Dolphen, Sakkayawong, Thiravetyan, &amp; Nakbanpote, 2007; Rozada, Otero, Garcia, &amp; Moran, 2007)</p> |
|---------------|---|---|--|

|               |   |   |   |
|---------------|---|---|---|
| Yoon Nelson   | $t_b = \tau + \frac{\tau}{k_{YN}} \ln \frac{C_b}{C_{in} - C_b}$                                 | $k_{YN}$ is the rate constant ( $\text{min}^{-1}$ );<br>$\tau$ is 50% breakthrough time | The rate of decrease in the probability of adsorption is proportional to the coverage (Ayoob & Gupta, 2007) |
| Wheeler Jonas | $t_b = \frac{MC_{max}}{QC_i} - \frac{\rho C_{max}}{k_v C_i} \ln \left( \frac{C_i}{C_b} \right)$ | $k_v$ is the adsorption rate constant ( $\text{s}^{-1}$ )                               | Perfect plug flow;<br>Pseudo-first order;<br>(Lodewyckx, Wood, & Ryu, 2004)                                 |
| Clark         | $\ln \left( \frac{C_{in}^{n-1} - C_b^{n-1}}{C_b^{n-1}} \right) = \ln A - rt$                    | n is for Freundlich parameter; A and r are the constants of the model                   | Combined with Freundlich isotherm;<br>Piston flow type;<br>Absence of dispersion<br>(Hamdaoui, 2006).       |

Among these empirical models, the Yoon Nelson and Wheeler-Jonas equations have been most widely used for various adsorption system because of the simplicity and readily available macroscopic parameters. The other models require special knowledge of several parameters,

which are not easily achievable (Wood, 2001; Wu, Claesson, Fangmark, & Hammarstrom, 2005).

Since the dynamic adsorption is a very complicated process, even the most theoretically rigorous models are simplified representations of actual conditions. As an example, their inherent shortages to express the wall effect, the distribution of adsorbent particle of different size in the bed, non-homogenous surface-active sites, and the mass transfer caused by momentum and heat transfer are usually assumed to be either negligible or uniform. However, knowing the govern equations, one can still adjust individual phenomenological coefficient to optimize the value through mathematical fitting or consideration.

#### 2.4.2 Adsorption isotherm

Adsorption could be considered as the term for the enrichment of gaseous or dissolved substances on the boundary surface of a solid media (the adsorbent). The surface of the adsorbent has so-called active sites where the binding forces between the individual atoms of the solid structure are not completely saturated by neighboring atoms. These active sites can bind foreign molecules which, when bound, are referred to as adsorption. The adsorption capacity (also named removal capacity, adsorptive power, loading) of an adsorbent resulting from the pore size and structure of its inner surface for a defined gas compound is normally represented as a function of the component in the carrier gas for the equilibrium conditions at constant temperature. This is also known as the adsorption isotherm. One can find in literature

several models describing the process of adsorption. The adsorption isotherm equations proposed from dynamic sorption experiments have been summarized in Table 2-6.

**Table 2-6 Summary of adsorption isotherm**

| Isotherm                            | $C_s = f(C_p)$  | Parameters  |
|-------------------------------------|---|---|
| Linear                              | $C_s = K_{ma}C_p$   | $K_{ma}$ is the partition coefficient or Henry's constant   |
| Langmuir                            | $\frac{C_p}{C_{se}} = \frac{1}{C_{max}K_L} + \left(\frac{1}{C_{max}}\right)C_p$   | $C_{max}$ is the maximum adsorption capacity (mg/g) and $K_L$ is the affinity constant (m <sup>3</sup> /mg) |
| Freundlich                          | $\ln C_{se} = \ln K_f + \frac{1}{n}C_p$   | n is Freundlich exponent and $K_f$ is Freundlich constant   |
| Dubinin-Radushkevich (D-R)          | $C_{se} = C_{max} \exp \left\{ -D \left[ RT \ln \left( \frac{P_0}{P} \right) \right]^2 \right\}$  | D is the microporosity constant (mL/J)  |
| Brunmauer, Emmett, and Teller (BET) | $\frac{\left(\frac{P_0}{P}\right)}{C_{se} \left(1 - \frac{P_0}{P}\right)} = \frac{1}{cC_s^*} + \frac{c-1}{cC_s^*} \left(\frac{P_0}{P}\right)$ | C is dimensionless constant; $C_s^*$ is the capacity required to form a monolayer of the adsorbate (mg/g)   |

Note:

$C_p$  is the equilibrium air phase concentration in the pores of sorbent ( $\text{mg}/\text{m}^3$ );

$C_{se}$  is the equilibrium adsorbate concentration in solid phase ( $\text{mg}/\text{g}$  solid);

$R$  is the gas constant ( $8.314 \text{ J}/(\text{mole K})$ );

$T$  is the operation temperature of the system ( $\text{K}$ );

$P_0$  is the sorbate saturation vapor pressure at temperature  $T$ ;

$P$  is the partial pressure of the sorbate in the gas

To further illustrate the adsorption isotherm, some of the typical adsorption isotherm profiles are presented in Figure 2-6.

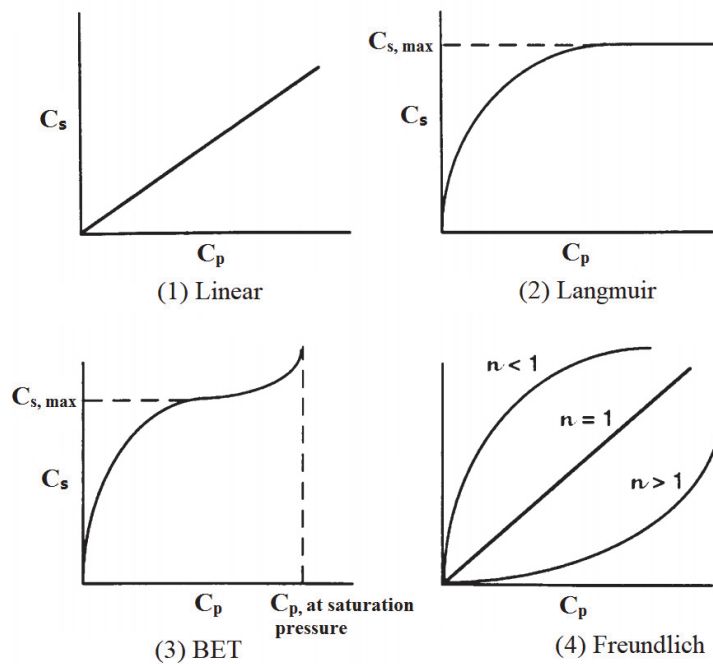


**Figure 2-6 Typical adsorption isotherm**

The linear adsorption is the simplest adsorption isotherm and is a special case for adsorption using Henry's law to define the discontinuity in concentration at two phase interfaces.

According to Henry's law at a constant temperature, the amount of a given gas that dissolves in a given type and volume of adsorbent is directly proportional to the concentration of that gas in equilibrium with the adsorbent. Thus, the partition coefficient,  $K_{ma}$ , is the same as the linear adsorption isotherm constant, Eq. (2-12).

$$K_{ma} = \frac{C_s}{C_p} \quad (2-12)$$

The linear adsorption isotherm coefficient could be found experimentally for each pair of adsorbate and adsorbent system. Figure 2-7 (Pei & Zhang, 2012) plots the adsorption isotherm at low concentration based on other researchers' data (Seo et al., 2009). This finding is very important because the majority of indoor VOCs present the concentrations below this limit.

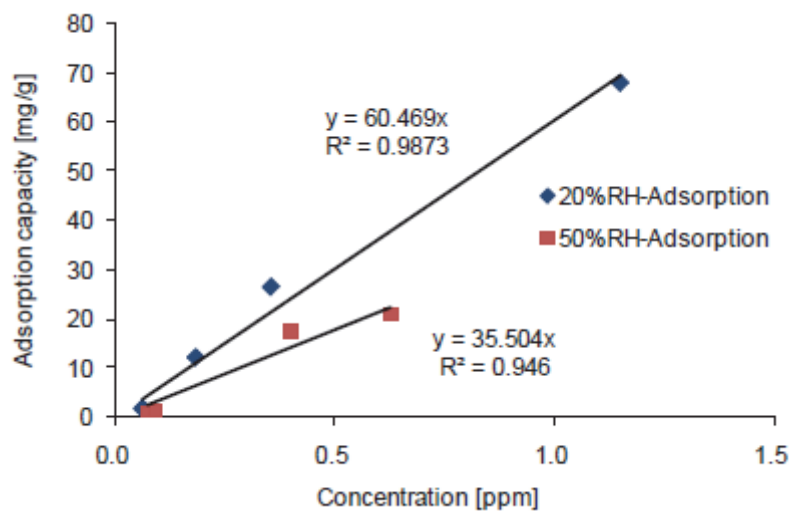


**Figure 2-7 Linearity of adsorption isotherm at low concentration (Pei & Zhang, 2012)**

Figure 2-7 demonstrated that the adsorption isotherm is very close to linear relation at very low concentration (lower than 1.5 ppm), but what is the upper limit concentration of the linear

isotherm? One guideline is 1 mg/m<sup>3</sup> (265 ppb) of toluene-activated carbon system which is recommended by (Seo et al., 2009).

Besides linear adsorption isotherm, Langmuir isotherm is widely used in physical adsorption process. The Langmuir adsorption isotherm can be applied under five assumptions: 1) ideal gas, 2) monolayer adsorption, 3) homogenous surface with the same affinity for all the active sites, 4) no interaction between adsorbed molecules and 5) localized stationary adsorbed gas molecules. The equation for Langmuir adsorption can be summarized as Eq. (2-13).

$$C_{se} = \frac{C_{max} K_L C_p}{1 + K_L C_p} \quad (2-13)$$

$K_L$  is a constant at a given temperature. This correlation converges to a limiting amount of adsorption capacity for high levels of gas concentration and reduces to the linear adsorption isotherm for low concentration levels. Langmuir adsorption isotherm can be applied for both physical adsorption and chemisorption.

Freundlich isotherm is an empirical model which can be simply described using Eq.(2-14)

$$C_s = K_F C_p^{1/n} \quad (2-14)$$

Where  $K_F$  and  $n$  are Freundlich parameters,  $n$  is usually larger than 1 and  $K_F$  is temperature dependent. Larger  $n$  indicates more nonlinear isotherm. A poor fit is often found at low concentration since it does not conform to Henry's law as one would expect according to the kinetic theory at low concentration region. Activated carbon generally have isotherm that obey the Freundlich model in the middle range of partial pressure, with less agreement at high pressures (Rouquerol, Rouquerol, Llewellyn, Maurin, & Sing, 2013).

The BET adsorption isotherm was developed by Brunauer, Emmett and Teller in 1938. They assume that the molecules adsorbed in the first layer on the carbon surface provide available sites for the second and subsequent layers. Molecules which are not in the first layer cannot



contact the surface of carbon atoms, therefore they act as saturated liquid with a different equilibrium constant from the first layer.

Axley (1994) stated that for sorption of air contaminant in building materials, Langmuir and linear isotherm are the most appropriate choices. For sorption of any gas phase contaminants in GAC, if its concentration is within one order of magnitude of its saturated value, the BET model should be applied. Freundlich and D-R isotherm are used for industrial sorbent which show a nonlinear equilibrium behavior (Axley, 1994). It has not been concluded that if the adsorption isotherm for low concentration region could be extrapolated linearly, especially when the equilibrium sorption capacities are determined at relative high concentration. For ~ppb level concentration in which performing the breakthrough tests is extremely difficult due to high demands of instrumentation and experimental time, so the most appropriate adsorption isotherm for ppb level has not been concluded.

### 2.4.3 Mechanistic model

Besides these empirical models, a number of mechanistic model based on the mass transfer principle in the packed bed system have been developed over decades in literatures (Ko, Porter, & McKay, 2003; K.-T. Liu & Weber Jr, 1981; Pei & Zhang, 2010; Popescu et al., 2013; Xu et al., 2013). Generally, three equations are derived from mass balance for the solid and gas phase, including the gas phase mass balance in the bed, solid phase mass balance in the equivalent spherical particle and adsorption isotherm at the gas-solid interface. The gas phase mass balance equation (bed equation), which is essentially the same in all the literature, has been

introduced in section 2.2.2. Considering the diffusion process inside the particle, three models with different degree of simplifications are summarized from literatures.

1) Homogeneous surface diffusion model (HSDM)

In the HSDM model, porous media is considered as pseudo-homogenous media and the resistance in the micropores is dominant. The concentration through the particle is essentially uniform, and the sorption rate should not depend on the size of particle (Ruthven, 1984). It is assumed that the contaminant adsorb at the external surface of the particles and then diffuse within the particles (Richard, Núñez, & Schweich, 2010). The basic mathematic for HSDM model is (Tien, 1994):

$$\frac{\partial C_s}{\partial t} = \frac{D_e}{r^2} \frac{\partial}{\partial r} \left( r^2 \frac{\partial C_s}{\partial r} \right) \quad (2-15)$$

With the initial and boundary conditions as

$$C_s = 0, \text{ at } t = 0$$

$$D_e \frac{\partial C_s(r_p, t)}{\partial r} = h_m (C_b - C_p), \text{ at } r = r_p$$

$$\frac{\partial C_s}{\partial t} = 0, \text{ at } r = 0$$

Note that a constant diffusion coefficient is considered. In fact, the effective or apparent diffusion coefficient,  $D_e$ , in HSDM is a lumped parameter but mainly contributed by surface diffusion coefficient as discussed in section 2.2.2.

2) Pore diffusion model (PDM)

In some cases, the macropore resistance is considered as supreme, there will be a concentration profile through the macroparticle, and the adsorption rate will depend on the particle size. To derive an expression for PDM model, it is assumed that a local equilibrium presents between

the adsorbed phase and the gas phase within the macropore at any specified radial position. This model describes that the VOC molecules diffuses through the pores of particle and then adsorbs on the internal surface of particle (pore wall)(Richard et al., 2010).

$$\frac{\partial C_p}{\partial t} + \frac{1-\varepsilon_p}{\varepsilon_p} \frac{\partial C_s}{\partial t} = \frac{D_e}{r^2} \frac{\partial}{\partial r} \left( r^2 \frac{\partial C_p}{\partial r} \right) \quad (2-16)$$

With the initial and boundary conditions

$$C_s = C_p = 0, \text{ at } t = 0$$

$$D_p \frac{\partial C_p(r_p, t)}{\partial r} = h_m(C_b - C_p), \text{ at } r = r_p$$

$$\frac{\partial C_s}{\partial t} = \frac{\partial C_p}{\partial t} = 0, \text{ at } r = 0$$

The diffusivity in the HSDM is based on the solid phase concentration gradient, and the diffusivity of PDM system is the effective pore diffusion. When the adsorption rate is linear, the two models can lead to an identical breakthrough curve due to the essentially the same mathematical expression (Weber & Chakravorti, 1974; Yang, 1988).

### 3) Pore surface diffusion model (PSDM)

We cannot ignore the possibility that the macropore and micropore diffusion are of similar order of magnitude. The PSDM combined HSDM and PDM models by assuming the pore diffusion and surface diffusion occur in parallel simultaneously. However, in most of the

studies, the PSDM model was ultimately reduced to HSDM or PDM model when one of the diffusion mechanism is dominating the process (Noll, 1991; Yu, Peldszus, & Huck, 2009).

$$\varepsilon_p \frac{\partial C_p}{\partial t} + (1 - \varepsilon_p) \frac{\partial C_s}{\partial t} = \varepsilon_p \frac{D_p}{r^2} \frac{\partial}{\partial r} \left( r^2 \frac{\partial C_p}{\partial r} \right) + (1 - \varepsilon_p) \frac{D_s}{r^2} \frac{\partial}{\partial r} \left( r^2 \frac{\partial C_s}{\partial r} \right) \quad (2-17)$$

Boundary and initial conditions are:

$$C_s = C_p = 0, \text{ at } t = 0$$

$$\varepsilon_p D_p \frac{\partial C_p(r_p, t)}{\partial r} + (1 - \varepsilon_p) D_s \frac{\partial C_s(r_p, t)}{\partial r} = h_m (C_b - C_p), \text{ at } r = r_p$$

$$\frac{\partial C_s}{\partial t} = \frac{\partial C_p}{\partial t} = 0, \text{ at } r = 0$$

The schematics of these three different models are presented in Figure 2-8, where  $C_b$  stands for the gas phase concentration in bulk air.

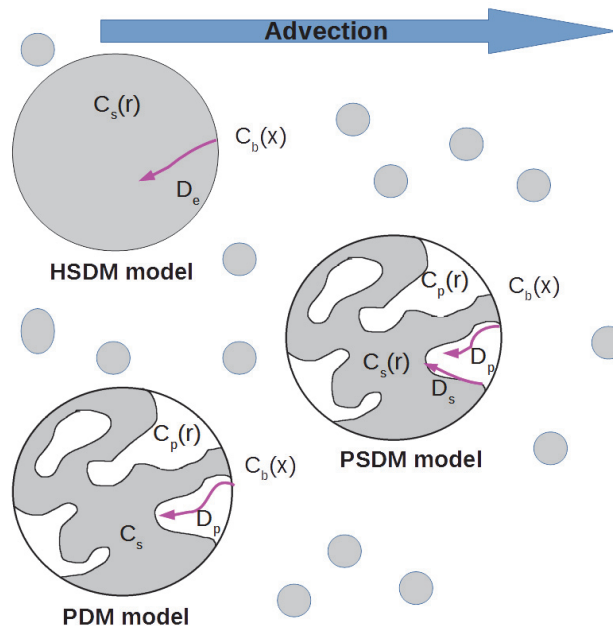


**Figure 2-8 Illustration of different adsorption model in packed bed**

## 2.5 Major findings

Testing sorbent bed filter at typical indoor air concentrations requires too much time which would be expensive and difficult for routine tests (Han, Guo, Pei, & Zhang, 2012; He et al., 2014; VanOsdell, Owen, Jaffe, & Sparks, 1996). Therefore, most of the tests were performed at high concentration which does not correspond to the concentration detected in indoor environment. Even though several studies reported the performance of activated carbon at relative low concentrations, but the media used and test conditions are not identical. Thus, little information is available about the performance of sorbent media to establish a correlation the performance at high and low concentration levels.

There are many studies regarding the influential factors on the performance of activated carbon filter, such as temperature, flow rate, relative humidity and pellet size, however not many tests were conducted to address the concentration effects on the adsorption performance.

Many models have been developed for predicting the performance of gaseous filter, however, no specific methodology has been demonstrated for differentiating the performance at high and low concentration levels. None of these predicting models have been validated at typical indoor concentration level (<100 ppb).

# 3 EXPERIMENTAL INVESTIGATION

## 3.1 Introduction

In order to understand the effects of concentration on the activated carbon packed-bed, a series of experiments were carried out at different concentration levels. In this chapter, the test system,

methodology, and materials are introduced, and then the results regarding the effects of concentration are discussed.

### 3.2 Test system and method

An air-cleaning technology test system (ACTTS, Figure 3-1) was used in this study. The main components of ACTTs are illustrated as a schematic diagram in Figure 3-2.

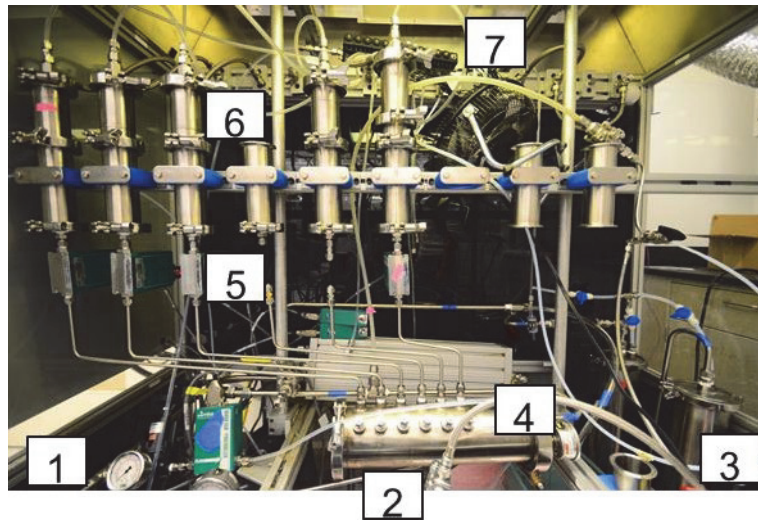


**Figure 3-1 Air-cleaning technology test system**

Where 1-pressurized supply air; 2-VOC generator; 3-humidifier; 4-mixing manifold; 5-mass flow controller; 6-test column; 7-switching valve.

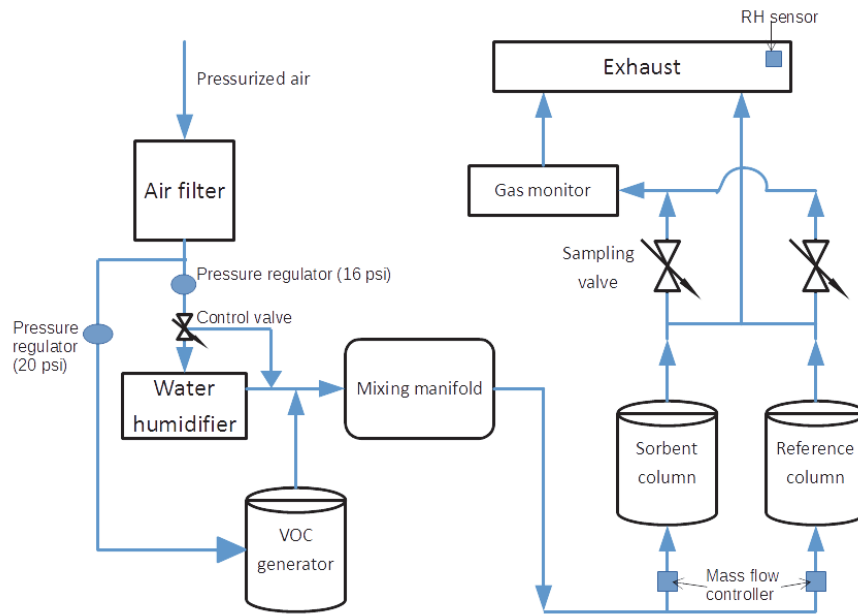


**Figure 3-2 Schematic of ACTTS system**

The ACTTS resides in a temperature-controlled enclosure that is maintained at a negative pressure to prevent any contamination to the lab space in case of any system leaks. The ACTTS has maximum of 8 channels, and only 4 channels were used for concurrent testing of different sorbent media with a single type of challenge VOC in this study. All the channels (test columns) were challenged by precisely the same inlet concentration (Guo et al., 2006). The system uses compressed and purified air supplied by the lab, which can be split into two flows. One is primary flow (with pressure controlled at 16 psi for supplying enough flow to all the channels), and the other is for the VOC generator (with pressure controlled at 20 psi). Air is directed by a three-way valve to achieve the appropriate flow rate between the water impinger and bypass line using a PID (proportional–integral–derivative) controller that takes signals from a humidity sensor located at the exhaust manifold of the system at the very end. The primary flow is then passed to a heat exchanger for stabilizing the air temperature to the desired setpoint and as a volumetric storage vessel, which provides thermally conditioned air to merge with the



VOC generation air. Each channel consists of a mass flow controller, specimen holder (test column), and a sampling valve along the flow direction. The mass flow controller controls the flow rate at a specific value between 0~30 LPM of the VOC mixed air through the test column. The controlled flow passes through the test column, a sampling T-connector, and the exhaust manifold. The sampling air flow are taken from the T-connector of each channel and connected to a row of switching valve. The valves are programmed to switch between each channel at a specified interval (5 minutes in this study), allowing the measurement device to sample the air from each T-connector in a certain sequence. Moreover, an additional valve has been added to provide a clean-air purge for the common sampling line and the measurement device. The purge occurs between sampling of adjacent channels. The measurement device (e.g., ppbRAE model 3000) is linked to the sample port from the row of switching valves. The measurement device has a sampling pump that operates continuously and measures the VOC concentrations at a certain time interval. A typical sampling sequence is programmed as follow.

- 1) Open the purge valve for channel 1 and close the other valves; the purge time lasts for a pre-selected time interval (e.g., 5 min).
- 2) Open the sampling valve for channel 1 and close the remaining valves; the sampling time lasts for a pre-selected time interval (e.g., 5 min)
- 3) Open the purge valve for channel 2 and close the other valves; the purge time lasts for a pre-selected time interval (e.g., 5 min).
- 4) Open the sampling valve for channel 2 and close all other valves; the sampling time lasts for a pre-selected time interval (e.g., 5 min)
- 5) Continue for all the 4 channels and loop back; repeat the procedure 1) and 2) for each channel until the completion of the test.

The entire ACTTS is constructed of stainless steel to avoid the undesired sorption effect by the wall of tubes and chambers. The sorbent media to be tested was carefully packed in an

ASHRAE standard 145.1 test column as shown in Figure 3-3. The length of sorbent bed,  $L$ , is packed as 1 inch in the standard, but it was changed to 1 cm and 3 mm in some of the tests in this study. Metal mesh and permeable pad were installed at the two ends of the sorbent bed to prevent the pellets from being blown out. The weight of the sorbent bed was measured before and after packing to determine the total amount of medium in the test specimen.

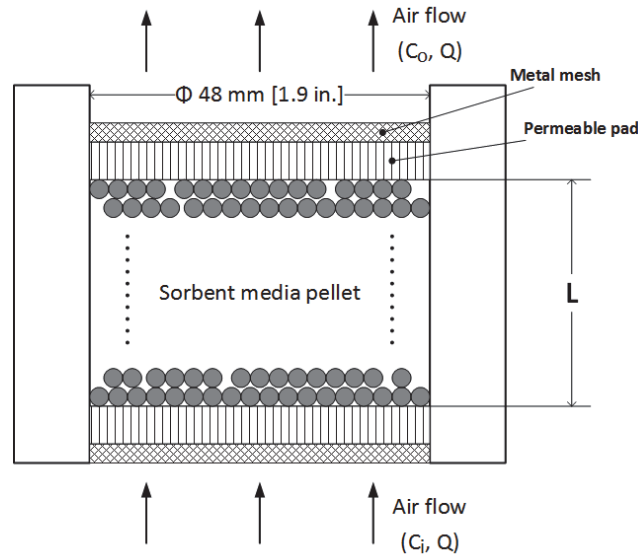


**Figure 3-3 Schematic of test column**

A VOC generation device was integrated in the ACTTS. There are two methods applied for VOC generation: bubbling method for high concentration VOC generation and heating permeation tube for low concentration VOC generation. A continuous VOC monitor for real-time measurement, ppbRAE model 3000, is selected for the air sampling. This VOC monitor uses photo-ionization detector (PID) technology. Air samples are continuously drawn in front of an ultraviolet lamp, which ionizes the VOC molecules to positive and negative ions, which are counted by the detector. The drawback of PID sensor which needs to be concerned is that the selectivity of VOCs when multi-compound exists, but the primary flow is pre-filtered where

moisture, particles (larger than 0.3 micron) and TVOCs (background concentration < 10 ppb) are removed.

### 3.3 Test material

Two virgin activated carbon were selected for tests: activated carbon OVC 4×8 (labeled as M#1) and AP4-60 (labeled as M#2), both from Calgon Carbon Corp (Figure 3-4). The

specifications are summarized in Table 3-1. M#1 has an irregular flat shape and M#2 is very close to a cylindrical shape.

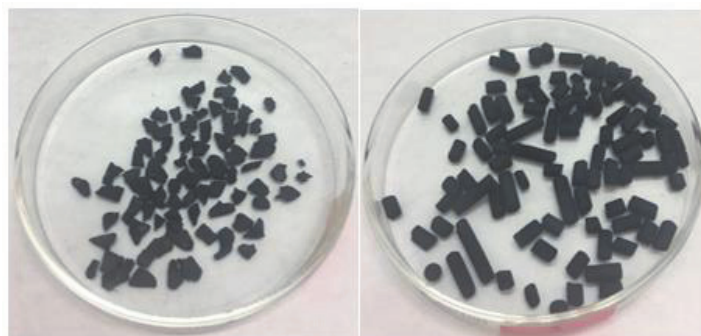


**Figure 3-4 Activated carbon M#1 (left) and M#2 (right)**

**Table 3-1 Test media**

| Media ID                                   | M#1                                  | M#2                               |
|--|--------------------------------------|-----------------------------------|
| Material                                   | Coconut base virgin activated carbon | Coal base virgin activated carbon |
| Shape                                      | Flat shell                           | Cylindrical pellet                |
| Size                                       | 4.75×2.36mm<br>(4×8 mesh)            | 4 mm pellet diameter              |
| Apparent density*                          | 0.45 g/cc                            | 0.49 g/cc                         |
| Porosity*                                  | 0.3                                  | 0.4                               |
| Target compounds specified by manufacturer | Toluene, O3                          | Toluene, O3                       |
| Type                                       | Physical sorbent                     | Physical sorbent                  |

\*Measured by the manufactures

Toluene is color-less, water insoluble and is commonly found in the indoor environment due to nail polish, paints, lacquers, rust inhibitor, adhesives and solvent based cleaning agents. Low

to moderate exposure to toluene can cause tiredness, weakness, drunken-type action, memory loss and hearing and color vision loss. A continuum of neurotoxic effects ranging from brain damage to degraded performance on psychometric tests has been observed. However, toluene is much less toxic than benzene which has similar molecular structure. Therefore, toluene has been widely used as a reference compound for total volatile organic compounds (TVOCs) in many studies. The vapor pressure of toluene is 22 mmHg at 20 °C and the boiling point is 111 °C. In this study, toluene is selected as the challenge gas to investigate the concentration effect of physical adsorption in the activated carbon filter/bed.

### 3.4 Test condition

Two series of experiments were performed to evaluate the performance of activated carbon packed bed at different concentrations, labeled as Test A and Test B. In the Test A series, the experiments were carried out following the ASHRAE standard 145.1 test conditions, but adding a 50 ppb inlet concentration test to investigate the sorbent media performance at typical indoor concentration. For Test B series, the sorbent bed length, L, was reduced to 1 cm from 2.54 cm (1 inch) to shorten the test period. The inlet concentration levels in Test B were

expanded to 4 different concentration levels. The test conditions were summarized in Table 3-2.

**Table 3-2 Test conditions**

| Parameter                      | Value   |      |         |   |     |     |
|--------------------------------|---------|------|---------|---|-----|-----|
|                                | Test A  |      | Test B  |   |     |     |
| Media bed depth, mm            | 25.4    |      | 10      |   |     |     |
| Test column diameter, mm       | 48      |      | 48      |   |     |     |
| Pellet diameter, mm            | 2~4     |      | 0.8~1   |   |     |     |
| Airflow rate m <sup>3</sup> /s | 4.72E-4 |      | 4.72E-4 |   |     |     |
| Residence time, s              | 0.1     |      | 0.039   |   |     |     |
| Temperature, °C                | 23±1    |      | 23±1    |   |     |     |
| RH, %                          | 47±5    |      | 33±5    |   |     |     |
| Inlet Concentration, ppm       | 100     | 0.05 | 50      | 5 | 0.5 | 0.1 |

It should not be overlooked that the pellet size in Test A and Test B are different. The pellets used in Test B are grounded by a grinding tool set shown in Figure 3-5, a. All the pellets are sieved through 0.8~1 mm mesh (Figure 3-5, b) before being packed into the test column to ensure a relative uniform pellet size. The grounded pellets are shown in Figure 3-5, c. The shape of the pellet is close to irregular particles after manual grinding and some smaller pellets still exist in the bulk material. These uncertainties may introduce some error to the mass transfer coefficient and total surface area estimations due to the complexity of sorbent bed structure. The influence will be discussed in Chapter 5. The purpose of grinding the pellet is to have at

least three layers of pellets in the test column so that the sorbent bed can maintain a good uniformity and the direct by-pass could be avoided. The sorbent bed structure is more uniform while the sorbent bed length is 10 times larger than the particle size.

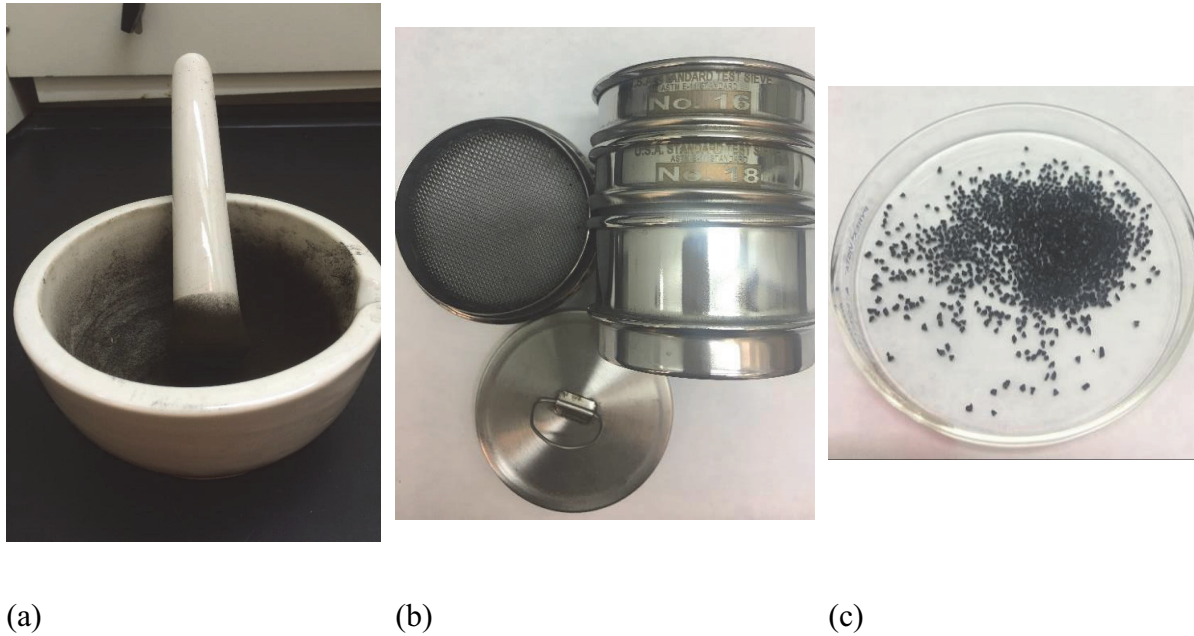


**Figure 3-5 Grinding tool set (a), sieving tool set (b) and ground pellet (c)**

### 3.5 Results and discussions

Figure 3-6 and Figure 3-7 show the results of Test A, which is the ASHRAE standard tests for M#1 and M#2 at high (107 ppm) and low (66 ppb) concentrations, respectively. For high concentration tests, as shown in Figure 3-6, M#1 has the longest service life in terms of 50% breakthrough time. In addition, M#2 shows a relatively high (~23%) initial breakthrough. This phenomenon is possibly caused by this large pellet size and shape of M#2. The bigger bed porosity could generate a “by-pass” effect due to the large pellet. In other words, not all the pollutants may have a chance to contact the media surface. Another probable reason is that the

internal diffusion becomes a controlling factor and takes a relative long time, so that the pollutant molecules cannot access the internal surface before exiting the sorbent bed.

Test results also indicate that the relative performance of these media at high and low concentrations could generally remain the same when comparing Figure 3-6 and Figure 3-7. The order of overall removal capacity and removal efficiency of M#1 and M#2 are consistent between high and low concentration tests. This conclusion can be further supported in previous work where more types of media were tested (He et al., 2014). Despite the consistency of relative performance, some differences are very interesting to note. Under low concentration, M#2 showed a breakthrough from 0 ppb instead of 23% initial breakthrough at high concentration since the concentration gradient under low concentration is much lower than that under high concentration. The direct by-pass seems less possible under the low concentration



condition (no initial breakthrough). Further explanation will be given in Chapter 4 from mechanistic modeling point of views.

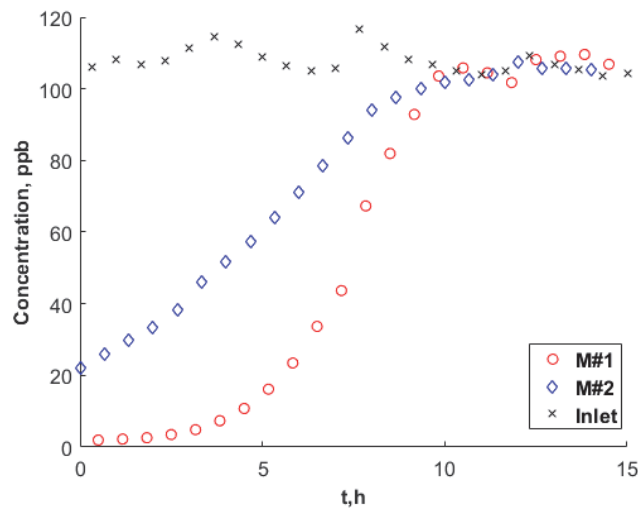


**Figure 3-6 Breakthrough curve of toluene,  $C_{in}=107\pm 3.4$  ppm, Test A**

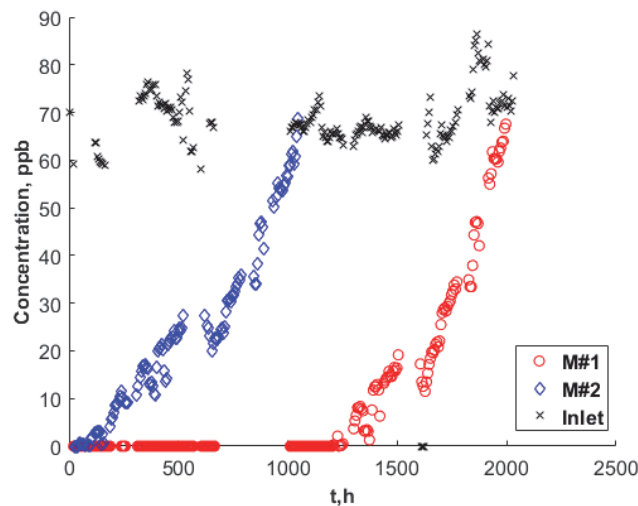


**Figure 3-7 Breakthrough curve of toluene,  $C_{in}=66.8\pm 8$  ppb, Test A**

The results of Test B at four different concentration levels such as 50 ppm, 5 ppm, 500 ppb and 100 ppb are presented in Figure 3-8, Figure 3-9, Figure 3-10 and Figure 3-11, respectively. Since the sorbent bed length is shorter than the ASHRAE 145.1 standard test (1 cm vs. 2.54 cm), the test period is significantly reduced for the Test B series. M#1 still has better overall

performance than M#2 regarding removal capacity and half breakthrough time. The difference is more obvious at lower concentration levels. It is worthy to mention that the inlet concentration in 5 ppm test (Figure 3-9) was not well-controlled due to the facility limitations. In the current ACTTS, the permeation tubes could not generate such high concentration of toluene at 100 °C which was already the maximum heating capacity due to safety consideration. Consequently, the 5 ppm challenge level was generated with bubbling method, which was difficult to maintain stable and last for long enough when the liquid level in the VOC generator became low. Practically, variable inlet concentration is closer to the real indoor application. It is still meaningful and interesting to present the data. Even though the very result cannot fully

represent the performance of M#1 and M#2 at a constant 5 ppm inlet concentration, they clearly state the differences in performance between the two media.

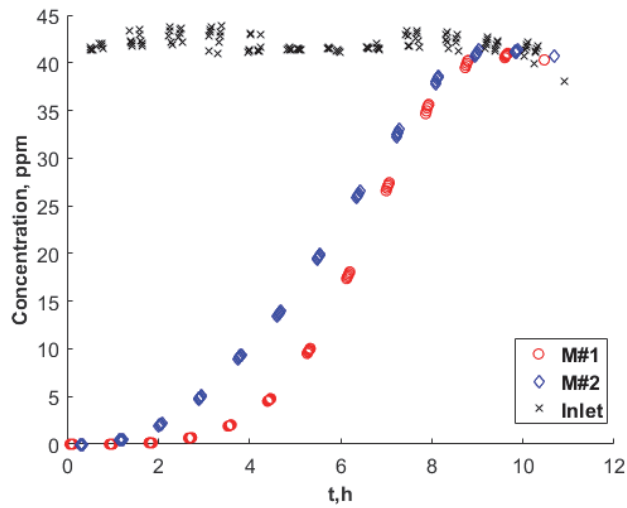


Figure 3-8 Breakthrough curve of toluene,  $C_{in}=50$  ppm ( $42\pm 0.8$  ppm), Test B

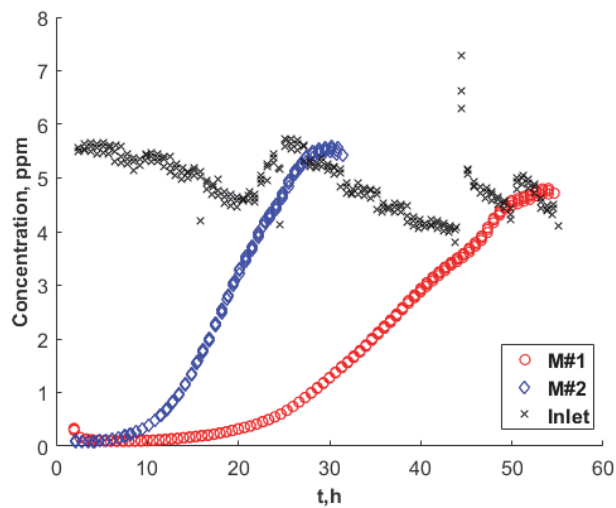
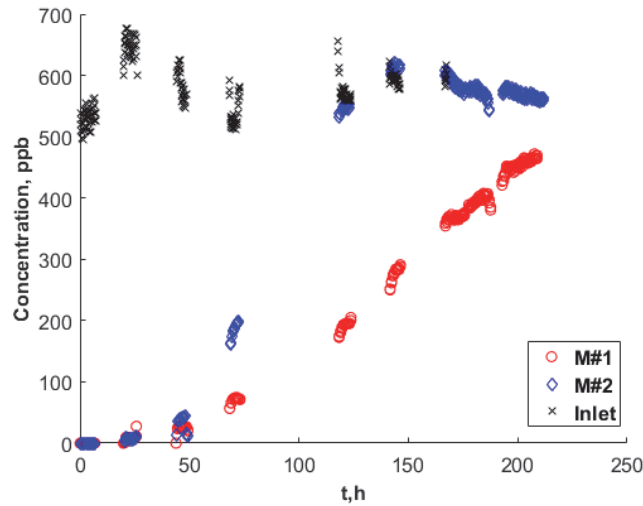
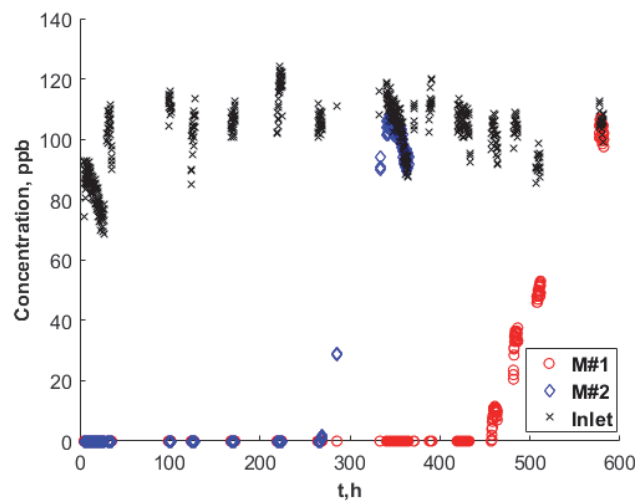


Figure 3-9 Breakthrough curve of toluene,  $C_{in}=5$  ppm ( $5\pm 0.37$  ppm), Test B



**Figure 3-10 Breakthrough of toluene,  $C_{in}=500$  ppb ( $563\pm 32.6$  ppb), Test B**



**Figure 3-11 Breakthrough curve of toluene,  $C_{in}=100$  ppb ( $103\pm 6.0$  ppb), Test B**

Even though the sorbent bed length and pellet size of Test B are different from Test A, the physical properties at microscale such as internal diffusion and adsorption should not be impacted. With the performance data of selected activated carbon at total 6 different concentration levels, the estimation of the correlation between the inlet concentration and partition coefficient becomes possible.

Apparently, the total adsorbed mass, or namely, removal capacity, in the activated carbon under different concentration levels is very different. The correlation between the partition coefficient

and inlet concentration is also very significant for characterizing the adsorption behavior of certain sorbent/VOC combination. The partition coefficient is linearly correlated to the removal

capacity which can be determined by integrating the breakthrough curve with respect to elapsed time. The partition coefficient  $K_{ma}$  is defined as Eqn. (3-1).

$$K_{ma} = \frac{Cr \cdot \rho_{true}}{C_{in}} \quad (3-1)$$

Where removal capacity, Cr (mg/mg), can be obtained via Eqn. (2-2) in the previous chapter.

The removal capacity and partition coefficients of all the pervious experiments (Test A and Test B) are listed in Table 3-3.

**Table 3-3 Summary of the removal capacity and partition coefficient at different concentration levels**

| Concentration level                 | M#1              |                       | M#2              |                       |
|-------------------------------------|------------------|-----------------------|------------------|-----------------------|
|                                     | Removal capacity | Partition coefficient | Removal capacity | Partition coefficient |
| 66 ppb (2.51e-7 mg/m <sup>3</sup> ) | 0.0388           | 1.83E+08              | 0.0143           | 70000000              |
| 100 ppb (3.8e-7 mg/m <sup>3</sup> ) | 0.0431           | 1.04E+08              | 0.0286           | 68400000              |
| 500 ppb(1.9e-4 mg/m <sup>3</sup> )  | 0.0718           | 2.85E+07              | 0.0403           | 1.90E+07              |
| 5 ppm (1.9e-3 mg/m <sup>3</sup> )   | 0.159            | 7.60E+06              | 0.0741           | 3.20E+06              |
| 42 ppm (1.6e-2 mg/m <sup>3</sup> )  | 0.222            | 1.39E+06              | 0.2268           | 1.18E+06              |
| 100 ppm (3.8e-2 mg/m <sup>3</sup> ) | 0.25             | 4.80E+05              | 0.13             | 3.70E+05              |

At very high concentration level, the partition coefficients of M#1 and M#2 are relative small and have little changes with increasing concentrations. When the concentration decreases below 5 ppm in this study, the partition coefficient rises dramatically. A generic correlation following power-law between partition coefficient and inlet concentration is proposed and

determined from the tests as shown in Figure 3-12. For better visualization purpose, the curve was converted into log-log scale as Figure 3-13.

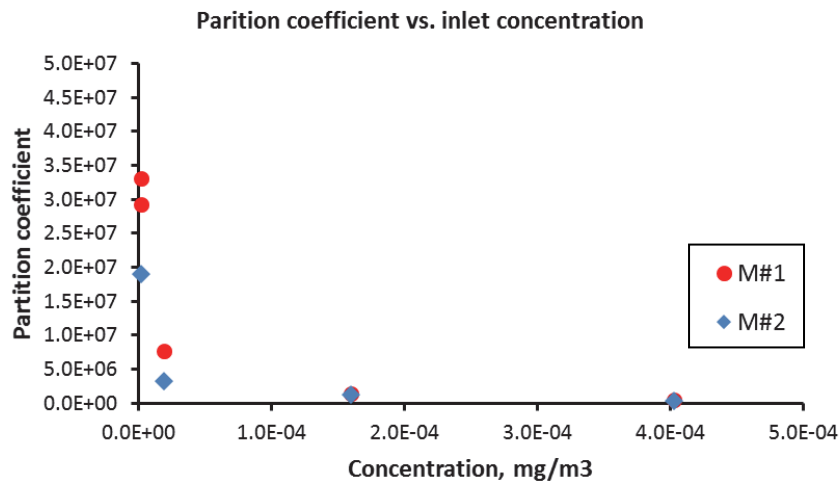


**Figure 3-12 Correlation of partition coefficient and inlet concentration**

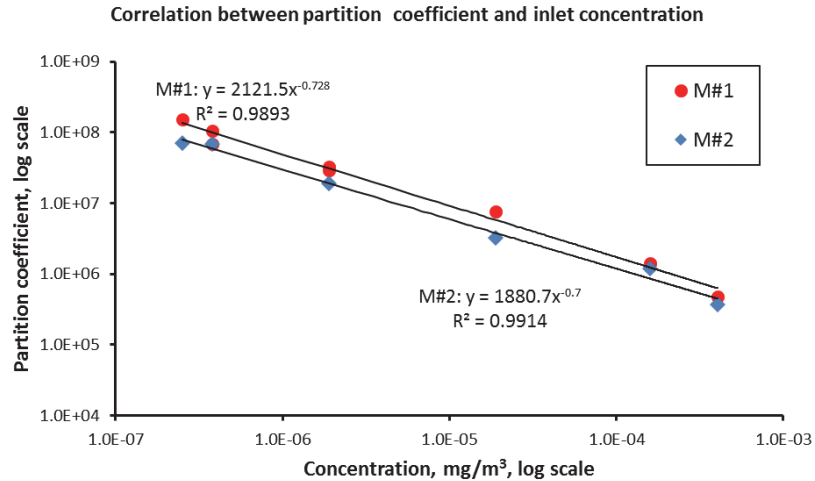


**Figure 3-13 Correlation of partition coefficient and inlet concentration, log axis**

This correlation can be summarized as Eqn. (3-2) or Eqn. **Error! Reference source not found.**, which is determined by two parameters related to the property of the carbon and VOC, a and



b. This correlation will be addressed in section 4.4. The correlation between partition coefficient and inlet concentration is named as P-C correlation in this study.

$$\begin{aligned} K_{ma,i} &= aC_{in,i}^b \\ \log(K_{ma,i}) &= a_i + b_i \cdot \log(C_{in,i}) \end{aligned} \quad (3-2)$$

Where,  $a_i = \log(a)$  , and  $b_i = b$  .

This correlation was not developed with the typical indoor concentration data provided in this study in the past. The previous extrapolations (e.g., Figure 2-7) that did not include enough data points at low concentration levels may result in an oversimplification of the partition coefficient.

### 3.6 Major findings

The single pass adsorption tests of activated carbon at ~ppb concentration levels could take an extremely long time to reach 100% breakthrough and be very difficult to perform in terms of low-concentration VOC generation and monitoring.

The sorbent media performs well at high concentration will also perform well at low concentration. In other words, the relative performance of adsorption in the tested activated carbon at low concentration could be indicated by the performance tests at high concentration. However, the relative ranking cannot represent the actual performance in engineering applications, which could be reflected by low concentration tests.

The removal capacity of activated carbon in terms of VOC mass removal per unit mass of sorbent decreased with decreasing challenge concentration. However, the partition coefficient, the ratio between sorbent and gas-phase concentration at equilibrium increased with the decrease of the concentration in a non-linear function. As a result, an empirical correlation, named generic P-C curve, is proposed and determined via a series of experiments including 2

types of activated carbon and 6 different concentration levels. The power-law function,  $K_{ma,i} = aC_{in,i}^b$  was found to represent the P-C correlation well, and hence proposed to be the generic form of the P-C correlation. The significance and application of this generic function will be further discussed in the next chapter.

# 4 MODELING AND SIMULATIONS

## 4.1 Introduction

Mathematical models that can predict the performance of adsorption filter media under different conditions are essential in the engineering design phase. The development of models intends to provide a useful tool for designing, selecting or replacing adsorption filter in the field based on the predicted filter performance in specified usage conditions. The fundamental process involved in the adsorption dynamic of the packed bed system includes: external convective mass transfer at the outer surface of sorbent particle, internal diffusion inside the pellet (within the pore air and on the internal surface) and adsorption of VOCs on the solid

matrix of the sorbent, such as activated carbon. In this chapter, two models are developed and evaluated with the experimental data obtained in Chapter 3.

## 4.2 Model Description

The major mass transport processes in section 2.2.2 can be described with three equations:

- Mass balance equation for the bulk gas transfer in the sorbent bed
- Mass balance equation within the pellet
- Adsorption isotherm equation

The models are based on the following assumptions:

- Plug flow, the velocity of the fluid is assumed to be constant across any cross-section
- Isotropic and spherical particles
- The bulk solution near a given particle is completely mixed
- Negligible radial dispersion in the sorbent bed
- Intraparticle transport is represented by the Fick's law
- Adsorbed phase and fluid phase are in equilibrium at the interface

### 4.2.1 Convective & Diffusion Mass Transfer with Constant Partition Coefficient (C&DMT-CP)

The mass balance equation in the sorbent bed is described as Eq. (4-1):

$$\frac{\partial C_b(x,t)}{\partial t} = D_{ax} \frac{\partial^2 C_b(x,t)}{\partial x^2} - u_s \frac{\partial C_b(x,t)}{\partial x} - \frac{(1-\varepsilon_b)}{\varepsilon_b} \rho_s \frac{\partial q(x,t)}{\partial t} \quad (4-1)$$

where  $D_{ax}$  is the axial dispersion coefficient,  $u_s$  is the superficial velocity in the bed.

Boundary conditions:

$$C_b(0,t) = C_{in}; \quad \frac{dC_b(L,t)}{dx} = 0,$$

Initial conditions:

$$C_b(0,0) = C_{in}, C_p(r, x, 0) = 0$$

This partial differential equation (PDE) has four terms:

- Accumulation term  $\frac{\partial C_b(x,t)}{\partial t}$ , accounts for the rate of accumulation/dissipation of the pollutants in an infinitely small control volume of the sorbent bed's gas phase.
- Advection term  $-u_s \frac{\partial C_b(x,t)}{\partial x}$ , presents the rate of mass transfer resulting from the fluid motion in the axial direction. The superficial velocity,  $u_s$ , is the average fluid velocity passing through the sorbent bed. It is correlated to the interstitial velocity,  $u_p$ , where  $u_p \cdot \varepsilon_b = u_s$ .
- Dispersion term  $D_{ax} \frac{\partial^2 C_b(x,t)}{\partial x^2}$ , also called dispersion or axial mixing, is an undesirable term while the fluid flows through the packed bed since it reduces the efficiency of the adsorption process. Molecular diffusion and turbulent mixing are identified as two main mechanisms that cause dispersion for a uniformly packed bed. Depending on the velocity in the bulk flow, either molecular diffusion or turbulent mixing becomes dominant. The Peclet number,  $Pe$ , is often used to evaluate the axial dispersion in the gas flow for packed bed system (Ruthven, 1984). Although the dispersion term is usually neglected against the advection term in most of the models, it should be noted that this is only reasonable with careful dimensionless analysis. Further discussion will be included in section 4.5.
- $\frac{(1-\varepsilon_b)}{\varepsilon_b} \rho_s \frac{\partial q(x,t)}{\partial t}$  is the accumulation rate of VOC in the sorbent, which can also be considered as the sink term that represents the rate at which the VOC mass transfer

from gas phase in the void of the bed to the activated carbon particle. In this study, the VOC molecules transport from flow in the bed across the laminar film adjacent to the

particle surface through convective mass transfer. A linear film transport theory is applied by using the convective mass transfer coefficient,  $h_m$  (Eq. (4-2)).

$$N_A = h_m [C_b(x,t) - C^*(x,t)] \quad (4-2)$$

As described in section 2.2.2, the mass transfer coefficient can be estimated from the correlation of Sherwood number, and  $h_m$  itself is only a function of the fluid components and conditions.

The mass balance equation within the particle is Eq. (4-3):

$$\begin{aligned} \varepsilon_p \frac{\partial C_p(x,r,t)}{\partial t} + (1-\varepsilon_p) \frac{\partial C_s(x,r,t)}{\partial t} = \varepsilon_p D_p \frac{1}{r^2} \frac{\partial}{\partial r} \left( r^2 \frac{\partial C_p(x,r,t)}{\partial r} \right) \\ + (1-\varepsilon_p) D_s \frac{1}{r^2} \frac{\partial}{\partial r} \left( r^2 \frac{\partial C_s(x,r,t)}{\partial r} \right) \end{aligned} \quad (4-3)$$

The adsorption isotherm is assumed as linear isotherm, Eq. (4-4)

$$C_s = K_{ma} C_p \quad (4-4)$$

Boundary conditions

$$\begin{aligned} C_b(0,t) &= C_m \\ \frac{dC_b(L,0)}{dx} &= 0, \\ \frac{\partial C_p(0,x,t)}{\partial r} &= 0 \\ \frac{\partial C_s(0,x,t)}{\partial r} &= 0 \\ h_m [C_b(x,t) - C^*(x,t)] &= \varepsilon_p D_p \frac{\partial C_p(r,x,t)}{\partial r} \end{aligned} \quad (4-5)$$

Initial conditions:

$$C_b(x,0)=0, C_p(r,x,0)=0, C_s(r,x,0)=0 \quad (4-6)$$

The detail derivation of the mass balance equations in sorbent bed and pellet are further presented in Appendix B.

#### 4.2.2 Convective & Diffusion Mass Transfer with Variable Partition Coefficient (C&DMT-VP)

Again, the mass transfer in sorbent bed is a transient process before 100% breakthrough. The amount of material adsorbed within a bed depends both on the position and time. Considering the time dependence, as fluid enters the bed, it meets the first few layers of adsorbent. Solute fills up some of the available sites. Soon, the adsorbent near the entrance is saturated and the fluid penetrates further into the bed until all solute is removed. Thus, the active region shifts downwind through the bed as time goes on. According to the mass transfer zone theory introduced in section 2.2.2, there is a concentration gradient along the sorbent bed, also called mass transfer zone (MTZ), as shown in Figure 4-1. The shape of the mass transfer zone depends on the bed structure, adsorption isotherm, flow rate and the diffusion characteristics. For example, favorable isotherms, like Langmuir isotherm or Freundlich, permit higher solid phase loadings at lower solution concentrations. They tend to start out steep and level out. Isotherms which start out flat are "unfavorable", since they only work well at high concentrations of solute. The wave front in the sorbent bed may change shape as it moves through the bed, and the mass transfer zone may broaden or diminish. Unfavorable isotherm tends to broaden. Favorable isotherm may broaden at first, but quickly achieve a constant pattern front, an asymptotic "S" shape. The high concentration regions move faster than the low concentration regions, and the



wave front steepens with time until a constant pattern front is developed. Some research named it as self-sharpening wave front (Seader & Henley, 2011).

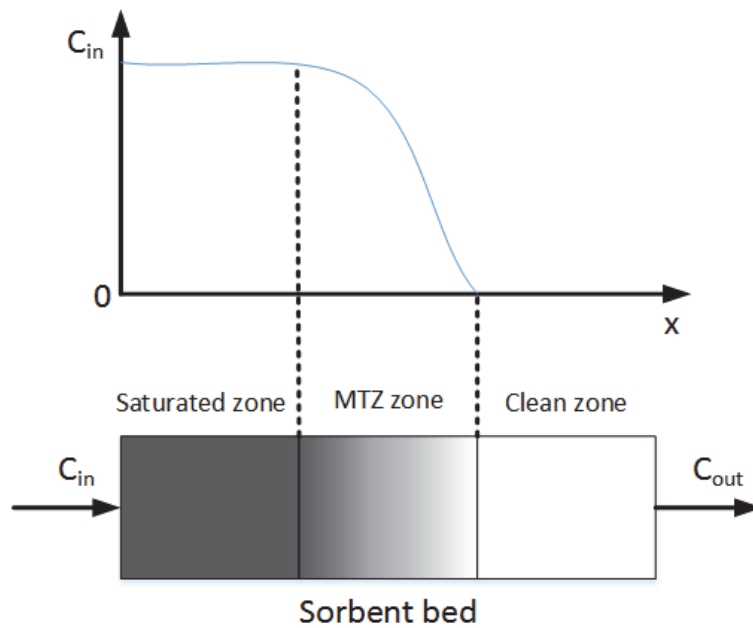


**Figure 4-1 Illustration of mass transfer zone in a sorbent bed**

With the knowledge obtained from Chapter 3, we are aware that partition coefficient is highly dependent on the concentration, especially at low concentration level. The C&DMT-CP model assumes that the partition coefficient is a constant in the entire system, however, the inlet concentration of each individual bed node is not the same until the entire sorbent bed is saturated. Consequently, the corresponding partition coefficient could be different with the moving MTZ and follow the P-C correlation determined in Chapter 3. When the wave front of the mass transfer zone is very steep, the variation of partition coefficient along the bed is negligible, but if the mass transfer zone length is relative large, the conventional

implementation method of model may introduce a significant error. As a result, a new model named C&DMT-VP is proposed in this study.

Compared with the C&DMT-CP model, the sorbent bed equation and the pellet equation of the new model remain the same, but the adsorption isotherm is no longer a linear isotherm. The power-law P-C correlation, Eq. (4-7), is applied in the C&DMT-VP model.

$$K_{ma} = a \cdot C_p^b \quad (4-7)$$

### 4.3 Model Implementation

#### 4.3.1 C&DMT-CP model implementation

To numerically solve the problem, the sorbent bed was spatially discretized using the finite difference scheme into  $n$  elements in the flow direction, each element consisting of  $m$  nodes to present the concentration gradient in the particle (Figure 4-2). This scheme was used by (Pei & Zhang, 2010) and adapted in the present study.

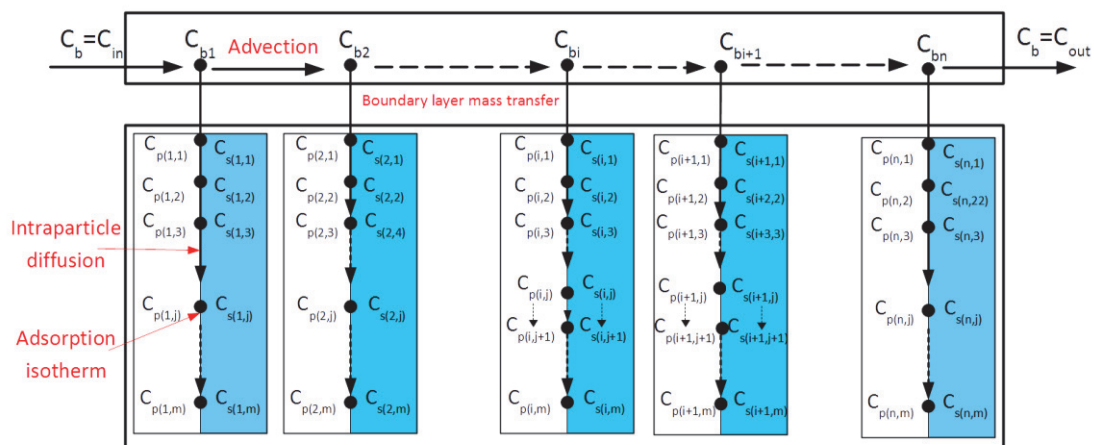


**Figure 4-2 Discrete representation of the sorbent bed**

A C++ numerical simulation program was implemented based on above models. The partial differential equations are transformed into a system of ordinary differential equations (ODEs)

by using the method of lines (MOLs). An open source package SUNDIAL::CVODE library (LLNL, 2007) was applied to solve this ODEs system. The VOC concentration is considered to be uniform within each pellet node,  $m$ , but they are different from one node to another. The

connections between the outermost node of single particle and the node in the bulk gas phase was defined according to the boundary condition.

The flow chart of the numerical simulation process is presented in Figure 4-3.

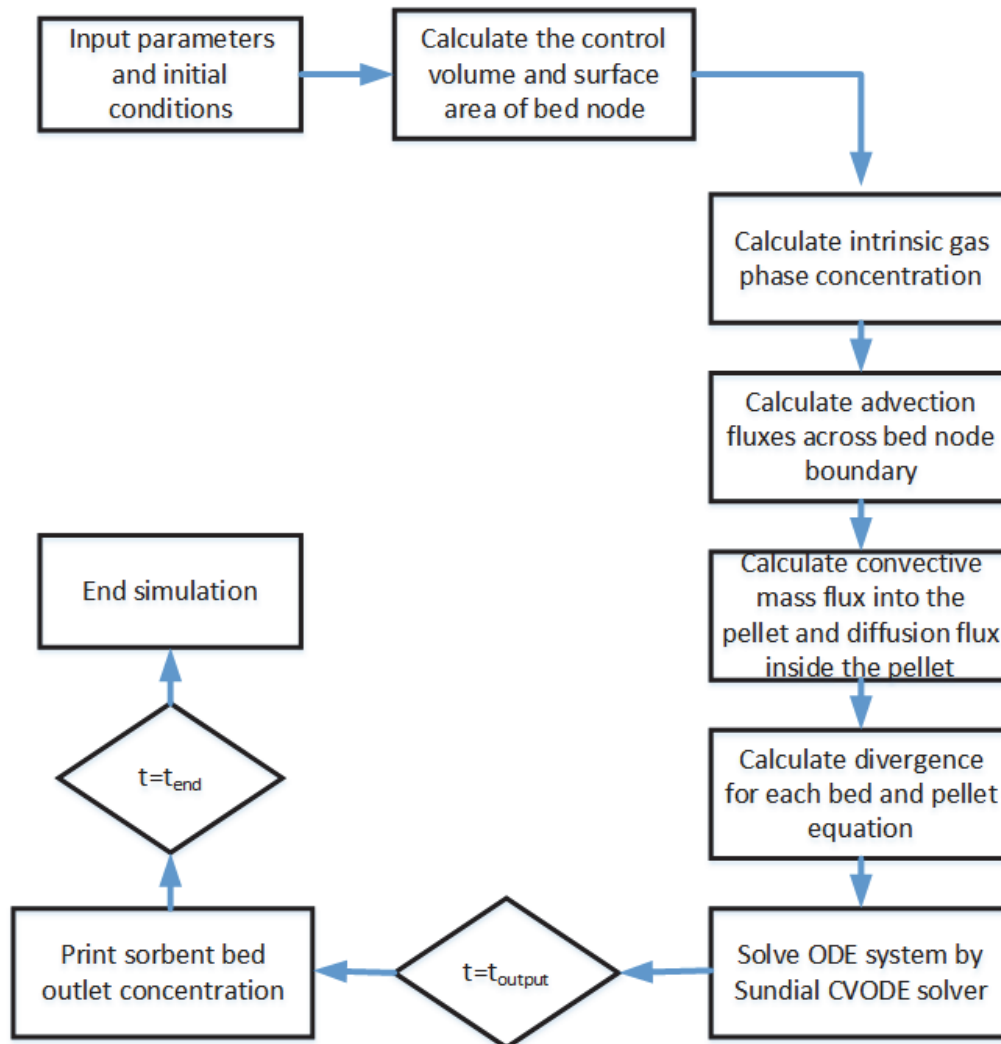


**Figure 4-3 Flow chart of simulation with the C&DMT-CP**

#### 4.3.2 C&DMT-VP model implementation

As shown in Figure 4-4, the partition coefficient  $K_i$  for bed node  $i$  is defined as a function of the inlet concentration of this node,  $C_b(i-1)$ , which is resulting from the previous bed node,  $i-$

1. The function of  $K_i$  is determined by the generic curve which was obtained by the experiments

carried out in Chapter 3. Consequently, the partition coefficient becomes different in each bed node and pellet node. At the entrance of sorbent bed, outer layer of the pellet, the partition coefficient exerts the minimum number.

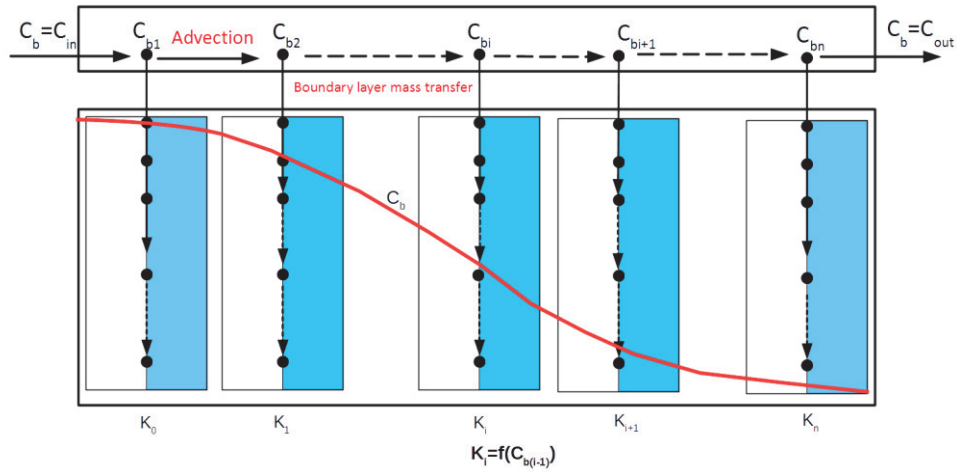


**Figure 4-4 Implement of P-C correlation in the model**

The flow chart of the new implementation of the method is represented in Figure 4-5.

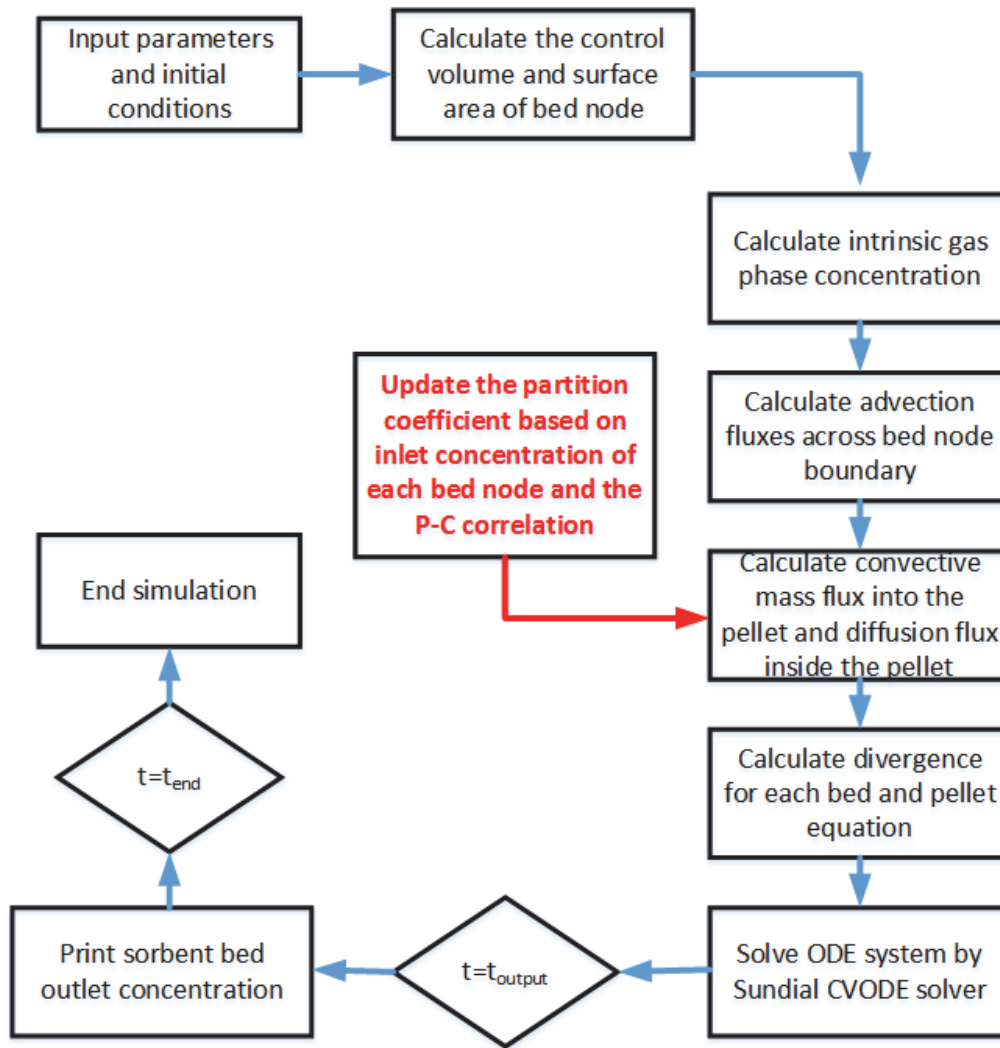


Figure 4-5 Flow chart of simulation with the C&DMT-VP

#### 4.4 Model evaluation

The simulation parameters for comparison between the modelling simulation and experimental data are summarized in Table 4-1. These parameters were obtained/estimated from either direct

measurements or existing literatures. The major difference between C&DMT-CP and C&DMT-VP simulation is the determination of partition coefficient.

**Table 4-1 Simulation parameters for adsorption tests**

|             |  | Test A                  | Test B          |            |
|-------------|--|-------------------------|-----------------|------------|
| Packed-bed  | Bed diameter, D, cm                    | 4.8                     | 4.8             | Measured   |
|             | Particle diameter, $d_p$ , mm          | 1.6 (M#1), 4 (M#2)      | 1               |            |
|             | Bed length, L, cm                      | 2.54                    | 1               |            |
|             | bed porosity, $\varepsilon_b$          | 0.328 (M#1), 0.4(M#2)   | 0.3             |            |
|             | Pellet porosity, $\varepsilon_p$       | 0.3 (M#1), 0.4(M#2)     |                 |            |
|             | mass transfer coefficient, $h_m$ , m/s | 0.069 (M#1), 0.05 (M#2) | 0.076           | Sh, Re, Sc |
| Environment | Inlet concentration, $C_i$ , ppm       | 100, 0.05               | 50, 5, 0.5, 0.1 | Measured   |
|             | Flow rate, Q, CFM                      | 1                       | 1               |            |
|             | Superficial velocity, $u_s$ , m/s      | 0.26                    | 0.26            |            |
| Media       | Pore diffusivity, $D_p$ , $m^2/s$      | 8e-6                    |                 |            |



|  |   |                               |  |
|--|---|-------------------------------|--|
| Surface diffusivity,<br>$D_s, m^2/s$                   | 5e-10   |                               | Literature<br><br>(Do, 2011;<br>Khazraei,<br>2014; Pei,<br>2011) |
| Partition<br>coefficient, $K_{ma}$ ,<br><br>(C&DMT-CP) | 100 ppm   | 4.8e5 (M#1),<br>3.7e5(M#2)    | Measured   |
|  | 50 ppm  | 1.39e6 (M#1), 1.2e6<br>(M#2)  |  |
|  | 5 ppm   | 7.6e6 (M#1), 3.6e6<br>(M#2)   |  |
|  | 500 ppb   | 2.85e7 (M#1), 1.7e7<br>(M#2)  |  |
|  | 50 ppb  | 1.15e8 (M#1),<br>6.12e7 (M#2) |  |
| P-C correlation<br><br>(C&DMT-VP)                      | $K_{ma}=2460.8 * C_p^{-0.713}$ (M#1)<br>$K_{ma}=1880.1 * C_p^{-0.70}$ (M#2) |                               | Measured<br>and<br>regressed                                     |

The mass transfer coefficient is estimated through the Wakao & Funazkri Correlation(Wakao & Funazkri, 1978b), which is already discussed in section 2.2.2:

$$Sh = 2.0 + 1.1Re^{0.6}SC^{1/3}$$

Where  $Re = \frac{u_s d_p}{\nu}$ ,  $Sh = \frac{h_m d_p}{D_m}$ ,  $Sc = \frac{\nu}{D_m}$ .

It is very important to address that the particle diameter,  $d_p$ , used in this study is an equivalent spherical diameter that given the same as the original pellet (i.e.,  $d_p = \frac{S_p}{\pi}$ , where  $S_p$  is the average surface area of original pellet). In this study, the original shape of M#1 and M#2 are considered as cuboid and cylindrical, respectively. The grounded pellet in test B is also considered as cuboid based on naked eye observation. All the geometric dimensions in this study are averaged by randomly measuring 15 pellets. The presented diameters in this study are all equivalent diameters unless specially noted otherwise.

#### 4.4.1 C&DMT-CP model evaluation

From Figure 4-6 to Figure 4-11, the simulation results through C&DMT-CP model are compared with the corresponding experimental data. It is very clear that the C&DMT-CP model can perform fairly well at the concentration level from 500 ppb to 100 ppm. As the concentration decreases, the discrepancy between predicted curve and the measured data increases. At 100 ppb concentration level (Figure 4-11), the model indicates that the breakthrough should occur at the very beginning of the test, which is a significant underestimation of the sorbent performance. The fact demonstrates that the C&DMT-CP model, which was considered as the most comprehensive model in the packed-bed system, cannot cover a wide range of VOC concentrations. The C&DMT-CP model also failed to predict the

initial breakthrough as shown in Figure 4-6 for Test M#2. The possible reasons will be addressed in the section of '4.5 Discussion'.

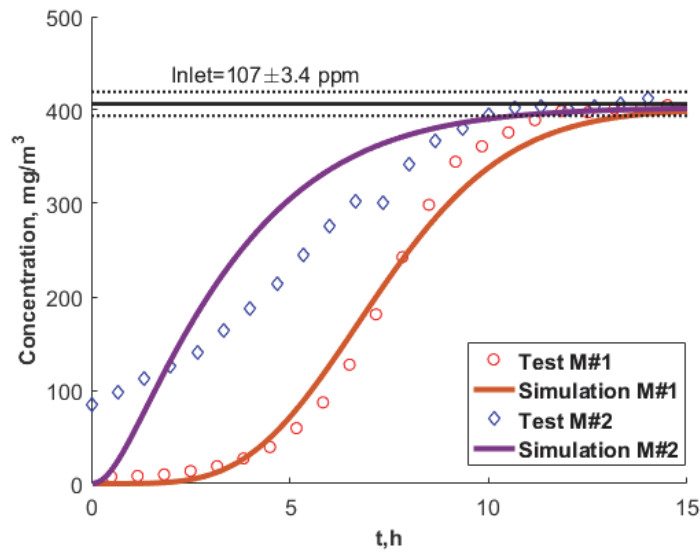


Figure 4-6 C&DMT-CP model simulation, 100 ppm

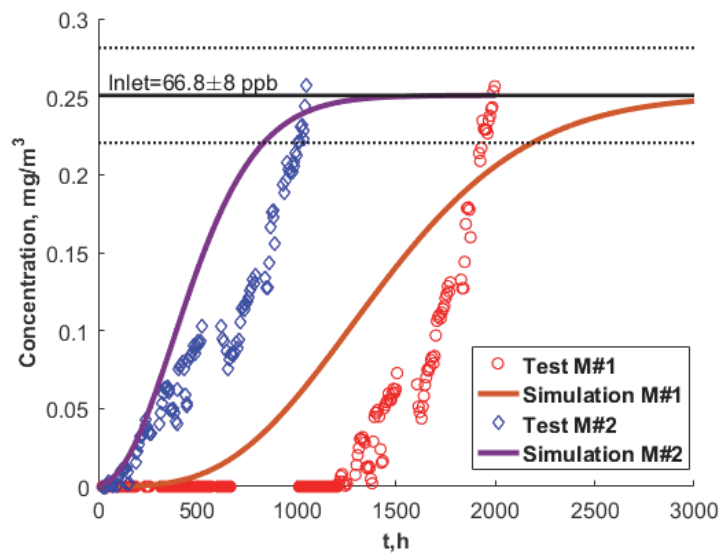


Figure 4-7 C&DMT-CP model simulation, 50 ppb

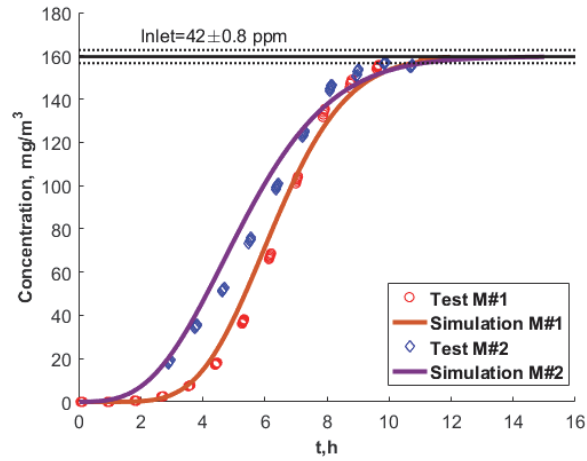


Figure 4-8 C&DMT-CP model simulation, 50 ppm

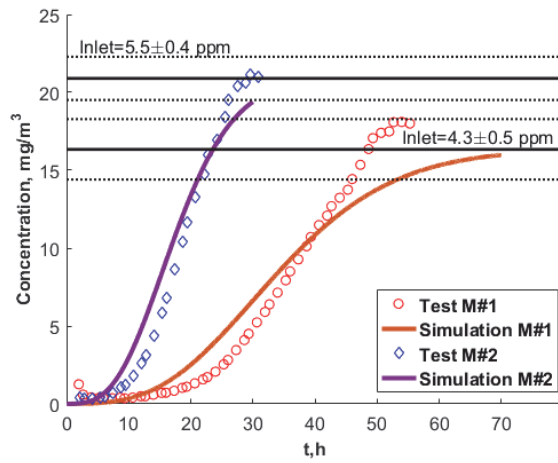


Figure 4-9 C&DMT-CP model simulation, 5 ppm

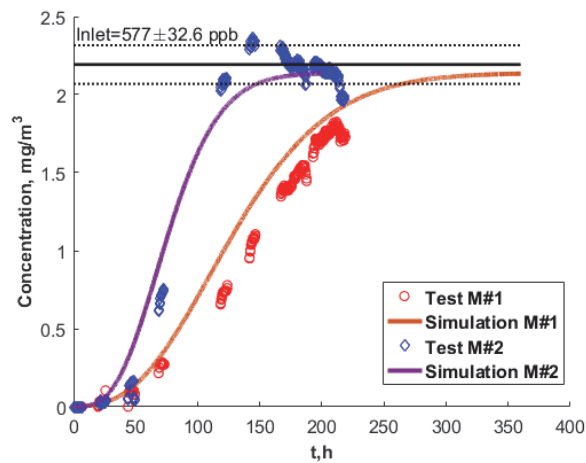


Figure 4-10 C&DMT-CP model simulation, 500 ppb

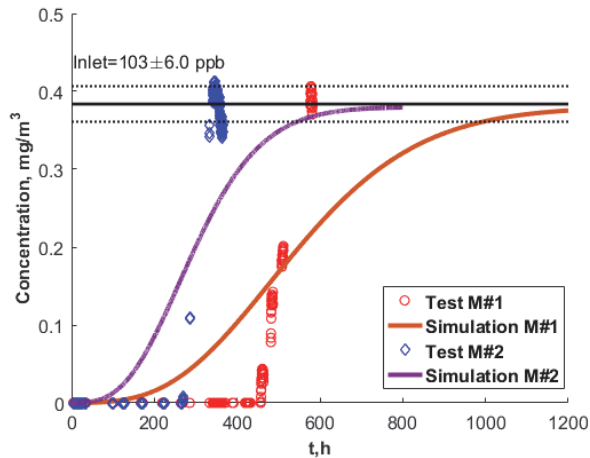


Figure 4-11 C&DMT-CP model simulation, 100 ppb

#### 4.4.2 C&DMT-VP model evaluation

For C&DMT-VP model simulation, the adsorption isotherm is obtained from the generic P-C correlation in section 3.6. By observing the simulation results in Figure 4-12~Figure 4-17, the fitting between experimental data and simulated curve is significantly improved compared with the C&DMT-CP model. Meanwhile, the C&DMT-VP model also successfully simulated the initial breakthrough for Test M#2 which the C&DMT-CP model failed to represent. It is very important to notice that the surface diffusion coefficient,  $D_s$ , was fitted through least-square regression in C&DMT-VP model. The coefficient of determination for each simulation,  $R^2$ , is also calculated. The reason for using regression to determine the surface diffusion coefficient is that it should be highly concentration-dependent in theory but usually being overlooked in previous studies due to the fact introduced in section 2.2.2. Because the pore diffusion coefficient is assumed to be constant, the  $D_s$  determined in the simulation should be considered

to represent the overall internal diffusivity when the partition coefficient is large. A further discussion is included in the next section.

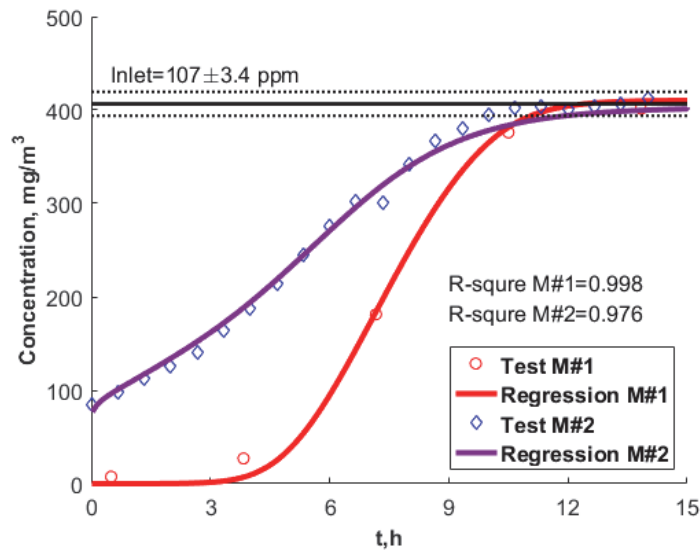


Figure 4-12 C&DMT-VP model simulation, 100 ppm, Test A

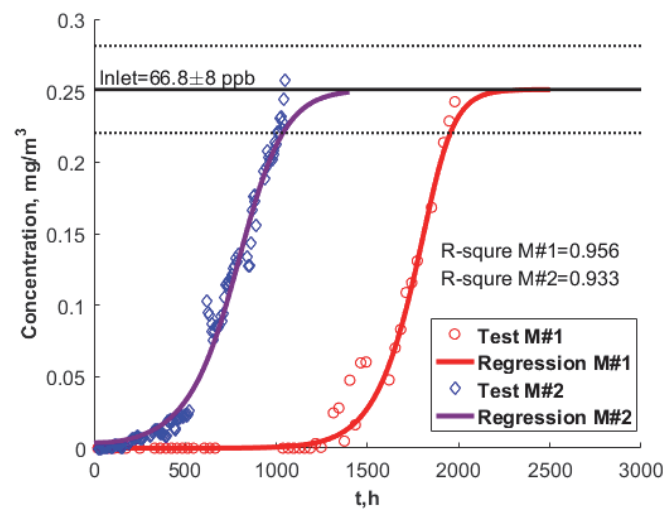


Figure 4-13 C&DMT-VP simulation, 50 ppb, Test A

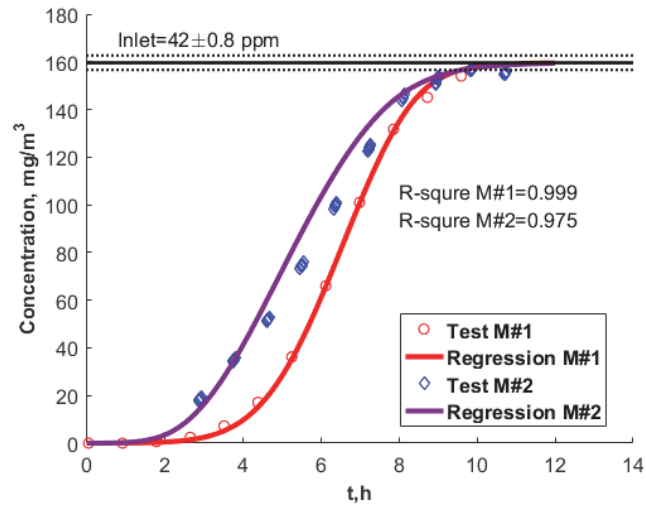


Figure 4-14 C&DMT-VP model simulation, 42 ppm, Test B

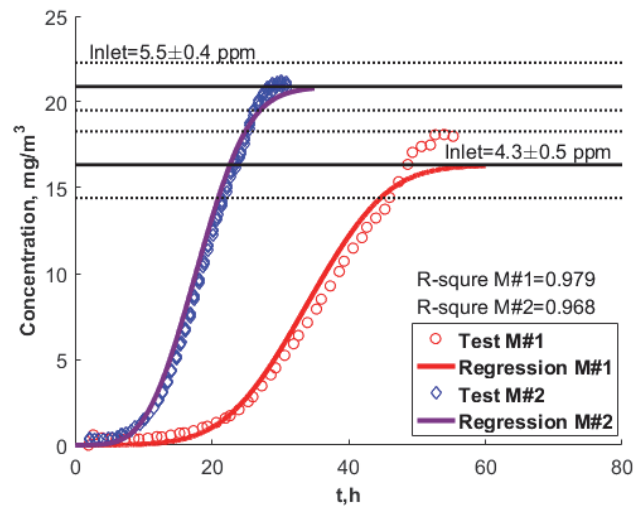


Figure 4-15 C&DMT-VP model simulation, 5 ppm, Test B

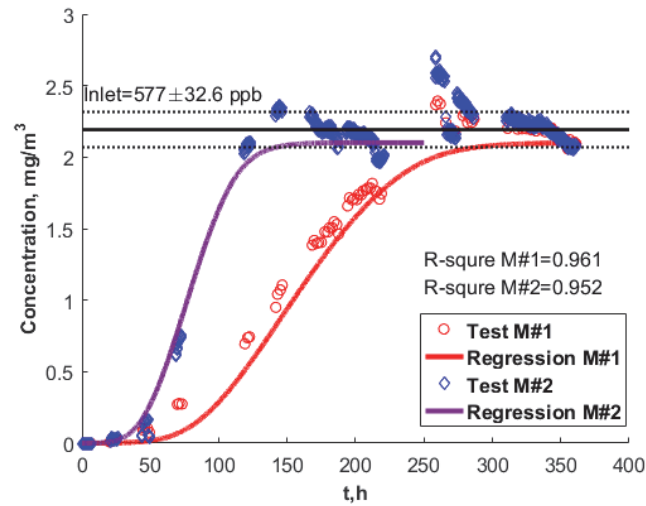


Figure 4-16 C&DMT-VP model simulation, 577 ppb, Test B

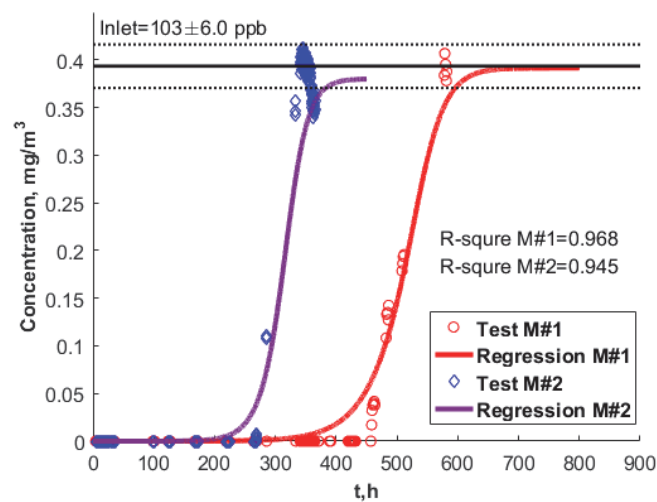


Figure 4-17 C&DMT-VP model simulation, 103 ppb, Test B

Biot number ( $Bi$ ) of each test is calculated via Equation (4-8) and presented in Table 4-2. It is considered as an analogous version of the  $Bi$  number in heat transfer, but applied in mass transfer process. In this study,  $Bi$  number is the ratio between the convective mass transfer at



the external surface of the pellet and the internal diffusion, which is mainly contributed by surface diffusion.

$$Bi = \frac{h_m \cdot d}{K_{ma} \cdot D_s} \quad (4-8)$$

A critical surface diffusion coefficient, 'D<sub>s, cri</sub>', is calculated for each test as well. The critical surface diffusion is defined as the surface diffusion coefficient when the Bi number equals 1, when the external convective mass transfer and internal diffusion are comparable. In this study, all the Bi numbers are larger than one, indicating a diffusion controlled process. The internal diffusion coefficient is the controlling factor for the overall mass transfer during the adsorption

process. The internal diffusion coefficient is the main reason for the gradual development of the curves from initial breakthrough to full breakthrough.

**Table 4-2 Summary of the determined  $D_s$  and  $Bi$  number**

| Concentration | h <sub>m</sub> , m/s | d, mm | K <sub>ma</sub> | D <sub>s, cri</sub> | D <sub>s, det</sub> | Bi   |
|---------------|----------------------|-------|-----------------|---------------------|---------------------|------|
| M#1           |                      |       |                 |                     |                     |      |
| 50 ppb        | 0.069                | 1.6   | 1.15E+08        | 9.12E-13            | 3.70E-14            | 24.6 |
| 100 ppb       | 0.076                | 1     | 1.07E+08        | 7.12E-13            | 4.40E-14            | 16.2 |
| 500 ppb       | 0.076                | 1     | 3.20E+07        | 2.38E-12            | 5.00E-14            | 47.5 |
| 5 ppm         | 0.076                | 1     | 7.61E+06        | 9.99E-12            | 8.00E-13            | 12.5 |
| 50 ppm        | 0.076                | 1     | 1.41E+06        | 5.39E-11            | 7.00E-12            | 7.7  |
| 100 ppm       | 0.069                | 1.6   | 4.80E+05        | 2.19E-10            | 7.50E-12            | 29.1 |
| M#2           |                      |       |                 |                     |                     |      |
| 50 ppb        | 0.032                | 2.02  | 70000000        | 1.83E-12            | 3.00E-13            | 6.1  |
| 100 ppb       | 0.076                | 1     | 68400000        | 1.11E-12            | 4.00E-13            | 2.8  |
| 500 ppb       | 0.076                | 1     | 1.90E+07        | 4E-12               | 6.00E-13            | 6.7  |

|         |       |      |          |          |          |      |
|---------|-------|------|----------|----------|----------|------|
| 5 ppm   | 0.076 | 1    | 3.20E+06 | 2.38E-11 | 9.00E-13 | 26.4 |
| 50 ppm  | 0.076 | 1    | 1.18E+06 | 6.44E-11 | 1.00E-12 | 64.4 |
| 100 ppm | 0.032 | 2.02 | 3.70E+05 | 3.46E-10 | 9.00E-11 | 3.8  |

## 4.5 Discussion

Both C&DMT-CP and C&DMT-VP model simulations were performed to compare with the experiments in ‘Chapter 3. Experimental Investigation’. Generally, C&DMT-CP model is able to simulate most of the tests at relative high concentration, such as 100 ppm, 50 pm, 5 ppm and 500 ppb (Figure 4-6, Figure 4-8, Figure 4-9 and Figure 4-10). However, the high initial breakthrough phenomenon of M#2 at 100 ppm is not picked up by C&DMT-CP model. This traditional model assumes that the partition coefficient is a constant in each sorbent layer along the entire sorbent bed. In Chapter 2, it has been concluded that the partition coefficient increases with decreasing inlet concentration. The selected media is very effective in toluene adsorption (favorable adsorption), resulting in a high concentration gradient along the longitude direction. The concentration of the wave front of the mass transfer zone should be very steep before all the adsorption sites are occupied even at high concentration. Hence, the constant partition coefficient assumption should not be applied for all the discretized bed layers and pellet layers in the model.

The performance of C&DMT-CP model at low concentration level, 66~100 ppb is not satisfactory, as Figure 4-7 and Figure 4-11. Large discrepancy and underestimated breakthrough time are identified in the simulation results. In C&DMT-CP model, the only

estimated parameter is the internal surface diffusion coefficient,  $D_s$ , so the effect of surface diffusion coefficient on the breakthrough deserves further investigation. In Figure 4-18, different order of magnitude of surface diffusion coefficient are applied in the simulation of M#1 in Test B, 100 ppb. It is shown that when the surface diffusion coefficient is smaller than the critical surface diffusion coefficient ( $D_s=1E-14 \text{ m}^2/\text{s}$ ), further decreasing the  $D_s$  only has slight change on breakthrough curve. It also underestimates the media performance since the VOCs molecules cannot access the internal pores when the diffusion resistance is very high. On the other hand, a large surface diffusion coefficient actually assumes a higher overall mass transfer rate that supposes to facilitate the simulation towards the experimental result (better early performance). However, as shown in Figure 4-18, increasing surface diffusion coefficient does not have significant effect once it is higher than the critical value ( $D_s=1E-14 \text{ m}^2/\text{s}$ ). When the surface diffusion coefficient is large, the controlling factor is not the internal diffusion but external mass transfer such as mass transfer coefficient and effective surface area. However, according to the calculation in Table 4-2, the Biot number of the tests in Test A and B are larger than one, which indicates an internal diffusion controlled process. On the other hand, C&DMT-CP model cannot simulate the experiments at low concentration even applying a very low surface diffusion coefficient either. The VOC molecules cannot enter the internal structure of activated carbon so the breakthrough occurs earlier. In conclusion, even considering the dependency of surface diffusion coefficient on concentration, the C&DMT-CP model cannot

well simulate the low concentration performance of the sorbent media with the conditions included in this study.

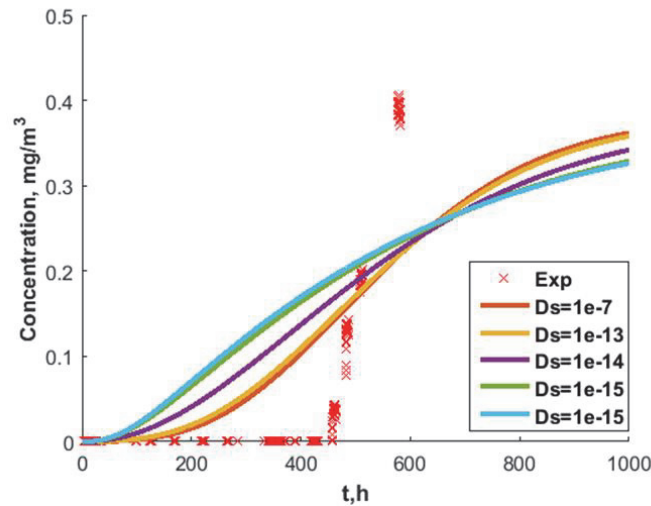


**Figure 4-18 Effect of surface diffusion coefficient in C&DMT-CP, M#1, Test B**

Figure 4-12~Figure 4-17 present the simulation results of C&DMT-VP model. A significant improvement is observed in C&DMT-VP model simulations. The high initial breakthrough phenomenon of M#2 at high concentration and the performance of both media at low concentration are successfully simulated with acceptable agreement. It is important to remind that the major update in C&DMT-VP model is the use of generic P-C curve obtained through the experiments in Chapter 3. The partition coefficient is relative small in the entrance region of the sorbent bed, and reach its maximum in the exit region. The similar gradient of partition coefficient also applies in the pellets, for example, the partition coefficient at the external surface is smaller than it at the center of the pellet according to the concentration gradient along the radius. This partition coefficient gradient in the C&DMT-VP model leads to a better early performance in simulation because the downstream bed layers will remain a large partition coefficient before the entire sorbent bed gets close to saturation. While most of the sorbent is saturated, the concentration of wave front becomes similar for all the bed layers, resulting in a

minimum partition coefficient and steep curve after the breakthrough point. It is more supportive to visualize the concentration within the sorbent bed at different locations to further understand the mass transfer zone movement in the testing column. Such concentration profile in high and low concentration simulations are presented in Figure 4-19 and Figure 4-20. At the high concentration, the concentration gradient in the sorbent bed is relative similar between C&DMT-CP model and C&DMT-VP model, especially at the initial time. However, at low inlet concentration, since the adsorption partition coefficient could change rapidly along the sorbent bed and pellet radius according to the power-law correlation summarized in Chapter 3, the difference between C&DMT-CP model and C&DMT-VP model becomes more significant at low concentration region. The concentration gradient in the sorbent bed is much steeper in C&DMT-VP simulation. In Figure 3-6, M#2 shows a 23% initial breakthrough at high concentration (~100 ppm). It is possibly a result of such a dependence of partition coefficient on the inlet concentration of each control volume. For example, during the initial period, each layer of bed/pellet would face a very high concentration, hence the partition coefficient could be very small resulting in an overall poor performance. When the mass transfer zone forms the

regular shape, the activated carbon surfaces at downstream start to present a higher partition coefficient. This mass transfer zone keeps moving to the exit of sorbent bed as  $x/L=1.0$ .

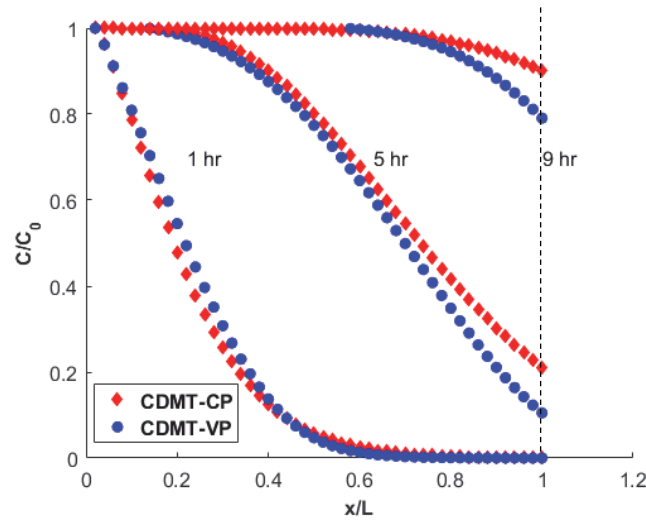


**Figure 4-19 Concentration profile in the sorbent bed ( $x/L$ , normalized bed location),  
M#1, 100 ppm, Test A.**

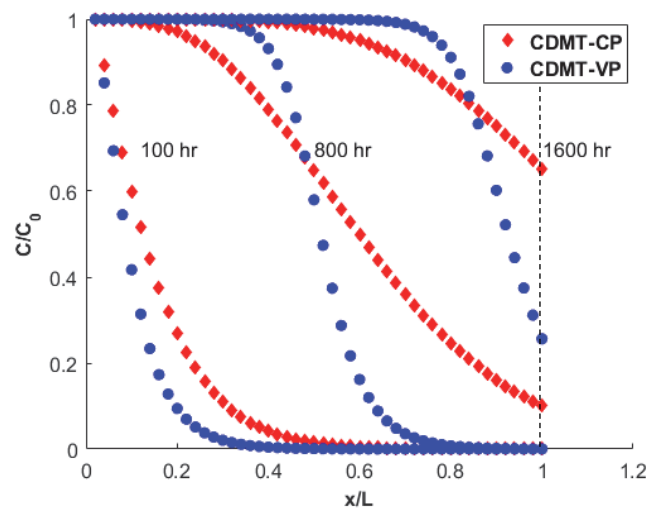


**Figure 4-20 Concentration profile in the sorbent bed ( $x/L$ , normalized bed location),  
M#1, 50 ppb, Test A**



## 4.6 Major findings

C&DMT-CP model could generally simulate the performance of sorbent media at high concentration levels that ranges from 500 ppb~100 ppm, but it was not able to simulate the performance at low concentration, ~100 ppb, which is usually found in indoor environment. In addition, C&DMT-CP model did not perform well when an initial breakthrough occurred at high concentration. The most possible reason is that the assumption of constant partition coefficient in all the bed layers may not be valid.

C&DMT-VP model showed a better performance at low concentration range, and successfully simulated the initial breakthrough of M#2 at high concentration (original pellet size). The overall performance of C&DMT-VP model suggests that the mechanistic model is more advanced and promising for developing a model-based testing and evaluation method for the prediction of sorbent media performance at typical indoor concentration levels.

# 5 MODEL-BASED TESTING METHOD FOR PREDICTING MEDIA PERFORMANCE AT LOW CONCENTRATIONS

## 5.1 Introduction

This chapter demonstrates an innovative model-based testing and evaluation method to predict the performance of physical sorbent media bed at low concentrations (~ppb levels). Based on the knowledge gained from previous experimental and modelling results, the effecting factors of sorbent media performance can be classified into three categories, such as Media, Environment and Species or named, MES (Figure 5-1). Apparently, most of factors can be measured physically, but a few important input parameters are experimentally difficult to determine, such as surface diffusion coefficient and partition coefficient (at low concentration). The model-based testing and evaluation method provides a practical way to determine these

parameters and simulate the real performance of physical adsorption media at very low challenge concentrations.

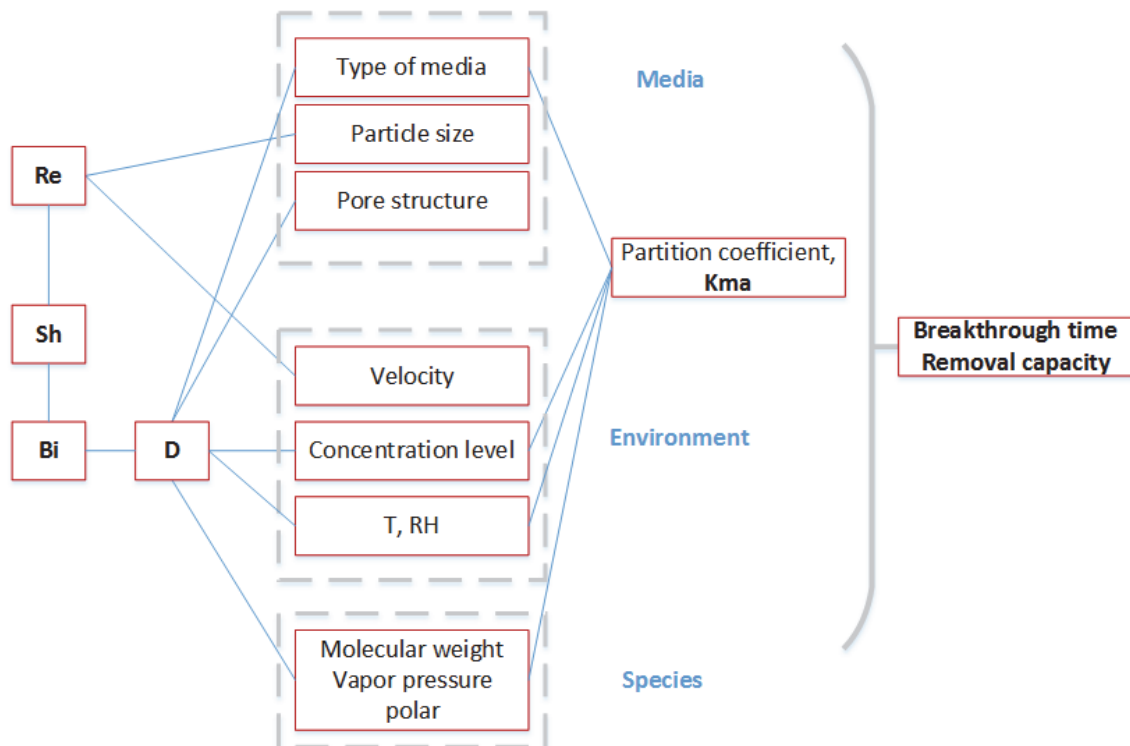


**Figure 5-1 Effecting factors of media sorption performance, MES**

## 5.2 Model-based testing and evaluation method

The components and procedure of model-based testing and evaluation are illustrated in Figure 5-2. The purpose of this method is to simulate the performance of a sorbent media's performance at practical conditions, including concentration level, media configuration and environmental condition. Conducting a low concentration test would be very challenging and time consuming, however, the model-based testing and evaluation method has a great potential to achieve the goal without performing the long-term experiment. Firstly, laboratory accelerated test must be conducted for the selected media and target challenge gas. For example, activated carbon and toluene are selected in this study. The corresponding measurements and

test results shall provide details of MES data and breakthrough curve as input parameters for a regression with CDMT-VP model. Then, the P-C correlation of a specific combination of media and challenge gas could be determined per the regression. Finally, the CDMT-VP model is performed again with the MES data of the target test conditions for simulation. In this study, the simulation results with simulation parameters determined from the accelerated tests are compared with the long-term & low concentration experimental data to validate the evaluation procedures.

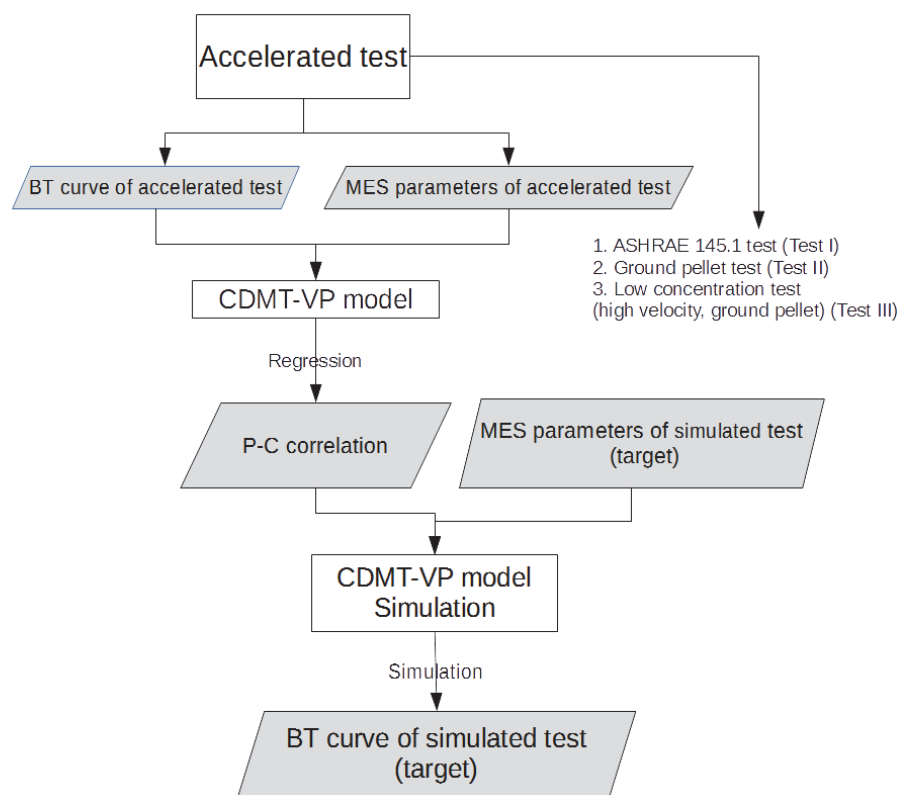


**Figure 5-2 Model-based evaluation method**

### 5.3 Determination of P-C correlation through accelerated tests

The pre-requisite tests (accelerated test) could be carried out at either high or low concentration for a specific combination of sorbent media and target VOC gas. Three accelerated methods were explored and evaluated in this study. The original ASHRAE 145.1 standard test at an elevated concentration is already a typical accelerated test, as Test A described in Table 3-2.

To further shorten the test time, the length of sorbent bed could be reduced. While decreasing length of sorbent bed, however, the pellet size must be reduced as well, so that the uniformity of the sorbent bed could be maintained, such as Test B (Table 3-2).

Further thoughts on accelerating the test for the determination of the P-C curve motivates a development of a new test method in this study. Considering the MES factors that could contribute to the test period, the test column in the new test was designed as Figure 5-3. The pellet diameter was grounded to average 1 mm which is approximately by one third of the sorbent bed length. The flow velocity was raised to 1.24 m/s. In order to achieve this face velocity, a new test column with 22 mm diameter was used due to the limit of the supplied air flow rate in the current ACTTS (Figure 5-3). This new test method was performed for both M#1 and M#2 activated carbon at an inlet concentration of 100 ppb. Thanks to the greatly reduced sorbent bed length and high flow velocity, the test method could be finished within a short time at low concentration level.

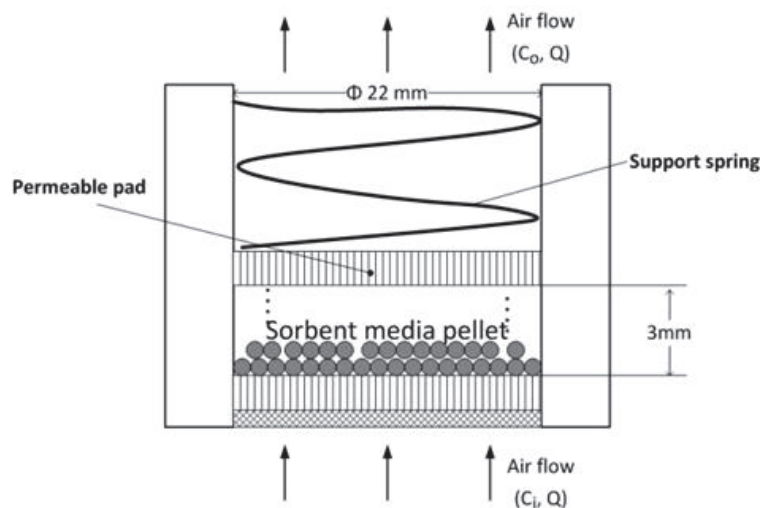


**Figure 5-3 Schematic of accelerated test (Test III)**

So far, the ASHRAE 145.1 standard test (labelled as Test I in this Chapter), the test with short sorbent bed and ground pellet (labelled as Test II) and the new developed test (labelled as Test

III) are used to determine the P-C curve and validate the model-based testing and evaluation method. The detailed test conditions are presented in Table 5-1.

**Table 5-1 Test conditions of accelerated tests**

|                            | Test I  | Test II   | Test III  |
|----------------------------|---|---|---|
| Concentration<br>(toluene) | 100 ppm   | 50 ppm  | 100ppb  |
| Pellet size and<br>shape   | OVC: 4x8 mesh size flat<br>shell<br><br>AP4-60: 4mm diameter<br>cylindrical | Granular 1mm<br>equivalent diameter<br>(grounded) | Granular 1mm<br>equivalent diameter<br>(grounded) |
| Bed depth                  | 1" (25.4 mm)  | 10 mm   | 3 mm  |
| Test column<br>diameter    | 48 mm   | 48 mm   | 22 mm   |
| Test media<br>volume       | 45 cm <sup>3</sup>  | 17.7 cm <sup>3</sup>                              | 1.14 cm <sup>3</sup>                              |
| Velocity                   | 0.26 m/s  | 0.26 m/s  | 1.24 m/s  |

The parameters used for Test I and Test II simulations have been listed in Table 4-1, so repeat is avoided intentionally.

## 5.4 Results and discussion

The test results of Test I and Test II have been presented in Chapter 3 (Figure 3-6 and Figure 3-8). The results of test III is shown in Figure 5-4. Due to the increased inlet velocity and small sorbent amount, the low concentration test was finished within 80 hours for both M#1 and M#2. The breakthrough curves are clear and complete. Thus, this test method is considered as valid and applicable for physical adsorption test. The initial breakthrough is zero, and a steep rise

occurs after the breakthrough point. The adsorption behaviour is consistent with the previous low concentration tests.

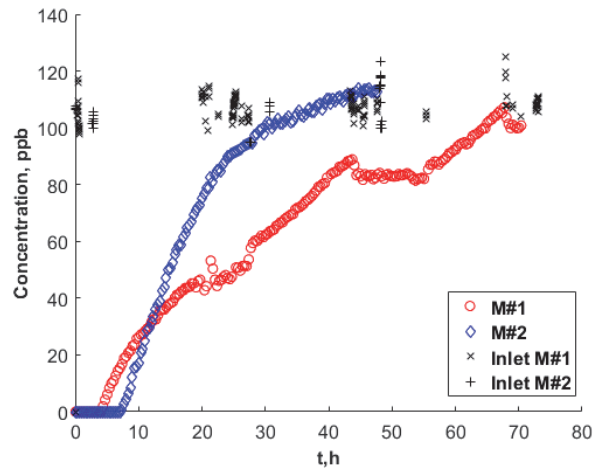


**Figure 5-4 Breakthrough of low concentration-accelerated test, (M#1:  $107 \pm 9$  ppb; M#2:  $99 \pm 4$  ppb)**

The C&DMT-VP model developed in Chapter 4 was applied to simulate Test III and determine the corresponding P-C curve through regression. The parameters used in the simulation are listed in Table 5-2, and the result is shown in Figure 5-5.

**Table 5-2 Simulation parameters for Test III**



|             |                                      |   |
|-------------|--------------------------------------|---|
| Packed bed  | Bed length, mm                       | 3   |
|             | Bed diameter, mm                     | 22  |
|             | Particle porosity                    | 0.3 (M#1), 0.4(M#2)   |
|             | mass transfer coefficient, m/s       | 0.187   |
| Environment | Inlet concentration, ppb             | 107   |
|             | Superficial velocity, m/s            | 1.24  |
|             | Pore diffusivity, $D_p$ , $m^2/s$    | $8e-6$  |
|             | Surface diffusivity, $D_s$ , $m^2/s$ | $5e-13$   |
| Media       | P-C correlation (C&DMT-VP)           | $K_{ma}=100*C_p^{-0.927}$ (M#1)<br>$K_{ma}=1200*C_p^{-0.729}$ (M#2) |

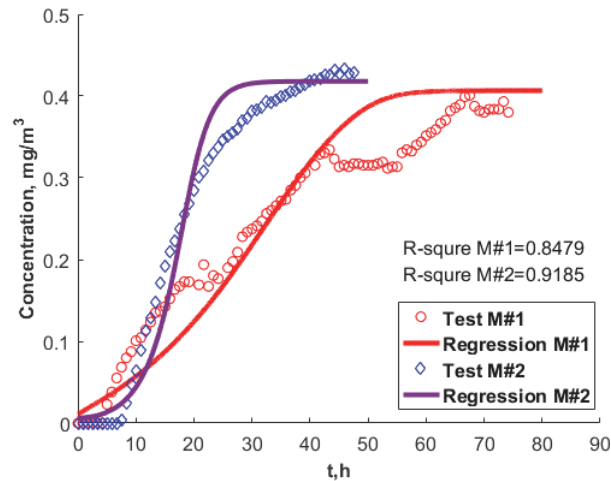


**Figure 5-5 Regression through low concentration-accelerated test, 100 ppb**

Up to now, the three sets of required data for model-based testing and evaluation method are completely collected through Test I, Test II and Test III. Following the procedures in Figure 5-2. The P-C curves of M#1 and M#2 are determined from Test I, Test II and Test III, respectively (Figure 5-6 and Figure 5-8). For better visualization, these P-C curves are plotted in a log-log scale as shown in Figure 5-8 and Figure 5-9. For M#1, the Test I, Test II and the Generic curve (obtained in Chapter 3) provide very similar P-C curve, while the P-C curve determined from Test III is slightly different in 0.1~2 mg/m<sup>3</sup> concentration range. For M#2, the P-C curve determined by the three tests are almost identical. In theory, all the P-C curves for a given combination of sorbent and sorbate should be identical regardless the methods of

determination. The differences may be attributed to experimental error in this study. Test III is more difficult to perform due to the very small amount of sorbent media in the bed.

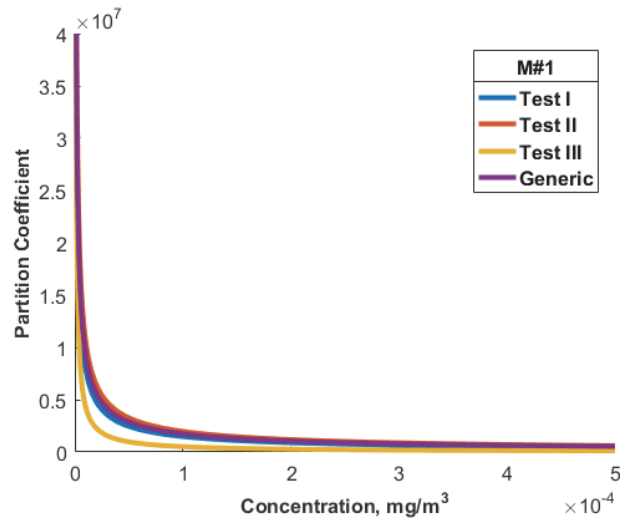


**Figure 5-6 Determination of the P-C curve, M#1**

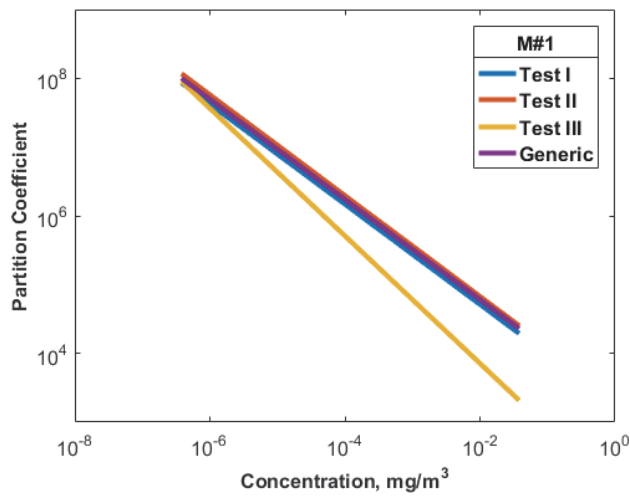


**Figure 5-7 Determination of the P-C curve, M#1(log scale)**

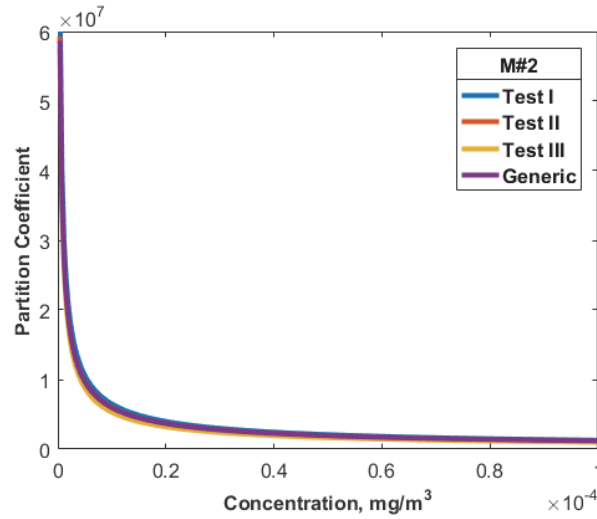


**Figure 5-8 Determination of the P-C curve, M#2**

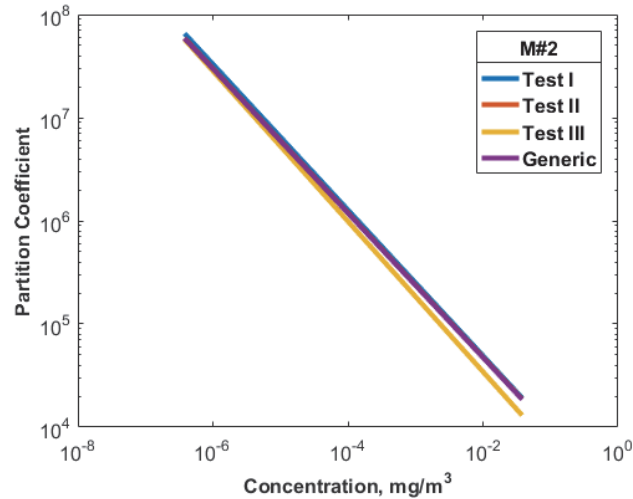


**Figure 5-9 Determination of the P-C curve, M#2(log scale)**

To verify the model-based testing and evaluation method, the tests for original pellet of M#1 and M#2 under ASHRAE 145.1 standard test condition at 66 ppb inlet concentration (long-term and low concentration test) are used for validation purpose, also named target test for short. The detailed test conditions and simulation parameters have been introduced in Table 4-1. The P-C curves determined from Test I, Test II and Test III are applied in the C&DMT-

VP model to predict the performance of M#1 and M#2 at target test conditions. The prediction results are compared with the experimental data of target tests for verification.

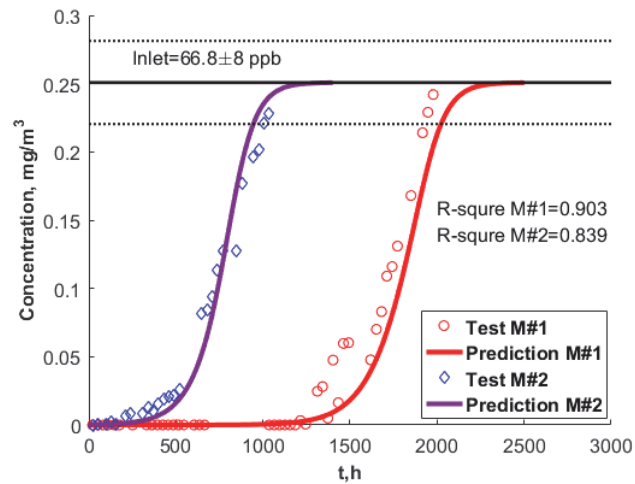


**Figure 5-10 Prediction of 50 ppb performance based on the P-C curve from the accelerated test I: ASHRAE standard test (100 ppm)**

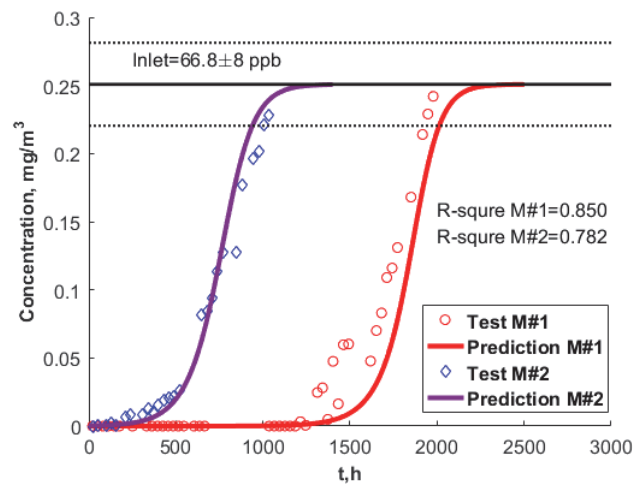


**Figure 5-11 Prediction of 66 ppb performance based on the accelerated test II: ground pellet test (50 ppm)**

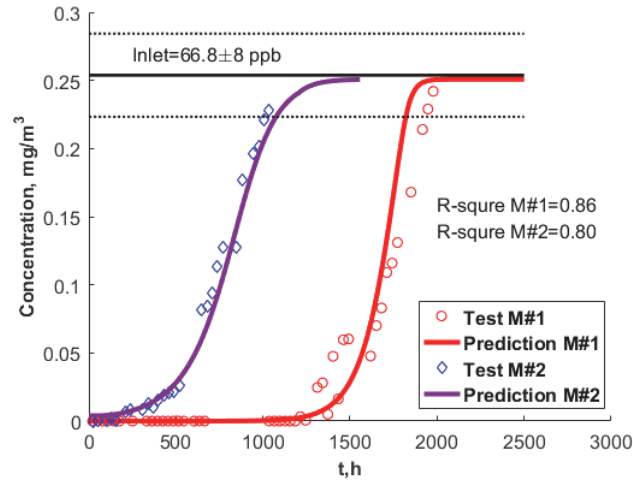


**Figure 5-12 Prediction of 66 ppb performance based on the accelerated test III: low concentration-accelerated test (100 ppb)**

The prediction results are presented in Figure 5-10, Figure 5-11 and Figure 5-12. The discrepancy between simulation and experiment data could be considered as acceptable in HVAC applications. The initial breakthrough time, 50% breakthrough time and removal capacity are well predicted by the model-based testing and evaluation method when the P-C curve is determined by an accelerated test.

## 5.5 Major findings

Based on the knowledge gained in Chapter 3 and Chapter 4, an innovative model-based testing and evaluation method is developed in Chapter 5. The major findings are:

1. The P-C correlation could provide an improved description of the physical adsorption process for a particular Media-VOC combination. It could be determined not only through a series experiments under different concentration levels, but also from a single accelerated test, such as ASHRAE 145.1 standard test (Test I), high concentration ground pellet test (Test II) and low concentration ground pellet test (Test III).
2. Three P-C correlations for each tested sorbent media are determined by the three different tests. All the P-C correlations are applied and evaluated by comparing with the

experimental data of target tests. The simulation results have a good agreement with the experiments.

3. A new model-based testing and evaluation method is developed, illustrated and validated to simulate the performance of activated carbon at very low concentration level. The application of this method requires the MES data of the target test and the corresponding P-C correlation determined by an accelerated test.
4. The three accelerated test methods evaluated were promising to be introduced as a standard test method and procedure for estimating the P-C correlation and the surface diffusion coefficient.

# 6 SUMMARY AND CONCLUSIONS

## 6.1 Introduction

Physical adsorption media in a duct system or a stand-alone air purifier is the most widely used intervention to reduce the indoor VOCs concentration. The concentration of VOCs that exists in indoor air are usually at ~ppb levels. However, the majority of previous studies focus on the tests at high concentration levels because the experiments are easier to perform and measure. Even though some recent experimental studies were conducted at typical indoor concentration levels, there is no validated mechanistic model that could simulate the sorbent media performance at such low concentration region. This study presents a comprehensive work including both the experimental investigation and model development for the activated carbon type media at very low concentrations (<100 ppb). Leveraging the knowledge gained in experiments and modelling, a model-based testing and evaluation method is developed and verified. The prediction of physical adsorption media performance at very low concentration can be achieved through such a new method which specially requires a P-C correlation curve that is determined from an accelerated test, which is also developed in this study.

## 6.2 Physical adsorption test at different concentration levels

In the experimental investigation, it can be concluded that a tested physical adsorption media that performs well at high concentration will also perform well at low concentration. The removal capacity at 100% breakthrough depends on the challenge concentration (also called inlet concentration) greatly. The higher the challenge concentration, the large the removal capacity at 100% breakthrough. The partition coefficient, mass transfer coefficient, and



diffusion coefficient are three key parameters describing the VOC transport and storage characteristics on the sorbent media. The tests at 6 different concentration levels show that the partition coefficient increases with decreasing inlet concentration. The correlation between partition coefficient and inlet concentration can be summarized into a power-law empirical equation, also named P-C curve (Partition Coefficient-Concentration curve).

Two mechanistic models are developed and evaluated following the experimental investigation. The major difference between C&DMT-CP model and C&DMT-VP model is the assumption regarding the dependence of partition coefficient. In the C&DMT-CP model, the partition coefficient is defined as a constant number everywhere in the sorbent bed, and is determined by the integration of upper area of complete breakthrough curve. However, the C&DMT-VP model assumes that the partition coefficient varies with the challenge concentration during the adsorption process. When the high concentration gradient occurs along the longitude of the sorbent bed and radius of the pellet, the partition coefficient could be determined by the air phase pollutant concentration right at the interface by using the P-C curve. These two models are compared with experimental data. C&DMT-CP can simulate the high concentration tests but not low concentration tests. C&DMT-VP model performs well at both high and low concentration by using a generic P-C curve determined from the experimental data of 6 concentration levels. In conclusion, the assumptions in C&DMT-VP model is more realistic when describing the adsorption process at low concentration levels.

### 6.3 Model-based testing and evaluation method

Finally, an innovative model-based testing and evaluation method is developed based on the knowledge obtained in this study. The method requires 1) an accelerated test to generate a breakthrough curve at either high or low challenge concentration level; 2) a mechanistic model, namely, C&DMT-VP, to determine the correlation between partition coefficient and inlet concentration, known as P-C curve; 3) the MES parameters of the target test to generate a

prediction. Eventually, the new method is able to predict the result of the target test by using the P-C curve and MES parameters. The prediction results of two type of activated carbon showed a good agreement with the low concentration experimental data obtained independent of the model-based testing and evaluation method.

## 6.4 Recommendations for future works

The following section represents some possible research directions for future studies.

1. More experimental data for different type of VOC and sorbent combinations need to be fully investigated to validate the universality of the conclusions in section 6.3.
2. In practice, some parameters are experimentally difficult to measure, such as pellet porosity, bed porosity and pellet size. A lot of physical properties of activated carbon are estimated based on literatures. A more convenient method for measuring these physical properties will be very beneficial.
3. This study mainly focused on physical adsorption process, but there are many other filter types such as chemisorbent and catalyst that are used for air cleaning. The performance of such sorbents at low concentration levels are still very difficult to test or simulate, and need further investigation.
4. The modelling/simulation tool for model-based testing and evaluation method needs to be improved. A user-friendly interface with the C&DMT-VP model developed in current study would be very useful for both engineers and designers.

# 7 APPENDICES

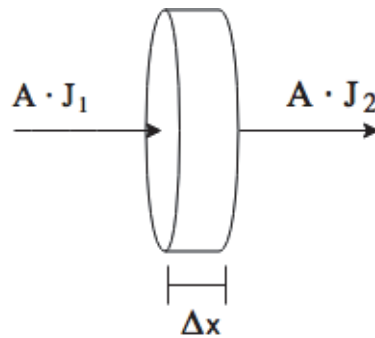
## Appendix A Specification of monitoring device

The compact ppbRAE 3000 is a comprehensive VOC gas monitor and datalogger for hazardous environments. This PID device monitors VOCs using a photoionization detector with a 9.8 eV, 10.6 eV UV-discharge lamp. The specifications of ppbRAE 3000 are listed in Table 7-1.

**Table 7-1 Specifications for ppbRAE 30000**

| Category           | Specifications   |
|--------------------|--|
| Range              | 0.999-199.9 ppm  |
| Resolution         | 1 ppb for 0-999 ppb; 10 ppb for 0.01-9.99 ppm; 100 ppb for 0.1-199.9 ppm   |
| Accuracy           | ±20 ppb or 10% of reading whichever is larger with 10.6 eV lamp            |
| Response time      | <5s calibrated with isobutylene gas  |
| Sensor             | Planar, dual-channel photoionization sensor with super bright 10.6 eV lamp |
| Sampling flow rate | 400 cc/min   |

## Appendix B. Derivation of sorbent bed equation and pellet equation



### i. Bed equation:

In the sorbent bed, a cylindrical control volume with cross area  $A$  and thickness  $\Delta x$  is taken.

The mass balance in this control volume can be presented as: [change rate of gas-phase

concentration in the control volume]=[in at x]-[out at x+Δx]+[adsorbed by the pellets in the control volume]

$$\varepsilon_b V \frac{\partial C_b}{\partial t} = A(J_1 - J_2) - (1 - \varepsilon_b)S$$

$$J_2 = J_1 + \frac{\partial J}{\partial X} \Delta X$$

Where J is the mass flux passing the control volume, S is the adsorption rate from gas-phase in the sorbent bed to the pellets in the control volume. It is considered as the sink term, so a negative sign is assigned to this term.

$$\frac{\partial C_b}{\partial t} = -\frac{\partial J}{\partial X} - \frac{(1 - \varepsilon_b)S}{\varepsilon_b V}$$

At the boundary of the pellet,  $S = A_p h_m (C_b - C^*)$ , where  $A_p$  is the total available outer surface area of the pellets in the control volume.

The mass flux through the control volume includes both advection and dispersion,

$$J = J_{advection} + J_{dispersion}$$

According to the conservation of mass, the flow rate of the VOC passing through the control

volume  $Q = C_b \cdot \Delta X \cdot A$ , thus  $J_{advection} = \frac{Q}{A \Delta t} = \frac{\Delta X}{\Delta t} C_b = u_s C_b$ .

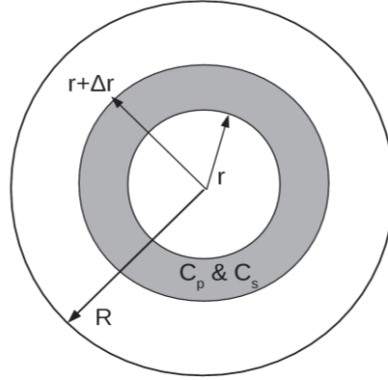
The dispersion flux is  $J_{dispersion} = -D_{ax} \frac{\partial C_b}{\partial X}$ , according to diffusion theory.

Substitute and rearrange the equation, the mass balance equation in the sorbent bed is:

$$\frac{\partial C_b}{\partial t} = D_{ax} \frac{\partial^2 C_b}{\partial X^2} - u_s \frac{\partial C_b}{\partial X} + \frac{(1 - \varepsilon_b)R}{\varepsilon_b V}$$

ii. Pellet equation:

[Adsorption rate of VOC within a shell of thickness  $\Delta r$ ] = [In at  $r$ ]-[Out at  $r+\Delta r$ ]



$$\varepsilon_p V_s \frac{\partial C_p}{\partial t} = \varepsilon_p (J_p \cdot 4\pi r^2 |_{r} - J_p \cdot 4\pi r^2 |_{r+\Delta r})$$

$$(1 - \varepsilon_p) V_s \frac{\partial C_s}{\partial t} = (1 - \varepsilon_p) (J_s \cdot 4\pi r^2 |_{r} - J_s \cdot 4\pi r^2 |_{r+\Delta r})$$

$$J_p = -D_p \frac{\partial C_p}{\partial r}; J_s = -D_s \frac{\partial C_s}{\partial r}$$

Where  $\frac{4\pi r^2}{V_s} = \Delta r$ ,  $J_p$  is the mass flux in the pore air and  $J_s$  is the mass flux in the adsorbent

(on the internal surface).

As a result, the pellet equation can be summarized as:

$$\varepsilon_p \frac{\partial C_p}{\partial t} + (1 - \varepsilon_p) \frac{\partial C_s}{\partial t} = \varepsilon_p D_p \frac{1}{r^2} \frac{\partial}{\partial r} \left( r^2 \frac{\partial C_p}{\partial r} \right) + (1 - \varepsilon_p) D_s \frac{1}{r^2} \frac{\partial}{\partial r} \left( r^2 \frac{\partial C_s}{\partial r} \right)$$

## Appendix C. Computer program (C++) for Simulation Model

The models described in Chapter 4 were realized with C++ language. Each model was implemented with a cpp file. The partial differential equation systems were discretized into a system of ordinary differential equations by using the control volume method, and solved by SUNDIAL-CVODE open source solver.

CDMT-CP:

```
#include <iostream>
#include <fstream>
#include <vector>
#include <iomanip>
#include <cmath>
#include <numeric>
#include <sstream>
using namespace std;
#define USE_CVODE_INTEGRATOR
#include <sundials/sundials_types.h>
#include <sundials/sundials_math.h>
#include <nvector/nvector_serial.h>
#include <cvode/cvode.h>
#include <cvode/cvode_band.h>
// Directory for outputs
const char * OUTPUT_DIR = "..\\..\\..\\Simulations\\";
struct simulation_data_t {
int n;
int m;
vector<double> c; // gas-phase concentration in bed and pellet
vector<double> f; // fluxes between bed cells
vector<double> sigma; // mass transfer into pellet or intrapellet diffusion fluxes
vector<double> r; // radius of each pellet cell, m
vector<double> A_p; // surface area of each pellet cell, m^2
vector<double> V_shell; //volume of each pellet cell/shell, m^3
double e_b; // bed porosity
double e_p; // pellet porosity
double A; //cross-section area
```

```

double V_rev; //control volume
double n_p; // number of pellet in each bed node
//double A_pellet; // pellet surface area in control volum
//double R; // equvalant pellet radius in each bed cell;
double dr; //distance between each pellet cell;
double c_inlet; // inlet concentration
double u; // in-coming velocity
double K; // partition coefficient
double K_f; // mass transfer coefficient
double D_p; // intrapellet effective pore diffusion coefficient
double D_s; // surface diffusion coefficient
double D_app; // apparent diffusion coefficient
double sum_mass; // total mass stored in media bed m
double in_mass; // total mass go into the media bed
double out_mass; // total mass go out the media bed
double dif_mass; // in_mass - out_mass
double duration; // simulation duration
double output_dt; // output time step
double max_sim_dt; // max simulation time step
};
// Prototype
int system_function(realtype t, N_Vector y, N_Vector ydot, void * f_data);
int integrateExplicitly(double t_next_output, N_Vector v, N_Vector v_dot, double *
t,simulation_data_t * simdata);
int main(int argc, char * argv[]) {
simulation_data_t simdata;
simdata.n = 200; // number of cells of bed
simdata.m = 100; // number of cells of each pellet
simdata.e_b = 0.365;
simdata.e_p = 0.33;
simdata.A = 0.0018; // m2
double len = 0.025; // m
double r = 0.0025; // pellet radius
simdata.K_f = 1.0; //m/s, mass transfer coefficient
simdata.K = 9e+06;//*11; // partition coefficient
simdata.D_p = 5.82e-08*10 ; // diffusion coefficient
simdata.D_s = 5e-7; //m2/s
simdata.c_inlet = 1.2e-5; // kg/m3(gas) 1 ppm

```



```

simdata.u = 0.26; // m/s
simdata.duration = 10* 3600;
simdata.max_sim_dt = 240;
simdata.output_dt = 480;

simdata.c.resize(simdata.n*(simdata.m+1));
simdata.f.resize(simdata.n+1);
simdata.sigma.resize(simdata.n*simdata.m);
simdata.r.resize(simdata.m);
simdata.A_p.resize(simdata.m);
simdata.V_shell.resize(simdata.m);
simdata.D_app =simdata.D_p; /* simdata.e_p + 0*(1 - simdata.e_p) * simdata.K *
simdata.D_s);//(simdata.e_p+(1-simdata.e_p)*simdata.K);
simdata.V_rev = len*simdata.A/simdata.n;
double V_sp = 4*3.14*r*r*r/3; //volume of single pellet
double A_sp = 4*3.14 *r*r; // surface of single pellet
simdata.n_p = simdata.V_rev * (1-simdata.e_b)/ V_sp; // number of pellet in each V_rev
simdata.dr = r/simdata.m;
simdata.sum_mass = 0; // total mas stored in bed
simdata.in_mass = 0; // total mass go into the bed
simdata.out_mass = 0; // total mass go out the bed
//calculate A_p for each pellet cell
for(int j=0; j<simdata.m; j++){
simdata.r[j]=(simdata.m-j)*simdata.dr;
simdata.A_p[j]=4*3.14*simdata.r[j]*simdata.r[j];
}
//calculate V_shell for each pellet cell
for (int j=0; j<simdata.m-1; j++){
simdata.V_shell[j]=4.0/3*3.14*(simdata.r[j]*simdata.r[j]*simdata.r[j] - simdata.r[j+1] * simdata.r[j+1]
* simdata.r[j+1]);
}
simdata.V_shell[simdata.m-1]=4.0/3*3.14*simdata.r[simdata.m-1]*simdata.r[simdata.m-1]*simdata.r[simdata.m-1];
stringstream output_name;
output_name << OUTPUT_DIR << "OutletConcentration_Simulation_MD"<< ".out";
string output_filename = output_name.str();

```

```

ofstream output_outlet(output_filename.c_str());
// write header required for CHAMPS ChartView
output_outlet << "# Delphin 5 Output file\n";
output_outlet << "# TYPE = FIELD\n";
//output_outlet << "# PROJECT_FILE = "\n";
output_outlet << "# CREATED = now\n";
output_outlet << "# QUANTITY = Outlet concentration\n";
output_outlet << "# SPACE_TYPE = SINGLE\n";
output_outlet << "# TIME_TYPE = NONE\n";
output_outlet << "# VALUE_UNIT = mg/m3\n";
output_outlet << "# TIME_UNIT = h\n";
output_outlet << "\n";
output_outlet << "ELEMENTS = 1\n\n";
// set default output accuracy
output_outlet.precision(10);
output_outlet.flush();
output_name.clear();
output_name.str("");
// also increase precision for console output
cout.precision(10);
// first create a vector for the solution variables
N_Vector v = N_VNew_Serial(simdata.n*(simdata.m+1));
// specify initial conditions
for (int i=0; i<(simdata.m+1)*simdata.n; ++i)
NV_DATA_S(v)[i] = 0;
double t = 0;
// CVODE memory pointer
void * cvodeMem = CVodeCreate(CV_BDF, CV_NEWTON);
double relTol = 1e-5; // Relative tolerance
double absTol = 1e-5; // Absolute tolerances
CVodeMalloc(cvodeMem, system_function, t, v, CV_SS, relTol, &absTol);
// create banded solver
int bandwidth = 1; // only connected to the next cell
bandwidth = (bandwidth+1)*(simdata.m+1) - 1;
int result = CVBand(cvodeMem, simdata.n*(simdata.m+1), bandwidth, bandwidth);
CVodeSetFdata(cvodeMem, &simdata);
// set CVODE initial step size

```

```

CVodeSetInitStep(cvodeMem, 1e-2);
// set CVODE maximum step size
CVodeSetMaxStep(cvodeMem, simdata.max_sim_dt);
// set CVODE minimum step size
CVodeSetMinStep(cvodeMem, 1e-5);
try {
// start the simulation
double t_end = simdata.duration;
double dt_output = simdata.output_dt;
cout << "Starting simulation" << endl;
double t_next_output = dt_output;
while (t < t_end) {
// integrate until next output time point
int res = CVode(cvodeMem, t_next_output, v, &t, CV_NORMAL); // or CV_ONE_STEP
if (res < 0) {
switch (res) {
case CV_TOO_MUCH_WORK : break; // just go on with integrating
case CV_ILL_INPUT :
throw runtime_error("CVODE Error: Wrong input...");
default :
throw runtime_error("CVODE Error: Unknown error");
}
}
else {
// calculate new solution:  $y = y + dt * y_{dot}$ 
double * yp = NV_DATA_S(v);
// only output if past an output time point
if (t + 1e-6 > t_next_output) {
// catch up with the last output time point
while (t + 1e-6 > t_next_output) t_next_output += dt_output;
// calculate output quantities
simdata.sum_mass = 0;
for (int i=0; i < simdata.n; i++) {
simdata.sum_mass += yp[i*(simdata.m+1)]* simdata.V_rev;
for(int j=1; j<= simdata.m; j++) {
simdata.sum_mass += yp[i*(simdata.m+1)+j]* simdata.n_p * simdata.V_rev;
} //end for
}
}
}
}

```

```

} //end for
simdata.in_mass += simdata.f[0]* dt_output;
simdata.out_mass += simdata.f[simdata.n]* dt_output;
simdata.dif_mass = simdata.in_mass - simdata.out_mass;
// write output data into output files
double outlet_c = NV_DATA_S(v)[(simdata.n-1)*(simdata.m+1)]/simdata.e_b;
double outlet_cmgm3 = outlet_c*1000000;
output_outlet << t/3600 << "\t" << outlet_cmgm3 << endl;
cout << setw(10) << left << t/3600 << "\t"
<< setw(15) << left << outlet_cmgm3 << "\t"
<< setw(20) << left << simdata.sum_mass << " "
<< setw(15) << left << simdata.dif_mass << endl;
} //end if
} //end else
} // while
} // try

catch (std::exception & ex) {
cout << ex.what() << endl;
}
//CvodeFree(&cnodeMem);
N_VDestroy_Serial(v);
}

// function to calculate the divergences of your balance equations
int system_function(realtype t, N_Vector y, N_Vector ydot, void *f_data) {
// y - contains the solution variables (mass densities)
// ydot - store here the divergences of all balance equations
// t - current time point
// f_data - pointer to your local data vector
double * values = NV_DATA_S(y);
double * derivatives = NV_DATA_S(ydot);
simulation_data_t * simdata = reinterpret_cast<simulation_data_t*>(f_data);
// Use readability improvements, so that the code below is easier to follow and
// also faster (Andreas)
std::vector<double> & c = simdata->c;
unsigned int n = simdata->n;

```

```

unsigned int m = simdata->m;
double e_b = simdata->e_b;
double e_p = simdata->e_p;
double K = simdata->K;
double V_rev = simdata->V_rev;
std::vector<double> & V_shell = simdata->V_shell;
// first loop over all cells and calculate concentrations
for (unsigned int i=0; i<n; i++) {
unsigned k = i*(m + 1); // the bed node index
c[k] = values[k]/e_b;
}
// this is the gas phase concentration in pellet
for (unsigned int i=0; i<n; i++) {
for (unsigned j=1; j<=m; j++) {
unsigned k = i*(m + 1); // the bed node index
simdata->c[k+j] = values[k+j] / (e_p + K*(1-e_p)) / (V_shell[j-1]/V_rev);
//simdata->c[i*(simdata->m+1)+j] = values[i*(simdata->m+1)+j]/(simdata->e_p / simdata->K + (1-
simdata->e_p))/(simdata->V_shell[j-1]/simdata->V_rev);
}
}
// then loop over all sides and calculate the convective fluxes
simdata->f[0] = simdata->c_inlet*simdata->A*simdata->u;
for (unsigned int i=1; i<=n; i++) {
simdata->f[i] = simdata->c[(i-1)*(m+1)]*simdata->A*simdata->u;
}
//then loop over all bed and calculate the mass transfer/diffusion fluxes
for (unsigned int i=0; i<n; i++) {
unsigned int k = i*m; // = i*simdata->m = flux index into first pellet
unsigned int k_bed = k + i; // = i*(simdata->m+1) = index of bed node
// mass transfer flux kg/s into a single pellet
simdata->sigma[k] = simdata->K_f * simdata->A_p[0] * (simdata->c[k_bed]-simdata->c[k_bed+1]);
// diffusion flux between pellet shells
for (unsigned int j=1; j<m; j++) {
simdata->sigma[k + j] = simdata->D_app * simdata->A_p[j]*( simdata->c[k_bed+j] -
simdata->c[k_bed+j+1])/simdata->dr;
}
}
// then loop over all elements again and calculate divergences

```

```

for (unsigned int i=0; i<n; i++) {
unsigned int k = i*m; // = i*simdata->m = flux index into first pellet
unsigned int k_bed = k + i; // = i*(simdata->m+1) = index of bed node
// bed equation
derivatives[k_bed] = (simdata->f[i] - simdata->f[i+1] - simdata->sigma[k] * simdata->n_p)/V_rev;
// pellet equations
for (unsigned int j=1; j<m; j++){
derivatives[k_bed+j] = (simdata->sigma[k+j-1] - simdata->sigma[k+j])/V_rev;
}
//pellet equation for most inner node
derivatives[k_bed + m] = simdata->sigma[k + m - 1]/V_rev;
}
return 0; // all ok

```

CDMT-VP:

```

#include <iostream>
#include <fstream>
#include <vector>
#include <iomanip>
#include <cmath>
#include <numeric>
#include <sstream>
using namespace std;
#define USE_CVODE_INTEGRATOR
#include <sundials/sundials_types.h>
#include <sundials/sundials_math.h>
#include <nvector/nvector_serial.h>
#include <cvode/cvode.h>
#include <cvode/cvode_band.h>
// Directory for outputs
const char * OUTPUT_DIR = "..\\..\\..\\Simulations\\";
struct simulation_data_t {
int n;
int m;
vector<double> c; // gas-phase concentration in bed and pellet
vector<double> f; // fluxes between bed cells
vector<double> sigma; // mass transfer into pellet or intrapellet diffusion fluxes

```

```

vector<double> r; // radius of each pellet cell, m
vector<double> A_p; // surface area of each pellet cell, m^2
vector<double> V_shell; //volume of each pellet cell/shell, m^3
double e_b; // bed porosity
double e_p; // pellet porosity
double A; //cross-section area
double V_rev; //control volume
double n_p; // number of pellet in each bed node
//double A_pellet; // pellet surface area in control volum
//double R; // equvalant pellet radius in each bed cell;
double dr; //distance between each pellet cell;
double c_inlet; // inlet concentration
double u; // in-coming velocity
double K; // partition coefficient
double K_f; // mass transfer coefficient
double D_p; // intrapellet effective pore diffusion coefficient
double D_s; // surface diffusion coefficient
double D_app; // apparent diffusion coefficient
double sum_mass; // total mass stored in media bed
double in_mass; // total mass go into the media bed
double out_mass; // total mass go out the media bed
double dif_mass; // in_mass - out_mass
double duration; // simulation duration
double output_dt; // output time step
double max_sim_dt; // max simulation time step
};
// Prototype
int system_function(realtype t, N_Vector y, N_Vector ydot, void * f_data);
int integrateExplicitly(double t_next_output, N_Vector v, N_Vector v_dot, double *
t,simulation_data_t * simdata);
int main(int argc, char * argv[]) {
simulation_data_t simdata;
simdata.n = 50; // number of cells of bed
simdata.m = 10; // number of cells of each pellet
simdata.e_b = 0.36;
simdata.e_p = 0.3;
simdata.A = 0.0018; // m2 //small bed
double len = 0.025; // m

```

```

double r = 0.00076; // pellet radius
simdata.K_f = 0.069; //m/s, mass transfer coefficient
simdata.K = 1.5e8; // partition coefficient
simdata.D_p = 8.22e-6 ; // diffusion coefficient
simdata.D_s = 4e-13; //m2/s
simdata.c_inlet = 66*3.8e-9; // kg/m3(gas)
simdata.u = 0.26; // m/s
simdata.duration = 1200;
simdata.max_sim_dt = 120;
simdata.output_dt = 120;

string input_file = "input.txt"; // this is the default name and location of the input file

// check if we have command line arguments
if (argc > 1) {
    input_file = argv[1];
}
// check if input file exists
ifstream in(input_file.c_str());
if (in){
in >> simdata.n
>> simdata.m
>> simdata.e_b
>> simdata.e_p
>> simdata.A
>> len
>> r
>> simdata.K_f
>> simdata.K
>> simdata.D_p
>> simdata.D_s
>> simdata.c_inlet
>> simdata.u
>> simdata.duration
>> simdata.max_sim_dt
>> simdata.output_dt;

```



```

cout << "Using data from input file " << input_file << "." << endl;
}
in.close();
simdata.c.resize(simdata.n*(simdata.m+1));
simdata.f.resize(simdata.n+1);
simdata.sigma.resize(simdata.n*simdata.m);
simdata.r.resize(simdata.m);
simdata.A_p.resize(simdata.m);
simdata.V_shell.resize(simdata.m);
simdata.D_app = simdata.D_p * simdata.e_p + (1 - simdata.e_p) * simdata.K * simdata.D_s;
simdata.V_rev = len*simdata.A/simdata.n;
double V_sp = 4*3.14*r*r*r/3; //volume of single pellet
double A_sp = 4*3.14 *r*r; // surface of single pellet
simdata.n_p = simdata.V_rev * (1-simdata.e_b)/ V_sp; // number of pellet in each V_rev
simdata.dr = r/simdata.m;
simdata.sum_mass = 0; // total mas stored in bed
simdata.in_mass = 0; // total mass go into the bed
simdata.out_mass = 0; // total mass go out the bed
//calculate A_p for each pellet cell
for(int j=0; j<simdata.m; j++){
simdata.r[j]=(simdata.m-j)*simdata.dr;
simdata.A_p[j]=4*3.14*simdata.r[j]*simdata.r[j];
}
//calculate V_shell for each pellet cell
for (int j=0; j<simdata.m-1; j++){
simdata.V_shell[j]=4.0/3*3.14*(simdata.r[j]*simdata.r[j]*simdata.r[j] - simdata.r[j+1] * simdata.r[j+1]
* simdata.r[j+1]);
}
simdata.V_shell[simdata.m-1]=4.0/3*3.14*simdata.r[simdata.m-1]*simdata.r[simdata.m-1]*simdata.r[simdata.m-1];
stringstream output_name;
output_name << OUTPUT_DIR << "OutletConcentration_Simulation_MD" << ".out";
string output_filename = output_name.str();
ofstream output_outlet(output_filename.c_str());
// write header required for CHAMPS ChartView
output_outlet << "# Delphin 5 Output file\n";
output_outlet << "# TYPE = FIELD\n";
output_outlet << "# PROJECT_FILE = " << input_file << "\n";

```

```

output_outlet << "# CREATED = now\n";
output_outlet << "# QUANTITY = Outlet concentration\n";
output_outlet << "# SPACE_TYPE = SINGLE\n";
output_outlet << "# TIME_TYPE = NONE\n";
output_outlet << "# VALUE_UNIT = mg/m3\n";
output_outlet << "# TIME_UNIT = h\n";
output_outlet << "\n";
output_outlet << "ELEMENTS = 1\n\n";
// set default output accuracy
output_outlet.precision(10);
output_outlet.flush();
output_name.clear();
output_name.str("");
// also increase precision for console output
cout.precision(10);
// first create a vector for the solution variables
N_Vector v = N_VNew_Serial(simdata.n*(simdata.m+1));
// specify initial conditions
for (int i=0; i<(simdata.m+1)*simdata.n; ++i)
NV_DATA_S(v)[i] = 0;
double t = 0;
// CVODE memory pointer
void * cvodeMem = CVodeCreate(CV_BDF, CV_NEWTON);
double relTol = 1e-8; // Relative tolerance
double absTol = 1e-8; // Absolute tolerances
CVodeMalloc(cvodeMem, system_function, t, v, CV_SS, relTol, &absTol);
// create banded solver
int bandwidth = 1; // only connected to the next cell
bandwidth = (bandwidth+1)*(simdata.m+1) - 1;
int result = CVBand(cvodeMem, simdata.n*(simdata.m+1), bandwidth, bandwidth);
CVodeSetFdata(cvodeMem, &simdata);
// set CVODE initial step size
CVodeSetInitStep(cvodeMem, 1e-8);
// set CVODE maximum step size
CVodeSetMaxStep(cvodeMem, simdata.max_sim_dt);
// set CVODE minimum step size
CVodeSetMinStep(cvodeMem, 1e-8);

```

```

try {
// start the simulation
double t_end = simdata.duration;
double dt_output = simdata.output_dt;
cout << "Starting simulation" << endl;
double t_next_output = dt_output;
while (t < t_end) {
// integrate until next output time point
int res = CVode(cvodeMem, t_next_output, v, &t, CV_NORMAL); // or CV_ONE_STEP
if (res < 0) {
switch (res) {
case CV_TOO_MUCH_WORK : break; // just go on with integrating
case CV_ILL_INPUT :
throw runtime_error("CVODE Error: Wrong input...");
default :
throw runtime_error("CVODE Error: Unknown error");
}
}
else {
// calculate new solution:  $y = y + dt*y_{dot}$ 
double * yp = NV_DATA_S(v);
// only output if past an output time point
if (t + 1e-6 > t_next_output) {
// catch up with the last output time point
while (t + 1e-6 > t_next_output) t_next_output += dt_output; //???-10
// calculate output quantities
simdata.sum_mass = 0;
for (int i=0; i < simdata.n; i++) {
simdata.sum_mass += yp[i*(simdata.m+1)]* simdata.V_rev;
for(int j=1; j<= simdata.m; j++) {
simdata.sum_mass += yp[i*(simdata.m+1)+j]* simdata.n_p * simdata.V_rev;
} //end for
} //end for
simdata.in_mass += simdata.f[0]* dt_output;
simdata.out_mass += simdata.f[simdata.n]* dt_output;
simdata.dif_mass = simdata.in_mass - simdata.out_mass;
// write output data into output files

```

```

double outlet_c = NV_DATA_S(v)[(simdata.n-1)*(simdata.m+1)]/simdata.e_b;
double outlet_cmgm3 = outlet_c*1000000;
output_outlet << t/3600 << "\t" << outlet_cmgm3 << endl;
cout << setw(10) << left << t/3600 << "\t"
<< setw(15) << left << outlet_cmgm3 << "\t"
<< setw(20) << left << simdata.sum_mass << " "
<< setw(15) << left << simdata.dif_mass << endl;
} //end if
} //end else
} // while
} // try

catch (std::exception & ex) {
cout << ex.what() << endl;
}
//CvodeFree(&cvmem);
N_VDestroy_Serial(v);
} //end of main

// function to calculate the divergences of your balance equations
int system_function(realtype t, N_Vector y, N_Vector ydot, void *f_data) {
// y - contains the solution variables (mass densities)
// ydot - store here the divergences of all balance equations
// t - current time point
// f_data - pointer to your local data vector
double * values = NV_DATA_S(y);
double * derivatives = NV_DATA_S(ydot);
simulation_data_t * simdata = reinterpret_cast<simulation_data_t*>(f_data);
// Use readability improvements, so that the code below is easier to follow and
// also faster (Andreas)
std::vector<double> & c = simdata->c;
unsigned int n = simdata->n;
unsigned int m = simdata->m;
double e_b = simdata->e_b;
double e_p = simdata->e_p;
double K = simdata->K;
double V_rev = simdata->V_rev;

```

```

std::vector<double> & V_shell = simdata->V_shell;
// first loop over all cells and calculate concentrations
for (unsigned int i=0; i<n; i++) {
unsigned k = i*(m + 1); // the bed node index
c[k] = values[k]/e_b;
}
// this is the gas phase concentration in pellet
for (unsigned i=0; i<n; i++) {
for (unsigned j=1; j<=m; j++) {
node index                                unsigned k = i*(m + 1); // the bed
simdata->c[k+j] = values[k+j] / (e_p
+ 1747.9* pow(c[k+j-1],-0.748)*(1-e_p)) / (V_shell[j-1]/V_rev);
// simdata->c[i*(simdata->m+1)+j] = values[i*(simdata->m+1)+j]/(simdata->e_p / simdata->K + (1-
simdata->e_p))/(simdata->V_shell[j-1]/simdata->V_rev); 2121.5 * pow(c[k+j-1],-0.728)
}
}
// then loop over all sides and calculate the convective fluxes
simdata->f[0] = simdata->c_inlet*simdata->A*simdata->u;
for (unsigned int i=1; i<=n; i++) {
simdata->f[i] = simdata->c[(i-1)*(m+1)]*simdata->A*simdata->u;
}
//then loop over all bed and calculate the mass transfer/diffusion fluxes
for (unsigned int i=0; i<n; i++) {
unsigned int k = i*m; // = i*simdata->m = flux index into first pellet
unsigned int k_bed = k + i; // = i*(simdata->m+1) = index of bed node
// mass transfer flux kg/s into a single pellet
simdata->sigma[k] = simdata->K_f * simdata->A_p[0] * (simdata->c[k_bed]-simdata->c[k_bed+1]);
// diffusion flux between pellet shells
for (unsigned int j=1; j<=m; j++) {
simdata->sigma[k + j] = simdata->D_app* simdata->A_p[j]*( simdata->c[k_bed+j] -
simdata->c[k_bed+j+1])/simdata->dr;
} //2e-15 * pow(c[k_bed],16)
simdata->D_app
}
// then loop over all elements again and calculate divergences
for (unsigned int i=0; i<n; i++) {
unsigned int k = i*m; // = i*simdata->m = flux index into first pellet
unsigned int k_bed = k + i; // = i*(simdata->m+1) = index of bed node

```

```

// bed equation
derivatives[k_bed] = (simdata->f[i] - simdata->f[i+1] - simdata->sigma[k] * simdata->n_p)/V_rev;
// pellet equations
for (unsigned int j=1; j<m; j++){
derivatives[k_bed+j] = (simdata->sigma[k+j-1] - simdata->sigma[k+j])/V_rev;
}
//pellet equation for most inner node
derivatives[k_bed + m] = simdata->sigma[k + m - 1]/V_rev;
}
return 0; // all ok
}

int integrateExplicitly(double t_next_output, N_Vector v, N_Vector v_dot, double * t,
simulation_data_t * simdata)
{
    double dt = 1e-5;
    while (*t < t_next_output) {
        // calculate divergences
        int result = system_function(*t, y, y_dot, simdata);

        // calculate new solution: y = y + dt*y_dot
        double * yp = NV_DATA_S(y);
        double * y_dotp = NV_DATA_S(y_dot);
        for (int i = 0; i<(simdata->m + 1)*simdata->n; ++i) {
            yp[i] += dt*y_dotp[i];
        }

        // calculate the total VOC mass stored in media bed ??
        //simdata->sum_mass = std::accumulate(yp, yp + (simdata->m+1)*simdata->n, 0.0)*
simdata->V_rev;
        for (int i = 0; i < simdata->n; i++) {
            simdata->sum_mass += yp[i*(simdata->m + 1)] * simdata->V_rev;
            for (int j = 1; j <= simdata->m; j++) {
                simdata->sum_mass += yp[i*(simdata->m + 1) + j] * simdata->n_p *
simdata->V_rev;
            }
        }
        // calculte the total mass go out the media bed
    }
}

```

```

simdata->in_mass += simdata->f[0] * dt;
simdata->out_mass += simdata->f[simdata->n] * dt;
simdata->dif_mass = simdata->in_mass - simdata->out_mass;
// advance in time
*t += dt;
}
return 0;
}

```

## Appendix D. Method and procedure implemented in models for regression analysis with C&DMT-VP model

Regression method is used to determine unknown parameters, such as surface diffusion coefficient  $D_s$ , and P-C correlation. Constants (a and b). Most commonly, regression analysis estimates the conditional expectation of the variables given the independent variables – that is, the average value of the dependent variable when the independent variables are fixed. In this

study, the “to-be-determined” parameters are considered as the variable in the regression. The procedure is summarized in Figure D-1.

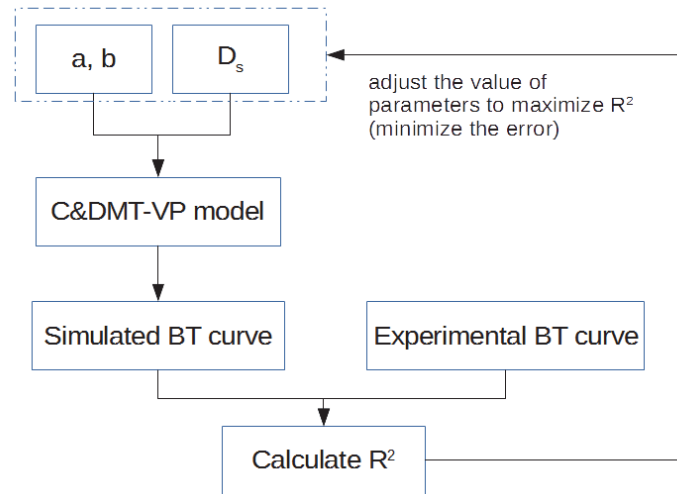


**Figure D-1 Procedure of regression method**

After completing an adsorption test, the partition coefficient  $K_{ma}$  for this test can be considered as know parameter. The correlation between  $a$  and  $b$  can be easily calculated per Eq. (3-2). Because the range of  $D_s$  is very large (in the magnitude of  $10^{-7} \sim 10^{-14}$ ), an algorithm must be applied to systematically adjust the parameter estimates to reduce the squared errors of prediction (SSE). For each iteration, the Levenberg–Marquardt algorithm in the MATLAB function package adjusts the parameter estimates in a manner that it predicts should reduce the SSE compared to the previous iteration. The connection between MATLAB and C++ is achieved by calling the Matlab function engine in the C++ script:

```

#include "MatlabEngine.hpp"
#include "MatlabDataArray.hpp"
#include <iostream>
void callFevalgcd() {

    // Pass vector containing MATLAB data array scalar
    using namespace matlab::engine;
  
```



```

// Start MATLAB engine synchronously
std::unique_ptr<MATLABEngine> matlabPtr = startMATLAB();

// Create MATLAB data array factory
matlab::data::ArrayFactory factory;

// Pass vector containing 2 scalar args in vector
std::vector<matlab::data::Array> args({
    factory.createScalar<int16_t>(30),
    factory.createScalar<int16_t>(56) });

// Call MATLAB function and return result
matlab::data::TypedArray<int16_t> result = matlabPtr->
    feval(convertUTF8StringToUTF16String("gcd"), args);
int16_t v = result[0];
std::cout << "Result: " << v << std::endl;
}

```

Once calling the function of regression in the MATLAB is enabled in the C++ script, the  $R^2$  value while comparing the simulated data and experimental data for each iteration can be calculated:

```

%calculate the R-squire value for Acc 100 ppb toluene and AC M#1 & M#2
clear;
clc;
filename = 'viz_chapt5_prediction.xlsx';
M = xlsread(filename,'Sheet1');
timeM1 = M(:,1);
concM1 = M(:,2);
timeM2 = M(:,3);
concM2 = M(:,4);
timeSimM1 = M(:,5);
concSimM1 = M(:,6);
timeSimM2 = M(:,7);
concSimM2 = M(:,8);
for i=1:2
    flag=i;
    if flag==1

```

```

%% Fit: 'untitled fit 1'.
[xData, yData] = prepareCurveData( timeSimM1, concSimM1 );

elseif flag==2
[xData, yData] = prepareCurveData( timeSimM2, concSimM2 );

end

% Set up fitype and options.
ft = fitype( 'a/(1+exp(b-c*x))', 'independent', 'x', 'dependent', 'y' );
opts = fitoptions( 'Method', 'NonlinearLeastSquares' );
opts.Display = 'Off';
opts.Lower = [0 0 0];
opts.StartPoint = [0.217583190739525 0.571412481591965 0.991198241873201];

% Fit model to data.
[fitresult, gof] = fit( xData, yData, ft, opts );
coefficient = coeffvalues(fitresult);
a = coefficient(1);
b = coefficient(2);
c = coefficient(3);
Ind = ~isnan(M(:,(flag-1)*2+1));
time_clear_trans=M(:,(flag-1)*2+1);
time_clear = time_clear_trans(Ind);

z=(a./(1+exp(b-c.*time_clear)));

%Ind = find(~isnan(concM1));
conc = M(:,(flag-1)*2+2);
conc_clear = conc(Ind);
n=length(conc_clear);
average_exp=1/n*sum(conc_clear);
SStot(flag) = sum ((conc_clear-average_exp).^2);
for i=1:n
temp(i)=conc_clear(i)-z(i);
end
SSres(flag) = sum((temp).^2);
R2(flag)=1-SSres(flag)/SStot(flag)

```

```

end
%plot the regressed BT curve
hold on

scatter(timeM1(1:5:end),concM1(1:5:end),'DisplayName','Test
M#1','marker','o','MarkerEdgeColor','r');
plot(timeSimM1,concSimM1,'DisplayName','Prediction M#1','MarkerEdgeColor',[0 0 1],...
'LineWidth',3,...
'Color','r');
scatter(timeM2(1:5:end),concM2(1:5:end),'DisplayName','Test
M#2','marker','d','MarkerEdgeColor','b');
plot(timeSimM2,concSimM2,'DisplayName','Regression M#2','linewidth',3,'MarkerEdgeColor','b');

t=length(timeM1);% plot the inlet concentration
cin=ones(3,t+1);
std=8*3.8e-3;
cin(2,:)=66*3.8e-3; cin(1,:)=cin(2,:)-std; cin(3,:)=cin(2,:)+std;
line(0:t,cin(2,:),'color','k','LineWidth',2)
line(0:t,cin(1,:),'color','k','LineWidth',1.5,'LineStyle',':');
line(0:t,cin(3,:),'color','k','LineWidth',1.5,'LineStyle',':');
textcin={'Inlet=66.8\pm8 ppb'};

text(250,0.27,textcin,'FontSize',12);

legend('Test M#1','Prediction M#1','Test M#2','Prediction M#2');
textstr={'R-squre M#1=0.903';'R-squre M#2=0.839'};
text(2000,0.15,textstr,'FontSize',12);
set(legend,'FontWeight','bold','FontSize',12);
axis([0,3000,0,0.3]);
set(gca,'fontsize',12,'xTick',0:500:3000)
xlabel('t,h','FontSize',12,'FontWeight','bold');
ylabel('Concentration, mg/m^3','FontSize',12,'FontWeight','bold');

hold off

```

# 8 REFERENCES

Axley, J. W. (1994). *Tools for the analysis of gas-phase air-cleaning systems in buildings*. American Society of Heating, Refrigerating and Air-Conditioning Engineers, Inc., Atlanta, GA (United States).

Ayoob, S., & Gupta, A. K. (2007). Sorptive response profile of an adsorbent in the defluoridation of drinking water. *Chemical Engineering Journal*, 133(1), 273–281.

Bohart, G. S., & Adams, E. Q. (1920). Some aspects of the behavior of charcoal with respect to chlorine. 1. *Journal of the American Chemical Society*, 42(3), 523–544.

Carratala-Abril, J., Lillo-Rodenas, M. A., Linares-Solano, A., & Cazorla-Amoros, D. (2009). Activated carbons for the removal of low-concentration gaseous toluene at the semipilot scale. *Industrial & Engineering Chemistry Research*, 48(4), 2066–2075.

Crittenden, J. C., & Weber, W. J. (1978). Predictive model for design of fixed-bed adsorbers: Parameter estimation and model development. *Journal of the Environmental Engineering Division*, 104(2), 185–197.

Delgado, J. (2006). A critical review of dispersion in packed beds. *Heat and Mass Transfer*, 42(4), 279–310.

Do, D. D. (1998a). *Adsorption analysis*. World Scientific.

Do, D. D. (1998b). *Adsorption Analysis: Equilibria and Kinetics*: (With CD Containing Computer Matlab Programs) (Vol. 2). World Scientific.

Dolphen, R., Sakkayawong, N., Thiravetyan, P., & Nakbanpote, W. (2007). Adsorption of Reactive Red 141 from wastewater onto modified chitin. *Journal of Hazardous Materials*, 145(1), 250–255.

Fiedler, N., Laumbach, R., Kelly-McNeil, K., Liroy, P., Fan, Z.-H., Zhang, J., ... Kipen, H. (2005). Health effects of a mixture of indoor air volatile organics, their ozone oxidation products, and stress. *Environmental Health Perspectives*, 113(11), 1542.

Fisk, W. J. (2008). CAN SORBENT-BASED GAS PHASE AIR CLEANING FOR VOCS SUBSTITUTE FOR VENTILATION IN COMMERCIAL BUILDINGS?

Foster, K. L., Fuerman, R. G., Economy, J., Larson, S. M., & Rood, M. J. (1992). Adsorption characteristics of trace volatile organic compounds in gas streams onto activated carbon fibers. *Chemistry of Materials*, 4(5), 1068–1073.

Goud, V. V, Mohanty, K., Rao, M. S., & Jayakumar, N. S. (2005). Prediction of mass transfer coefficients in a packed bed using tamarind nut shell activated carbon to remove phenol. *Chemical Engineering & Technology*, 28(9), 991–997.

Guo, B., Zhang, J. S., Nair, S., Chen, W., & Smith, J. (2006). VOC removal performance of pellet/granular-type sorbent media-: Experimental results. *ASHRAE Transactions*, 430–440.

Hamdaoui, O. (2006). Dynamic sorption of methylene blue by cedar sawdust and crushed brick in fixed bed columns. *Journal of Hazardous Materials*, 138(2), 293–303.

Han, K., Guo, B., Pei, J., & Zhang, J. (2012). Energy-efficient Reduction of Indoor Formaldehyde Exposure by Dynamic Integration of Air-cleaning and Ventilation: Final Report. Retrieved from <https://books.google.com/books?id=Bk15rgEACAAJ>

He, C., Chen, W., Han, K., Guo, B., Pei, J., & Zhang, J. S. (2014). Evaluation of filter media performance: Correlation between high and low challenge concentration tests for toluene and

formaldehyde (ASHRAE RP-1557). *HVAC&R Research*, 20(5), 508–521.

<https://doi.org/10.1080/10789669.2014.907096>

Henning, K.-D. (2001). Solvent recycling, removal, and degradation. *Handbook of Solvents*, ChemTec Publishing, Toronto, Canada, 1507–1570.

Khazraei Vizhemehr, A., Haghghat, F., Lee, C.-S., Kholafaei, H., & Lakdawala, N. (2014). Evaluation of Gas-Phase Filter Performance for a Gas Mixture. *CLEAN – Soil, Air, Water*, n/a-n/a. <https://doi.org/10.1002/clen.201300751>

Ko, D. C. K., Porter, J. F., & McKay, G. (2003). Mass transport model for the fixed bed sorption of metal ions on bone char. *Industrial & Engineering Chemistry Research*, 42(14), 3458–3469.

Laine, J., & Yunes, S. (1992). Effect of the preparation method on the pore size distribution of activated carbon from coconut shell. *Carbon*, 30(4), 601–604.

Levin, H., & Hodgson, A. T. (2006). VOC concentrations of interest in North American offices and homes. In *Proceedings Healthy Buildings* (pp. 233–238).

Li, L., Quinlivan, P. a., & Knappe, D. R. U. (2002). Effects of activated carbon surface chemistry and pore structure on the adsorption of organic contaminants from aqueous solution. *Carbon*, 40(12), 2085–2100. [https://doi.org/10.1016/S0008-6223\(02\)00069-6](https://doi.org/10.1016/S0008-6223(02)00069-6)

Liu, K.-T., & Weber Jr, W. J. (1981). Characterization of mass transfer parameters for adsorber modeling and design. *Journal (Water Pollution Control Federation)*, 1541–1550.

Liu, R.-T. (1990). Removal of volatile organic compounds in IAQ concentrations with short carbon bed depths. *Proceedings of Indoor Air*, 90, 177–182.

Lodewyckx, P., Wood, G. O., & Ryu, S. K. (2004). The Wheeler–Jonas equation: a versatile tool for the prediction of carbon bed breakthrough times. *Carbon*, 42(7), 1351–1355. <https://doi.org/10.1016/j.carbon.2004.01.016>

- Mohan, N., Kannan, G. K., Upendra, S., Subha, R., & Kumar, N. S. (2009). Breakthrough of toluene vapours in granular activated carbon filled packed bed reactor. *Journal of Hazardous Materials*, 168(2), 777–781.
- Mugge, J., Bosch, H., & Reith, T. (2001). Measuring and modelling gas adsorption kinetics in single porous particles. *Chemical Engineering Science*, 56(18), 5351–5360.
- Nelson, G. (1992). Gas mixtures: preparation and control. CRC Press.
- Noll, K. E. (1991). Adsorption technology for air and water pollution control. CRC Press.
- Patel, N. D., & Brown, M. W. (1994, December 27). Low VOC (volatile organic compounds), solvent-based ABS adhesives. Google Patents.
- Pei, J., & Zhang, J. (2010). Modeling of sorbent-based gas filters: Development, verification and experimental validation. *Building Simulation*, 3(1), 75–86. <https://doi.org/10.1007/s12273-010-0309-4>
- Pei, J., & Zhang, J. S. (2012). Determination of adsorption isotherm and diffusion coefficient of toluene on activated carbon at low concentrations. *Building and Environment*, 48, 66–76. <https://doi.org/10.1016/j.buildenv.2011.08.005>
- Pérez-Lombard, L., Ortiz, J., & Pout, C. (2008). A review on buildings energy consumption information. *Energy and Buildings*, 40(3), 394–398. <https://doi.org/https://doi.org/10.1016/j.enbuild.2007.03.007>
- Popescu, R. S., Blondeau, P., Jouandon, E., Costes, J. C., & Fanlo, J. L. (2013). Elemental modeling of adsorption filter efficiency for indoor air quality applications. *Building and Environment*, 66, 11–22. <https://doi.org/10.1016/j.buildenv.2013.01.025>
- Ranz, W. E., & Marshall, W. R. (1952). Evaporation from drops. *Chemical Engineering Progress*, 48(3), 141446.

Reguer, A., Sochard, S., Hort, C., & Platel, V. (2011). Measurement and modelling of adsorption equilibrium, adsorption kinetics and breakthrough curve of toluene at very low concentrations on to activated carbon. *Environmental Technology*, 32(7–8), 757–766. <https://doi.org/10.1080/09593330.2010.512297>

Richard, D., Núñez, M. de L. D., & Schweich, D. (2010). Adsorption of complex phenolic compounds on active charcoal: breakthrough curves. *Chemical Engineering Journal*, 158(2), 213–219.

Roberts, P. V, Cornel, P., & Summers, R. S. (1985). External mass-transfer rate in fixed-bed adsorption. *Journal of Environmental Engineering*, 111(6), 891–905.

Rouquerol, J., Rouquerol, F., Llewellyn, P., Maurin, G., & Sing, K. S. W. (2013). *Adsorption by powders and porous solids: principles, methodology and applications*. Academic press.

Rozada, F., Otero, M., Garcia, A. I., & Moran, A. (2007). Application in fixed-bed systems of adsorbents obtained from sewage sludge and discarded tyres. *Dyes and Pigments*, 72(1), 47–56.

Ruthven, D. M. (1984). *Principles of adsorption and adsorption processes*. John Wiley & Sons.

Scahill, J., Wolfrum, E. J., Michener, W. E., Bergmann, M., Blake, D. M., & Watt, A. S. (2004). A New Method for the Rapid Determination of Volatile Organic Compound Breakthrough Times for a Sorbent at Concentrations Relevant to Indoor Air Quality. *Journal of the Air &*



*Waste Management Association*, 54(1), 105–110.

<https://doi.org/10.1080/10473289.2004.10470879>

Seader, J. D., & Henley, E. J. (2011). Separation process principles.

Seo, J., Kato, S., Ataka, Y., & Chino, S. (2009). Performance test for evaluating the reduction of VOCs in rooms and evaluating the lifetime of sorptive building materials. *Building and Environment*, 44(1), 207–215.

Sing, K. S. W. (1985). Reporting physisorption data for gas/solid systems with special reference to the determination of surface area and porosity (Recommendations 1984). *Pure and Applied Chemistry*, 57(4), 603–619.

Sing, K. S. W. (1989). The use of gas adsorption for the characterization of porous solids. *Colloids and Surfaces*, 38(1), 113–124.

Thoenes, D., & Kramers, H. (1958). Mass transfer from spheres in various regular packings to a flowing fluid. *Chemical Engineering Science*, 8(3), 271–283.

Tien, C. (1994). Adsorption Calculations and Modeling. Butterworth-Heinemann Series in Chemical Engineering.

Treybal, R. E. (1980). Mass-transfer operations. *New York*.

van Vliet, B. M., & Weber Jr, W. J. (1981). Comparative performance of synthetic adsorbents and activated carbon for specific compound removal from wastewaters. *Journal (Water Pollution Control Federation)*, 1585–1598.

VanOsdell, D. W., Owen, M. K., Jaffe, L. B., & Sparks, L. E. (1996). VOC Removal at Low Contaminant Concentrations Using Granular Activated Carbon. *Journal of the Air & Waste Management Association*, 46(9), 883–890. <https://doi.org/10.1080/10473289.1996.10467524>

Vidic, R. D., Suidan, M. T., & Brenner, R. C. (1994). Impact of oxygen mediated oxidative coupling on adsorption kinetics. *Water Research*, 28(2), 263–268.

Wakao, N., & Funazkri, T. (1978a). Effect of fluid dispersion coefficients on particle-to-fluid mass transfer coefficients in packed beds. *Chemical Engineering Science*, 33(10), 1375–1384.  
[https://doi.org/10.1016/0009-2509\(78\)85120-3](https://doi.org/10.1016/0009-2509(78)85120-3)

Wakao, N., & Funazkri, T. (1978b). Effect of fluid dispersion coefficients on particle-to-fluid mass transfer coefficients in packed beds: Correlation of sherwood numbers. *Chemical*

*Engineering Science*, 33(10), 1375–1384. [https://doi.org/http://dx.doi.org/10.1016/0009-2509\(78\)85120-3](https://doi.org/http://dx.doi.org/10.1016/0009-2509(78)85120-3)

Weber, T. W., & Chakravorti, R. K. (1974). Pore and solid diffusion models for fixed-bed adsorbers. *AIChE Journal*, 20(2), 228–238.

Wolkoff, P. (1995). Volatile organic compounds sources, measurements, emissions, and the impact on indoor air quality. *Indoor Air*, 5(S3), 5–73.

Wood, G. O. (2001). Affinity coefficients of the Polanyi/Dubinin adsorption isotherm equations: A review with compilations and correlations. *Carbon*, 39(3), 343–356.

Wu, J., Claesson, O., Fangmark, I., & Hammarstrom, L.-G. (2005). A systematic investigation of the overall rate coefficient in the Wheeler–Jonas equation for adsorption on dry activated carbons. *Carbon*, 43(3), 481–490.

Xu, Z., Cai, J.-G., & Pan, B.-C. (2013). Mathematically modeling fixed-bed adsorption in aqueous systems. *Journal of Zhejiang University-SCIENCE A (Applied Physics & Engineering)*, 14(3), 155–176. <https://doi.org/10.1631/jzus.A1300029>

Yang, R. (1988). Gas separation by adsorption processes. Pergamon.

Yu, Z., Peldszus, S., & Huck, P. M. (2009). Adsorption of selected pharmaceuticals and an endocrine disrupting compound by granular activated carbon. 1. Adsorption capacity and kinetics. *Environmental Science & Technology*, 43(5), 1467–1473.

Bournemouth University, 2005, *Citing References*, [www.bournemouth.ac.uk/academic\\_services/documents/Library/Citing\\_References.pdf](http://www.bournemouth.ac.uk/academic_services/documents/Library/Citing_References.pdf).

[Accessed August 2006].



## VITA

**Name of Author:** Chuan He

**Place of Birth:** Harbin, Heilongjiang, China

**Date of Birth:** March 22, 1987

**Graduate and undergraduate school attended:**

Syracuse University, Syracuse, NY, USA

China University of Mining and Technology (Beijing), Beijing, China

**Degrees Awarded:**

M.S. Mechanical Engineering, 2013, Syracuse University

B.S. Fire Safety Engineering, 2010, China University of Mining and Technology (Beijing)

**Awards and Honors:**

Research assistant scholarship at Syracuse University, 2014~2016

**Professional Experience:**

Research assistant at Department of Mechanical and Aerospace Engineering, Syracuse University, 2013~2016

Teaching assistant at Department of Mechanical and Aerospace Engineering, Syracuse University, 2014

Research affiliate at Well Living Lab, Mayo Clinic, 2016~2018

Director at Delos Labs, Delos, NY, 2017

Senior Director at Delos Labs, Delos, NY. 2018